THE PEOPLE'S DEMOCRATIC REPUBLIC OF ALGERIA

الجمهورية الجزائرية الديمقراطية الشعبية

ⵜⵉⵅⵙⵉⵙⵓ ⵜⵉⵍⵅⵓⵙⵜ ⵜⵓⵢⵓⵣⵓⵍⵜ ⵜⵉⵏⵥⵓⵙⵓⵉⵜ

The Ministry of Higher Education and Scientific Research

وزارة التعليم العالي والبحث العلمي

UNIVERSITY OF SAAD DAHLEB BLIDA

Institute of Aeronautics and Space Studies

End-of-Studies Project for a MASTER's DEGREE

OPTION: AIRCRAFT PROPULSION

Topic :

Numerical Simulation and Analysis of Supersonic Combustion Chambers with Varied Mach Numbers and Cavity Configurations Using Ansys Fluent

REALISED BY :

Mr. HAMADA Mohamed Mouloud

SUPERVISED BY :

Dr : NECHE Ahmed

Dr : RENANE Rachid

Dr : ALLOUCHE Rachid

Blida, July 2024

Acknowledgements:

First and foremost, I would like to express my deepest gratitude to my family and friends. Your unwavering support, encouragement, and belief in my abilities have been the foundation upon which this academic journey was built. Without your love and understanding, this accomplishment would not have been possible.

I extend my sincere thanks to my advisors, Mr. Neche, Mr. Renane and Mr. Allouche, for their invaluable guidance, patience, and insights throughout this research. Your expertise and dedication have been instrumental in shaping this thesis, and I am profoundly grateful for your mentorship.

I am also indebted to the Chairman and members of the Jury for honoring my work with their presence and for their constructive feedback, which will greatly contribute to the improvement of this research.

My heartfelt appreciation goes to the faculty and staff at this Institute. Your exceptional teaching and support have provided me with the knowledge and skills necessary to undertake this project. Special thanks to all the great professors for your encouragement and assistance.

To my fellow classmates and friends, your camaraderie and collaborative spirit have made this journey enjoyable and enriching. The shared experiences, late-night study sessions, and mutual support have been invaluable.

Lastly, I extend my gratitude to all the participants who shared their experiences and insights for this thesis. Your contributions have infused this work with depth and authenticity.

This thesis stands as a testament to the collective efforts, support, and inspiration of all those involved. Thank you.

Ovation:

TO my mother,
My father,
My brothers,

To my loved ones and friends,

To all those who have contributed in any way to this work,

Thank you,

HAMADA Mohamed Mouloud.

Table of content :

Table of figures :

List of charts :

List of symbols :

ρ	Density,
u, v	Velocity components in x and y directions,
P	Pressure,
E	Total energy per unit mass,
H	Total enthalpy,
k	Thermal conductivity,
T	Temperature,
τ_{ij}	Stress tensor components,
S_x, S_y, S_E	Source terms,
Y_i	Mass fraction of species i,
D_i	Diffusion coefficient of species i,
R_i	Reaction rate of species i,
μ_i	Turbulent viscosity,
$\sigma_k, \sigma_\varepsilon$	Turbulent Prandtl numbers for k and ε,
G_k	Generation of turbulent kinetic energy due to mean velocity gradients,
$C_{1\varepsilon}, C_{2\varepsilon}$	Model constants,
$\eta_{c(x)}$	Combustion efficiency,
$\dot{m}_{H2(in)}$	The mass flow rate of the injected fuel,
$\dot{m}_{H2}$	Mass flow rate of unburned hydrogen,
Y_{H2}	Hydrogen mass fraction,
$A(x)$	Area.

In the Name of Allāh, the Most Gracious, the Most Merciful

ملخص :

تركز هذه الدراسة على المحاكاة العددية والتحليل العددي لحجرات الاحتراق فوق الصوتية، مع اختلاف أعداد الماك (Mach) وتصميمات التجويفات باستخدام Ansys Fluent 19.2. يعتمد النموذج الرياضي المستخدم على حل معادلات نافيير-ستوكس(NS) ، مع نمذجة الاضطراب باستخدام نهج رينولدز المتوسط نافيير-ستوكس (RANS) ونموذج الاضطراب القياسي K-ε. بالإضافة إلى ذلك، يُستخدم نموذج تفاعل الأنواع ذات المعدل المحدود/التبديد الدوامي finite-rate/eddy dissipation species reaction.

تبحث الدراسة في محركات SCRAMJET النافثة للهواء، والتي تشتهر بمعدل الدفع إلى الوزن العالي. ينصب التركيز على تصميم حاقن وقود الدعامة، حيث إنه ضروري لتحقيق احتراق فوق صوتي فعال. يتم التحقق من صحة النموذج من خلال مقارنة نتائج المحاكاة بالبيانات التجريبية. يتم فحص تصميمات متعددة لحاقن الوقود المحرك النفاث السريع، بما في ذلك نموذج تجويف مزدوج للاحتراق، وكذلك تصميمات مزدوجة الدعامة مع درجات متجهة للخلف، وغرفة احتراق محرك نفاث سريع DLR. يوفر التحليل رؤى قيمة حول كيف يمكن لتصميمات الدعامات المختلفة وتكوينات التجويف أن تعزز الكفاءة عند أرقام الماك (Mach) المختلفة، مما يوفر إرشادات لتحسين أداء محرك SCRAMJET في الدفع أثناء الطيران بسرعة تفوق سرعة الصوت.

الكلمات المفتاحية: محرك ذو احتراق أسرع من الصوت، SCRAMJET، RANS، الدفع.

Abstract :

This study focuses on the numerical simulation and analysis of supersonic combustion chambers, with varying Mach numbers and cavity configurations, using Ansys Fluent. The mathematical model used is based on resolving the Navier-Stokes (NS) equations, with turbulence modeled using the Reynolds-averaged Navier-Stokes (RANS) approach and the standard K-ε turbulence model. Additionally, a finite-rate/eddy dissipation species reaction model is used.

The study investigates air-breathing SCRAMJET engines, which are well known for their high thrust-to-weight ratio. Emphasis is placed on the design of the strut fuel injector, as it is crucial for efficient supersonic combustion. Model validation is achieved by comparing simulation results with experimental data. Various scramjet combustor configurations are examined, including a typical double cavity combustor, double-strut designs with backward-facing steps, and a DLR scramjet combustion chamber. The analysis provides valuable insights into how different strut designs and cavity configurations can enhance efficiency at different Mach numbers, offering guidance for optimizing SCRAMJET engine performance in high-speed flight propulsion.

Key Words: Supersonic combustion, SCRAMJET, Mach number, DLR scramjet, Reynolds-averaged Navier-Stokes (RANS), Navier-Stokes (NS), K-ε turbulence model, Finite-rate/eddy dissipation species reaction model, Propulsion, Combustion efficiency, Double-strut with backward facing steps, Air-breathing flight vehicle.

Resume :

Cette étude se concentre sur la simulation numérique et l'analyse des chambres de combustion supersoniques, avec des nombres de Mach et des configurations de cavités variés, en utilisant Ansys Fluent. Le modèle mathématique utilisé est basé sur la résolution des équations de Navier-Stokes (NS), avec la turbulence modélisée à l'aide de l'approche Reynolds-averaged Navier-Stokes (RANS) et du modèle de turbulence standard K-ε. De plus, un modèle de réaction des espèces à taux fini/dissipation des tourbillons est utilisé.

L'étude examine les moteurs SCRAMJET à respiration d'air, bien connus pour leur rapport poussée/poids élevé. L'accent est mis sur la conception de l'injecteur de carburant à longeron, car il est crucial pour une combustion supersonique efficace. La validation du modèle est réalisée en comparant les résultats de simulation avec les données expérimentales. Diverses configurations de combusteurs SCRAMJET sont examinées, y compris un combusteur à double cavité typique, des conceptions à double longeron avec des marches arrière et une chambre de combustion SCRAMJET du DLR. L'analyse fournit des informations précieuses sur la manière dont différentes conceptions de longerons et configurations de cavités peuvent améliorer l'efficacité à différents nombres de Mach, offrant des orientations pour optimiser les performances des moteurs SCRAMJET dans la propulsion de vol à haute vitesse.

Mots Cles: Supersonique combustion, SCRAMJET, RANS, Propulsion.

1. <u>Introduction :</u>

Supersonic combustion presents unique challenges and is critically important in the aerospace sector. As the aerospace industry continues to advance, there is a growing emphasis on controlling and enhancing supersonic and hypersonic combustion processes. Various technological tools are being utilized worldwide to optimize these systems for improved efficiency and reduced emissions.

Combustion, a primary method of energy conversion, generates thermal energy and is widely used in various sectors, including aviation, space exploration, and power generation. The aviation industry, in particular, is interested in achieving efficient and environmentally friendly combustion processes. Combustion involves exothermic and irreversible reactions between fuel and oxidizer, often resulting in pollutant emissions. To mitigate these emissions, numerical simulations, such as those using ANSYS Fluent, are crucial. Although computationally demanding, these simulations allow researchers to study combustion phenomena under different conditions, optimizing fuel consumption and reducing emissions.

Supersonic combustion, which occurs at speeds greater than the speed of sound, is vital for advanced propulsion systems, such as scramjets. This study utilizes ANSYS Fluent to simulate supersonic combustion, focusing on comparing different combustor geometries, including double cavity combustors and double-strut configurations with backward-facing steps. The aim is to evaluate the impact of these designs on combustion efficiency and understand the behavior of various thermodynamic factors. The simulations employ the RANS k-epsilon realizable turbulence model and investigate parameters such as density, mass fraction, pressure, Mach number, and temperature.

The thesis is structured as follows:

__Chapter 1:__ Introduces supersonic combustion, explores relevant concepts, reviews prior research, and identifies the geometries under study.

__Chapter 2:__ Presents the mathematical modeling of viscous, turbulent, reactive flow, detailing governing equations and turbulence models.

__Chapter 3:__ Describes the numerical methods employed, including solver configurations, boundary conditions, and meshing techniques within ANSYS Fluent.

__Chapter 4:__ Analyzes simulation results, comparing performance across different combustor configurations, and evaluating the influence of varied parameters.

__Conclusion:__ Summarizes key findings, discusses study limitations, and proposes directions for future research.

1. Chapter 1 :

Overview

1.1. Introduction :

1.1.1. State of Art :

Supersonic combustion technology, especially scramjet (Supersonic Combustion Ramjet) engines, is crucial for achieving efficient high-speed propulsion. These engines excel in hypersonic flight due to their high thrust-to-weight ratios, making them a focal point of research. The effective design of combustors, which mix fuel with air and sustain combustion at supersonic speeds, is essential.

- **Supersonic Combustion and Fuel Injectors:** Supersonic combustion involves burning fuel in an airstream moving faster than sound. Hydrogen is commonly used for its high energy content and quick ignition properties. Strut-based fuel injectors are vital for enhancing mixing performance, with designs such as single-strut and double-strut configurations, including backward-facing steps, proving effective.

- **Computational Fluid Dynamics (CFD):** CFD is crucial for analyzing and designing scramjet combustors. It allows researchers to model complex flow fields and predict combustion behavior using software like ANSYS Fluent. This involves solving the Reynolds-Averaged Navier-Stokes (RANS) equations along with turbulence and combustion models.

- **Cavity Flame Holders:** Cavity flame holders create recirculation zones that improve fuel-air mixing and stabilize the flame. Various cavity configurations have been studied to enhance combustion efficiency and stability.

- **Experimental Validation and Future Directions:** Experimental data from institutions like the National University of Defense Technology in China validate CFD models. Research continues to optimize combustor designs, improve fuel injection strategies, and explore new materials. Advances in diagnostics and high-performance computing are pushing the boundaries of supersonic combustion research.

This thesis contributes by comparing different combustor geometries, focusing on their impact on combustion efficiency, offering insights for next-generation scramjet engine designs.

1.1.2. Scramjet, Ramjet :

The name scramjet is an acronym for **Supersonic Combustion Ramjet**. A scramjet engine, hereafter referred to as a scramjet, is a type of jet engine designed to operate in the high-velocity regime usually associated with rockets. The scramjet belongs to a family of propulsion devices known as hypersonic air breathing vehicles. These devices use the surrounding atmosphere to propel various vehicles at velocities far exceeding the local speed of sound [1].

A ramjet engine which stands for **Ram Air Compression Jet Engine** operates by compressing incoming air using the vehicle's forward motion before mixing it with fuel and igniting the mixture. This type of engine is efficient at supersonic speeds but becomes inefficient at hypersonic speeds due to increased drag and thermal loads. The scramjet overcomes these limitations by allowing supersonic combustion, where the airflow remains supersonic throughout the engine, enhancing efficiency and performance at hypersonic velocities.

Figure 1-1-scramjet engine [24]
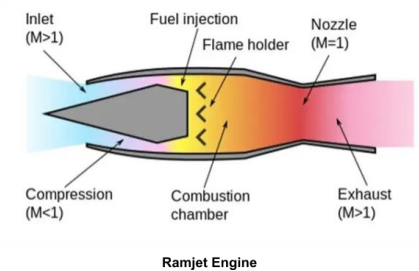
Figure 1-2-Ramjet engine [24]

Current aerospace technology development includes several applications for such hypersonic vehicles. One prominent example is reusable launch vehicles for space applications. A reusable launch vehicle that uses the surrounding atmosphere for propulsion could potentially reduce the cost of launching payloads into orbit by an order of magnitude. This cost reduction is crucial for the commercial utilization of space and future space exploration beyond the moon.

Hypersonic airbreathing vehicles also hold the potential to revolutionize commercial aviation. For instance, they could reduce the travel time for long-haul flights, such as from Stockholm to Sydney, to just a few hours. This paradigm shift in aviation could significantly impact global connectivity and transportation efficiency.

1.1.3. **History:**

❖ *Origins and Early Development of Ramjet :*

The concept of the ramjet, short for **Ram Air Compression Jet Engine**, dates back to the early 20th century. The idea was first proposed by French engineer René Lorin in 1913. Lorin's design envisioned an engine that would utilize the forward motion of an aircraft to compress incoming air, mix it with fuel, and ignite the mixture, thus generating thrust [2].

Figure 1-3-René Lorin [2]

❖ *World War II and Post-War Advances :*

Significant advancements were made during and after World War II. In the 1940s, German engineer Hans von Ohain [3] developed the first working ramjet engine, which was tested on a V-1 flying bomb [4]. Post-war, the United States and the Soviet Union conducted extensive research and development on ramjets. The 1950s saw the deployment of ramjet-powered missiles like the Bomarc missile [5] in the U.S. and the Soviet SA-4 Ganef [6].
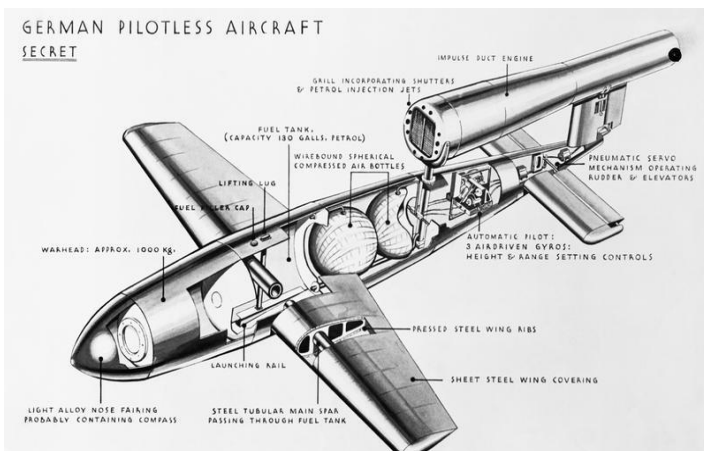
Figure 1-7-v1 flying bomb [4]
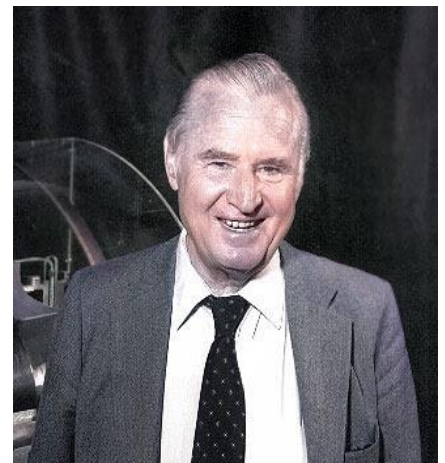
Figure 1-7-Hans von Ohain [3]
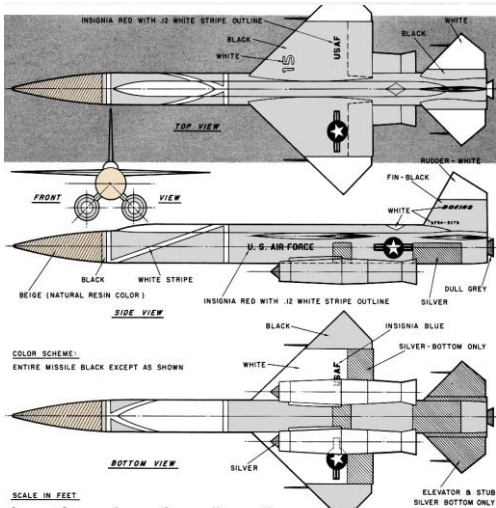
Figure 1-7-The BOMARC [5]

Figure 1-7-SA-4 Ganef [6]

9

❖ *Cold War and High-Speed Applications :*

The Cold War era brought further innovation, particularly in the development of high-speed aircraft and missiles. The Lockheed D-21 reconnaissance drone, which first flew in 1964, used a ramjet engine to achieve speeds over Mach 3. Despite the challenges of thermal management and materials capable of withstanding high temperatures, ramjet engines became a key technology for supersonic flight.

Figure 1-8-The Lockheed D-21 [21]

❖ *Concept and Early Research of Scramjet :*

The scramjet, short for **Supersonic Combustion Ramjet**, emerged from the limitations of the ramjet at hypersonic speeds. A scramjet allows for supersonic airflow throughout the entire engine, including the combustion chamber, thus improving efficiency at extremely high velocities. The concept was first seriously considered in the 1950s and 1960s as researchers sought ways to achieve sustained hypersonic flight.

❖ *Development and Testing :*

The first significant tests of scramjet technology occurred in the late 20th century. NASA's Hyper-X program (X-43) [7] was a major milestone. On November 16, 2004, the X-43A scramjet-powered aircraft set a record by flying at nearly Mach 10. This demonstrated the viability of scramjet propulsion for hypersonic flight [8].
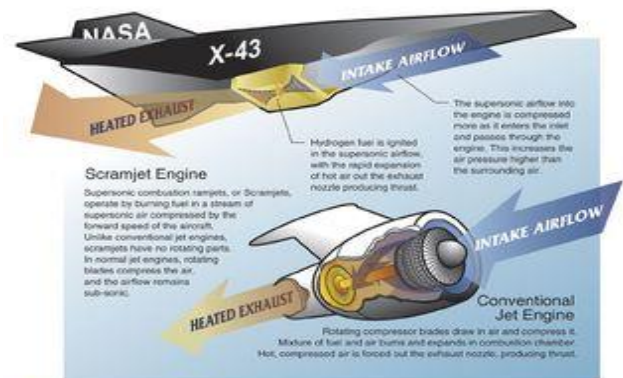
Figure 1-9-X-43 [8]

❖ *Modern Advances and Applications :*

In the 21st century, scramjet technology has continued to advance, driven by both military and civilian interests. DARPA's Falcon Project and the
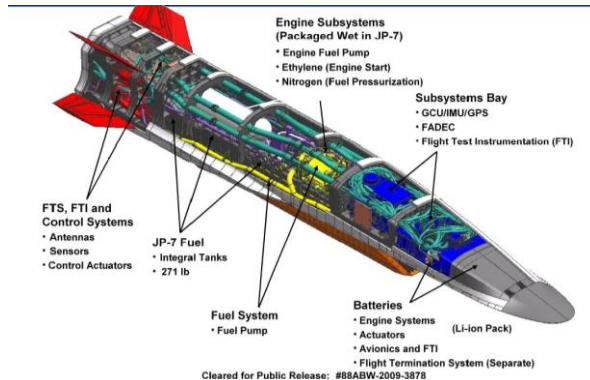
Figure 1-11-X-51A Waverider [23]

Figure 1-11-DARPA [22]

U.S. Air Force's X-51A Waverider, which achieved a flight speed of Mach 5.1 in 2013, are notable examples. These projects have shown the potential of scramjets for applications such as rapid global strike capabilities and more efficient access to space.

❖ *Significance and Future Prospects :*

Ramjet and scramjet engines represent significant technological advancements in aerospace propulsion. Ramjets enabled sustained supersonic flight and advanced missile technology, while scramjets hold the promise of practical hypersonic travel. Future developments in scramjet technology could revolutionize space launch systems, making space more accessible, and transform long-distance air travel by drastically reducing flight times.

❖ *Technical Technical challenges for scramjet engines :*

Scramjet and ramjet technologies offer both advantages and drawbacks. One of the key advantages of scramjets is their simple design, with few or no moving parts and a streamlined body. This simplicity leads to lower manufacturing costs compared to traditional rocket engines. Unlike rockets, scramjets do not require an onboard oxidizer for fuel combustion, reducing the need for carrying heavy oxidizing agents. For instance, NASA's Space Shuttle required large quantities of liquid oxygen, comprising about 75% of its total launch weight, solely for fuel combustion.

In contrast, ramjets operate at lower speeds than scramjets and do not require initial acceleration to high velocities for efficient operation. They can operate as a ramjet at lower speeds, offering flexibility in their use. However, ramjets face challenges in achieving efficient fuel combustion and optimal performance.

Both scramjets and ramjets require careful design to overcome technical challenges. They require structures for the suspension of engines, control systems, and additional equipment for acceleration, adding weight to the vehicle. To simplify design, many experts suggest using external, preferably reusable, rockets as a first stage for both types of engines. Additionally, the low thrust-to-weight ratio of scramjets and ramjets means they require more time to accelerate, following a flatter trajectory compared to vertically launched rockets. This prolonged exposure to hypersonic speeds increases the risk of atmospheric friction and heat buildup, requiring advanced heat insulation measures.

Another major challenge for both technologies is optimizing fuel combustion in the combustors. Current engines often combust only a fraction of the supplied fuel, generating minimal heat. This highlights the need for further research to improve fuel combustion efficiency. This work aims to enhance understanding of the complex flow dynamics in combustors.

❖ *About Ansys Fluent software :*

ANSYS Fluent is a powerful computational fluid dynamics (CFD) software package used for simulating fluid flow and heat transfer in a wide range of applications. It is widely used in industries such as aerospace, automotive, chemical processing, and turbomachinery to predict and optimize the performance of designs. Fluent offers a comprehensive set of features for modeling complex flow phenomena, including turbulence, combustion, multiphase flow, and heat transfer. Its user-friendly interface and robust solver make it a popular choice for engineers and researchers seeking to gain insights into fluid flow behavior and optimize their designs.

Figure 1-12-Ansys Fluent Logo [25]

In our simulation, we used it to model and analyze the fluid flow and combustion processes in the supersonic combustion chamber.

2. **Chapter II:**

Theoretical aspect

2.1. <u>Theory:</u>

2.1.1. <u>Introduction:</u>

This chapter provides a brief overview of the principles underlying Computational Fluid Dynamics and combustion modeling. It explains the governing equations and the numerical techniques used to solve them.

2.1.2. <u>Mathematical modeling of reacting flows :</u>

Combustion of gaseous fuels happens when fuel and an oxidant, such as air, mix at a molecular level and are heated to their ignition temperature, releasing chemically bound energy and forming combustion products. This energy release raises the temperature and causes the gases to expand, influencing the flow. Combustion can be categorized into pre-mixed combustion, where fuel and oxidizer are mixed before ignition, and diffusion combustion, where they mix during combustion.

Modeling combustion, especially in aerospace applications, involves complex processes including fluid mechanics, gas-phase chemical reactions, and chemical kinetics. Fluid mechanics principles have been established for over a century, with the Navier-Stokes equations, derived from Newton's laws of motion, serving as the foundation. These non-linear equations can rarely be solved analytically, necessitating numerical methods that discretize space and time into numerous computational cells and time steps for iterative solutions.

Most practical flows are turbulent, characterized by unpredictable velocity fluctuations governed by the Reynolds number. High Reynolds numbers create a vast scale range from energy input to dissipation at the Kolmogorov scale. To accurately resolve these flows, computational cells must be small enough to capture the smallest eddies, requiring significant computing power. Due to current computing limitations, direct simulation is feasible only for low Reynolds numbers in simple geometries. For high Reynolds numbers and complex geometries, simplifications like Reynolds-averaged Navier-Stokes (RANS) models are used, relying on statistical treatment of flow fluctuations.

Turbulence models simplify complex equations, while Large Eddy Simulation (LES) offers a more accurate alternative by simulating large eddies and modeling small-scale turbulence.

Despite its high computational cost, LES is becoming more practical with advanced computer clusters.

To simulate combustion, the Navier-Stokes equations are supplemented with a chemical reaction mechanism and a thermodynamic model. The reaction mechanism outlines how fuel and oxidant react and form products, while the thermodynamic model describes energy dissipation. This combined approach enables the simulation of complex combustion processes in engineering and scientific applications.

2.1.3. <u>Computational fluid dynamics :</u>

Computational Fluid Dynamics (CFD) is a specialized field within fluid mechanics that leverages computational techniques and algorithms to address and analyze fluid flow issues. Utilizing computers, CFD allows scientists and engineers to model the behavior of fluids (whether liquids or gases) across a wide range of conditions. This computational tool is essential for examining fluid mechanical processes, including mass, heat, and momentum transfer. The finite volume method, a prevalent numerical approach in CFD, is employed by the software tools used in this research.

2.1.4. <u>Governing equations and numerical approach :</u>

Understanding the internal flow characteristics of a scramjet combustor is crucial for analyzing its combustion behavior, especially in the context of reacting flow problems. The combustion process within the combustor is significantly influenced by flow variables. Due to the complexity and turbulence of the flow inside a scramjet combustor, the chosen governing equations must account for turbulent and compressible flow dynamics.

In this study, a two-dimensional computational model of the combustor was developed using Ansys Fluent 19.2 to conduct all simulations. The governing equations are formulated as Reynolds Averaged Navier-Stokes (RANS) equations to accurately capture the combustion behavior across a range of operating conditions and geometries. The RANS framework facilitates precise determination of shock wave positions and characteristics.

The flow governing equations and species transport equations are detailed in the references [9]. The computational model employs a density-based solver with a standard k-ε turbulence model. Hydrogen-air mixing reactions are modeled using a finite-rate/eddy dissipation approach, treating density as that of an ideal gas. This method avoids the need for Arrhenius

calculations, thereby reducing computational time and cost. Spatial discretization is performed using an implicit second-order upwind scheme.

For compressible and steady-state flows, the governing equations include continuity, momentum, and energy equations. These foundational equations are critical for capturing the intricate dynamics within the scramjet combustor.

❖ **Continuity Equation: [9]**

$$\frac{\partial \rho}{\partial t} + \frac{\partial (\rho u)}{\partial x} + \frac{\partial (\rho v)}{\partial y} = 0 \qquad (2.1)$$

❖ **Momentum Equations: [10]**

X-momentum:

$$\frac{\partial (\rho u)}{\partial t} + \frac{\partial (\rho u^2)}{\partial x} + \frac{\partial (\rho uv)}{\partial y} = -\frac{\partial P}{\partial x} + \frac{\partial \tau_{xx}}{\partial x} + \frac{\partial \tau_{xy}}{\partial y} + S_x \qquad (2.2)$$

Y-momentum:

$$\frac{\partial (\rho v)}{\partial t} + \frac{\partial (\rho uv)}{\partial x} + \frac{\partial (\rho v^2)}{\partial y} = -\frac{\partial P}{\partial y} + \frac{\partial \tau_{xy}}{\partial x} + \frac{\partial \tau_{yy}}{\partial y} + S_y \qquad (2.3)$$

❖ **Energy Equation: [11]**

$$\frac{\partial (\rho E)}{\partial t} + \frac{\partial (\rho u H)}{\partial x} + \frac{\partial (\rho v H)}{\partial y}$$
$$= \frac{\partial}{\partial x}\left(k \frac{\partial T}{\partial x}\right) + \frac{\partial}{\partial y}(k \frac{\partial T}{\partial y}) + \frac{\partial}{\partial x}(u_i \tau_{ij}) + \frac{\partial}{\partial y}(v_i \tau_{ij}) \qquad (2.4)$$
$$+ S_E$$

❖ **Species Transport Equation: [12]**

$$\frac{\partial (\rho Y_i)}{\partial t} + \frac{\partial (\rho u Y_i)}{\partial x} + \frac{\partial (\rho v Y_i)}{\partial y} = \frac{\partial}{\partial x}\left(\rho D_i \frac{\partial Y_i}{\partial x}\right) + \frac{\partial}{\partial y}\left(\rho D_i \frac{\partial Y_i}{\partial y}\right) + R_i \qquad (2.5)$$

❖ **Turbulence Model Equations (Standard k-ε Model):**

Turbulent Kinetic Energy (k): [13]

$$\frac{\partial (\rho k)}{\partial t} + \frac{\partial (\rho u k)}{\partial x} + \frac{\partial (\rho v k)}{\partial y}$$
$$= \frac{\partial}{\partial x}\left[\left(\mu + \frac{\mu_i}{\sigma_k}\right)\frac{\partial k}{\partial x}\right] + \frac{\partial}{\partial y}\left[\left(\mu + \frac{\mu_i}{\sigma_k}\right)\frac{\partial k}{\partial y}\right] + G_k - \rho\varepsilon \qquad (2.6)$$

Dissipation Rate (ε): [14]

$$\frac{\partial(\rho\varepsilon)}{\partial t} + \frac{\partial(\rho u\varepsilon)}{\partial x} + \frac{\partial(\rho v\varepsilon)}{\partial y}$$

$$= \frac{\partial}{\partial x}\left[\left(\mu + \frac{\mu_i}{\sigma_\varepsilon}\right)\frac{\partial\varepsilon}{\partial x}\right] + \frac{\partial}{\partial y}\left[\left(\mu + \frac{\mu_i}{\sigma_\varepsilon}\right)\frac{\partial\varepsilon}{\partial y}\right] + C_{1\varepsilon}\frac{\varepsilon}{k}G_k \qquad (2.7)$$

$$- C_{2\varepsilon}\rho\frac{\varepsilon^2}{k}$$

2.1.5. Why we use Hydrogen (H_2) in Supersonic Combustion?

Hydrogen (H_2) is often used in supersonic combustion, such as in scramjet engines, for several reasons:

❖ **High Energy Density**: Hydrogen has a high energy density per unit mass, which is crucial for achieving the high speeds required in supersonic combustion.

❖ **Fast Combustion Rate**: Hydrogen burns quickly and efficiently, which is important in the limited residence time available in the combustor of a scramjet engine.

❖ **Wide Flammability Range**: Hydrogen has a broad flammability range, allowing for more flexible operation conditions and better performance in varying flight regimes.

❖ **Lightweight**: Hydrogen is the lightest fuel, which helps in maintaining a favorable thrust-to-weight ratio, a critical factor in high-speed flight.

❖ **High Diffusivity**: Hydrogen has a high diffusion coefficient, which promotes rapid mixing with air, essential for efficient combustion in the very short timescales of supersonic flow.

❖ **Chemical Reaction for Hydrogen Combustion**

The primary chemical reaction for the combustion of hydrogen with oxygen in air is: [15]

$$2H_2 + O_2 \rightarrow 2H_2O$$
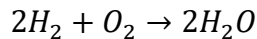
In the context of a scramjet combustor, the presence of nitrogen (N_2) in air must also be considered, though it does not participate directly in the combustion reaction. The overall reaction in the presence of air (which is approximately 21% O_2 and 79% N_2 by volume) can be simplified as:

$$2H_2 + O_2 + 3.76N_2 \rightarrow 2H_2O + 3.76N_2$$
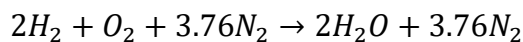
This reaction assumes complete combustion and ideal mixing conditions [16].

2.1.6. CFD errors:

When modeling flow with Computational Fluid Dynamics (CFD), it's crucial to be aware of the limitations. There are several potential sources of errors and uncertainties, which can be categorized as follows:

➤ Discretization Errors:

Spatial Discretization Errors: Occur when the continuous partial differential equations are approximated using discrete grid points. This error depends on the grid resolution; finer grids typically reduce discretization error.

Temporal Discretization Errors: Arise when time-dependent equations are discretized over discrete time steps. Smaller time steps reduce these errors but increase computational cost.

➤ Modeling Errors:

Turbulence Modeling Errors: Inaccuracies arising from the use of turbulence models (e.g., RANS, LES, DNS) to approximate the effects of turbulence. Each model has its own limitations and assumptions.

Boundary Condition Errors: Errors that occur due to incorrect or approximate boundary conditions applied in the simulation. Inaccurate boundary conditions can significantly affect the solution.

Initial Condition Errors: Errors stemming from inaccurate initial conditions in transient simulations. The solution can be highly sensitive to initial conditions, particularly in unsteady flows.

➤ Numerical Errors:

Round-Off Errors: Occur due to the finite precision of computer arithmetic. These errors are generally small but can accumulate over many iterations.

Convergence Errors: Errors that occur if the iterative solution process is stopped before reaching an acceptable level of convergence. Non-converged solutions can be significantly inaccurate.

Grid-Related Errors:

Grid Independence: Errors due to insufficient grid resolution or poor grid quality. Ensuring grid independence by performing grid refinement studies can help mitigate this error.

Non-Orthogonal Grid Errors: Occur when using non-orthogonal grids, which can introduce additional errors in the numerical solution.

➢ **Algorithmic Errors:**

Solution Algorithm Errors: Errors related to the choice and implementation of the numerical algorithms used for solving the equations. Different algorithms can have varying levels of accuracy and stability.

➢ **Physical Model Errors:**

Simplified Physical Models: Errors due to the use of simplified physical models that do not fully capture the complexity of the real physical phenomena (e.g., assuming incompressibility when compressibility effects are significant).

➢ **User Errors:**

User Input Errors: Mistakes in specifying input parameters, boundary conditions, or other simulation settings. These errors are often a result of human oversight or misunderstanding of the physical problem.

➢ **Mitigation Strategies**

To reduce these errors, CFD practitioners should:

- Perform grid and time step refinement studies.

- Validate models against experimental or analytical data.

- Use appropriate turbulence models for the flow regime.

- Ensure proper boundary and initial conditions.

- Verify the numerical solution by checking residuals and convergence criteria.

- Use high-quality grid generation techniques and tools.

By carefully addressing these potential sources of error, the accuracy and reliability of CFD simulations can be significantly improved.

3. **Chapter III :**

NUMERICAL

RESOLUTION

3.1. Physical model and numerical approach:

The mixing efficiency of fuel and air in a scramjet combustor is significantly impacted by the formation of shear layers. A well-established technique to produce these shear mixing layers is the use of cavity flame holders within the combustor. This study employs a computational model featuring parallel cavities designed to enhance the combustor's mixing performance by creating shear layers. The computational geometry was developed using Ansys Fluent 19.2 in DesignModeler, based on an experiment conducted by Yang et al. at the National University of Defense Technology in China. The combustor design includes parallel cavities spaced 40 mm apart, with an 8 mm cavity depth and a 45° aft wall angle. Hydrogen fuel is injected at sonic speed through 2 mm diameter injectors [15]. Detailed dimensions of the geometry are provided in both 2D and isometric views, as shown in Figures.
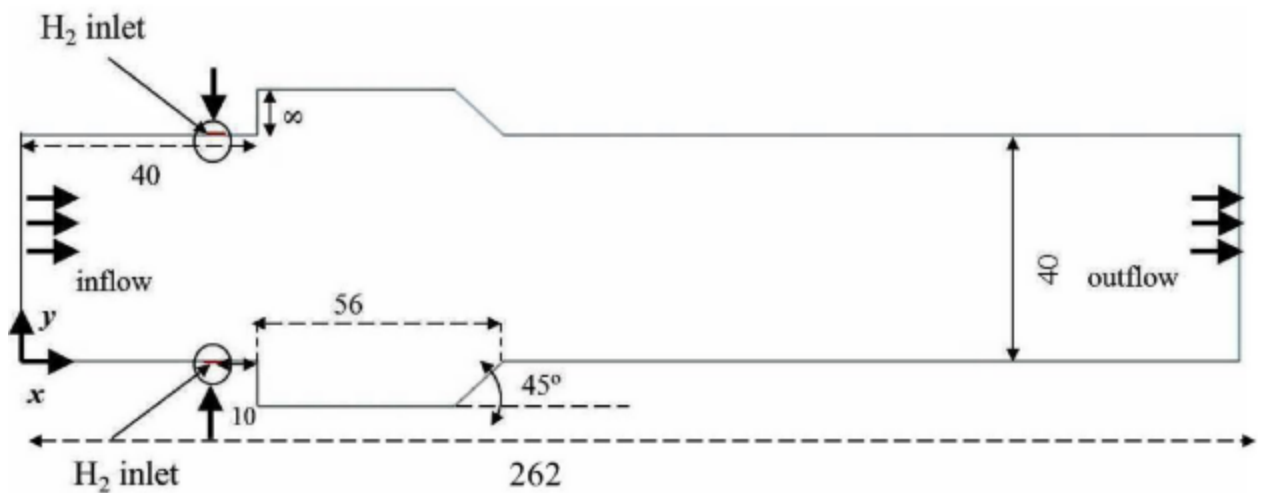

Figure 3-1-Schematic of 2D computational domain of double-cavity Scramjet combustor (all dimension in mm).
[27]

In another geometry, developed using Ansys Fluent 19.2 but adapted for SpaceClaim, a schematic diagram of the DLR scramjet model is provided. Air enters the combustion chamber at a Mach number of 2.0. The combustor has an entrance height of 50 mm and a length of 300 mm. Hydrogen fuel (H2) is injected sonically through the bottom of a wedge-shaped strut. From x = 58 mm onwards, the upper wall of the combustor diverges at an angle of 3°. The wedge-shaped strut is positioned 25 mm from the entrance in the center of the combustor and is 32 mm long with a half-angle of 6° [17]. Other details of the DLR scramjet model are shown in the accompanying figure.
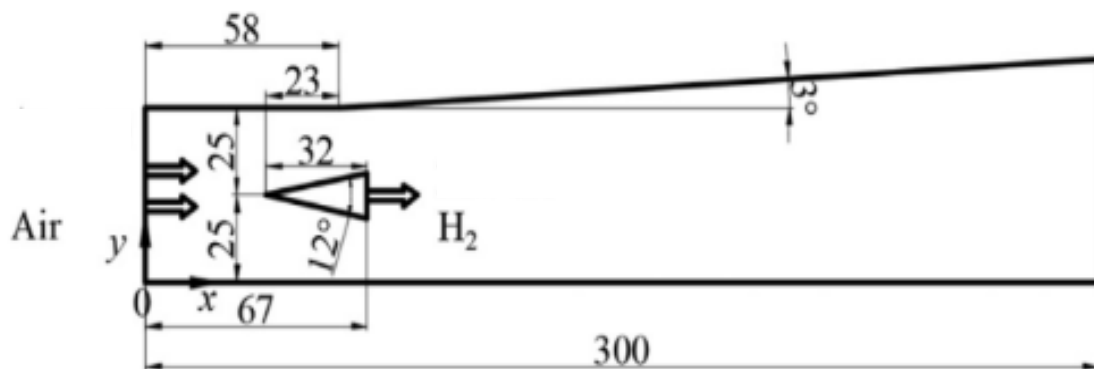

Figure 3-2-The schematic diagram of the DLR scramjet combustor [19].

To further improve combustion and mixing performance, a double-strut configuration with backward-facing steps is also used in this geometry [17]. Each strut has a backward-facing step with a height of 2 mm and a length of 9 mm. These double-struts are symmetrically positioned about the central axis, with fuel injected laterally at the center of the backward-facing steps. A gap of 4 mm exists between the two struts, representing the perpendicular
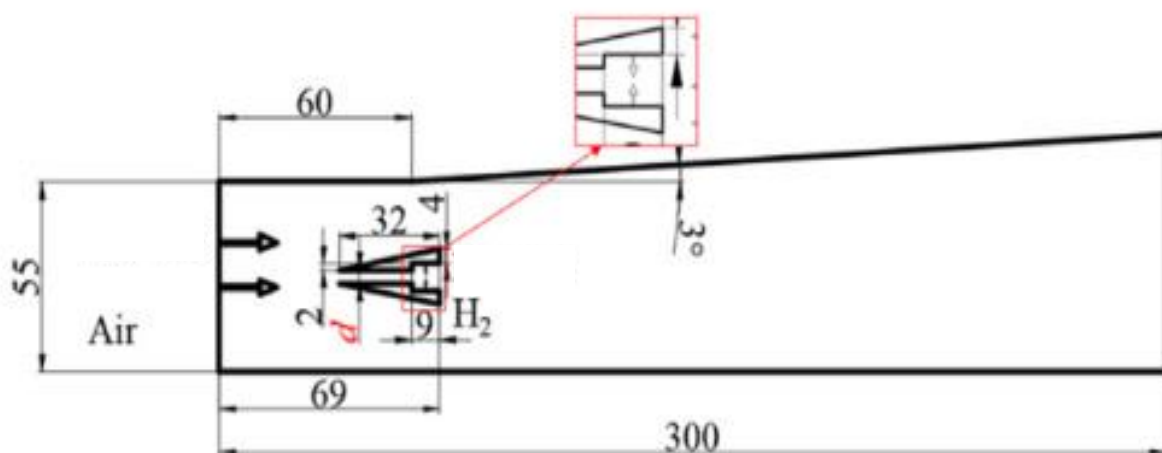

Figure 3-3-The schematic diagram scramjet combustor for the double-strut with back. [17]

22

distance. This lateral injection method is different from the horizontal injection used in other double-strut configurations [17].

The geometry is a sketch created in DesignModeler with the appropriate angle of cavity and fuel-injector. Named selections are defined for all the boundaries. This is the final geometry:
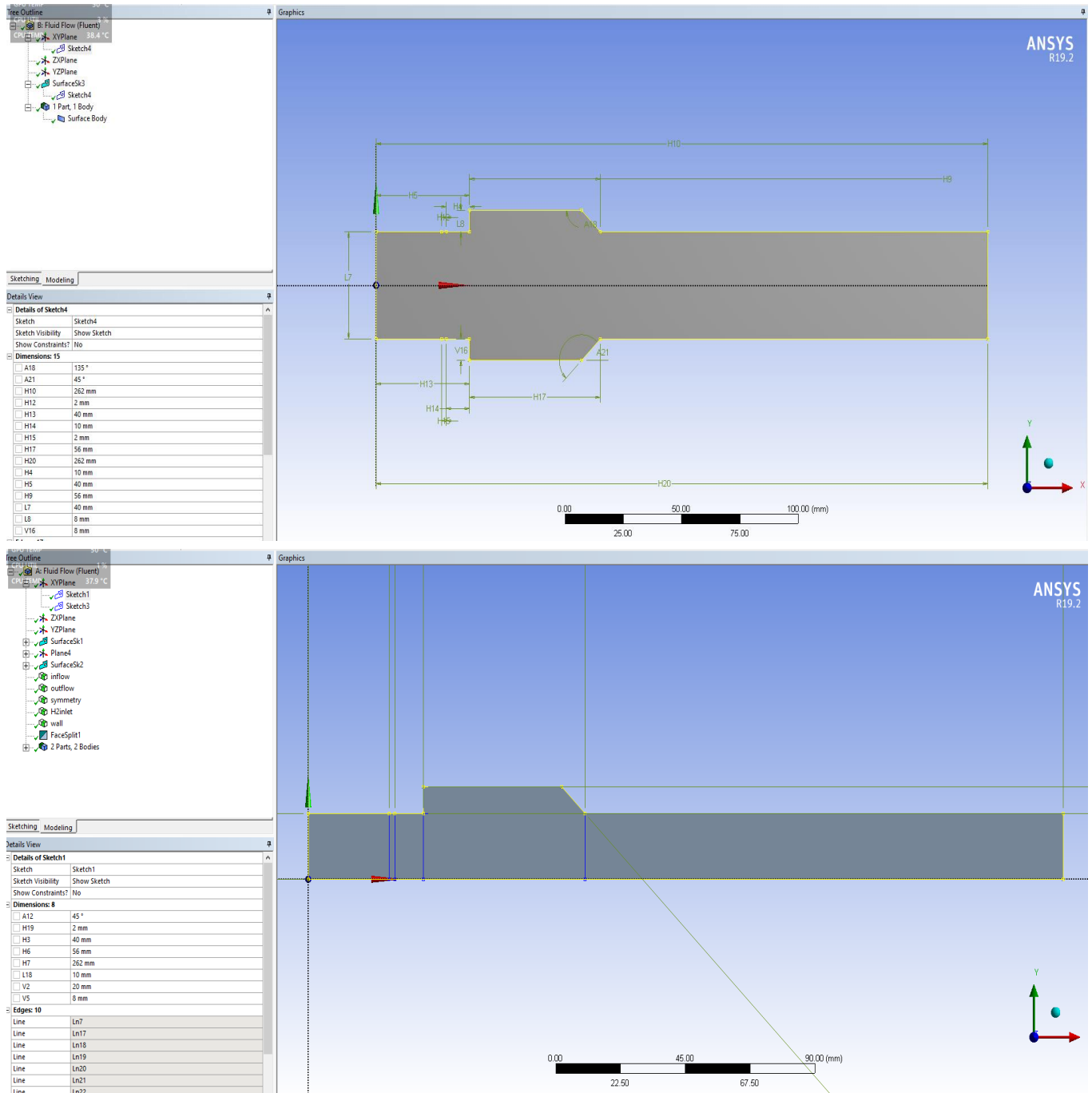

Figure 3-4-2D schematic of double-cavity Scramjet combustor in DesignModeler.

The geometry is a sketch created in Space Claim with the appropriate angles of cavity and fuel-injector, this geometry is converted into a surface using the pull tool. Named selections are defined for all the boundaries. This is the final geometry for a case:
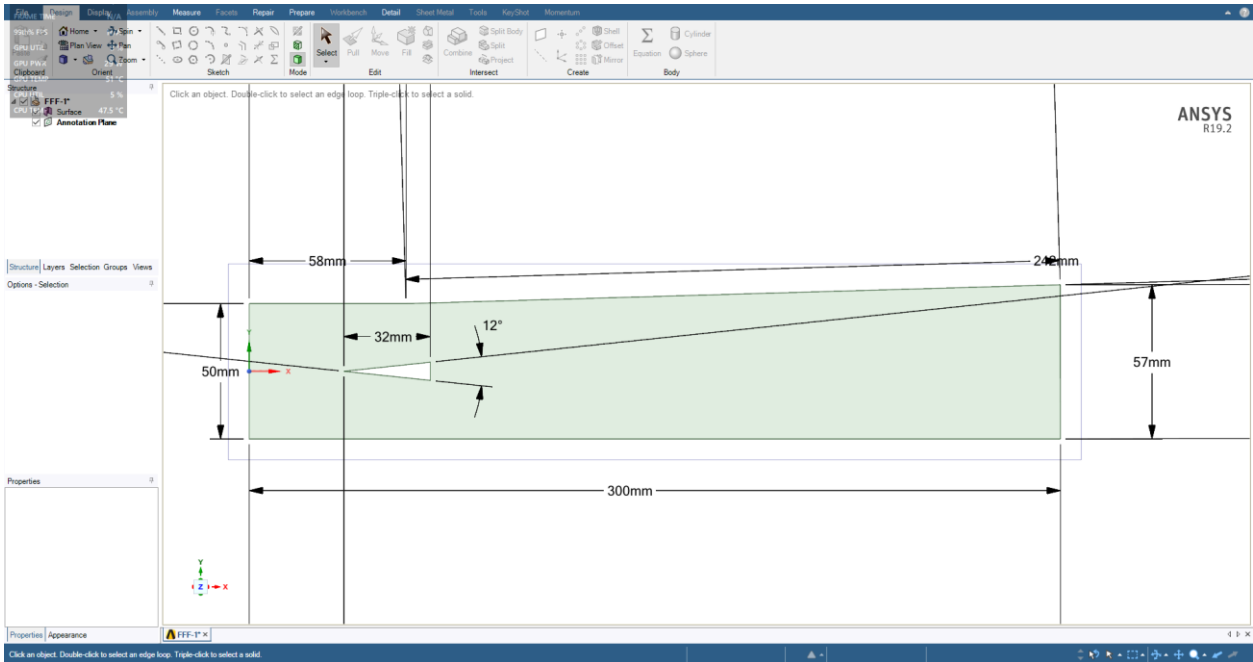

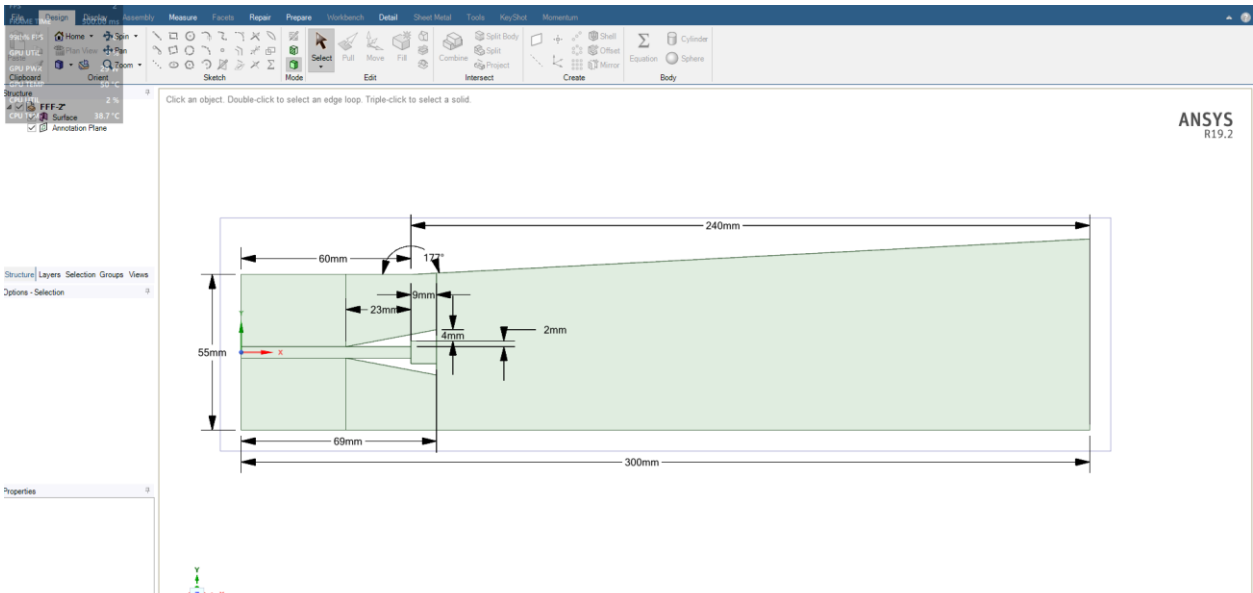*Figure 3-5-2D schematic of the DLR scramjet combustion chamber in SpaceClaim.*

Figure 3-6-2D schematic of scramjet combustor for the double-strut with backward facing steps in SpaceClaim.

Added a cavity to the double-strut with backward facing steps combustor chamber :
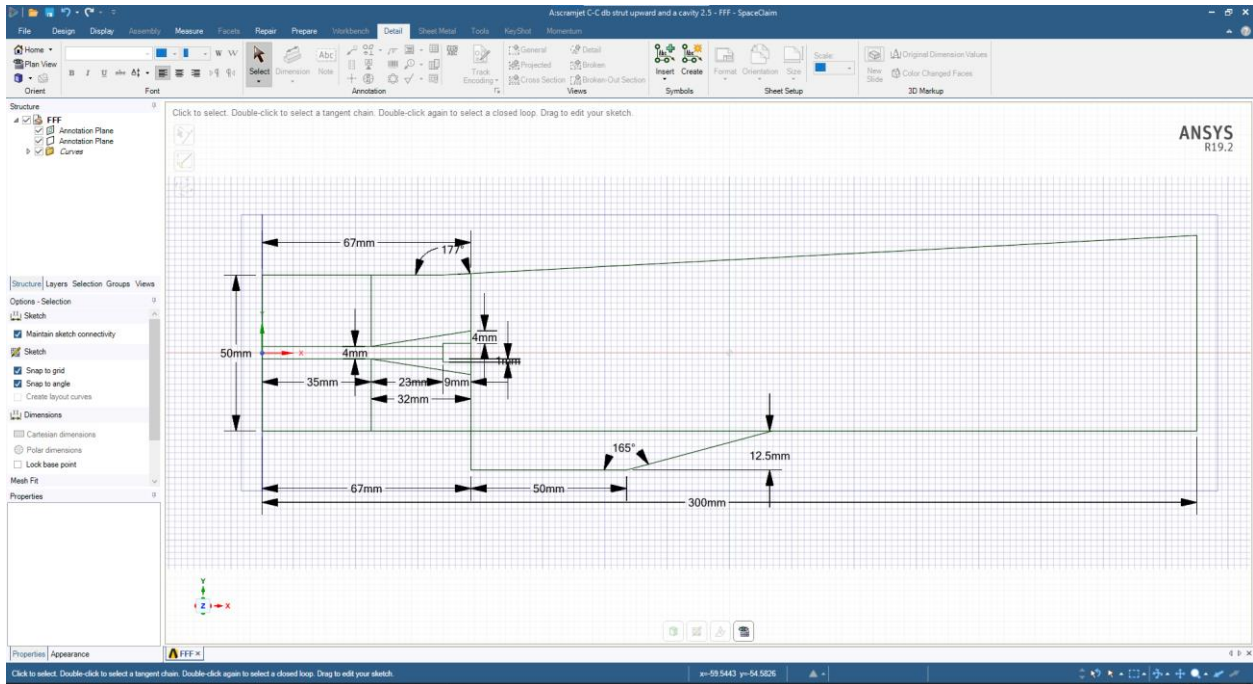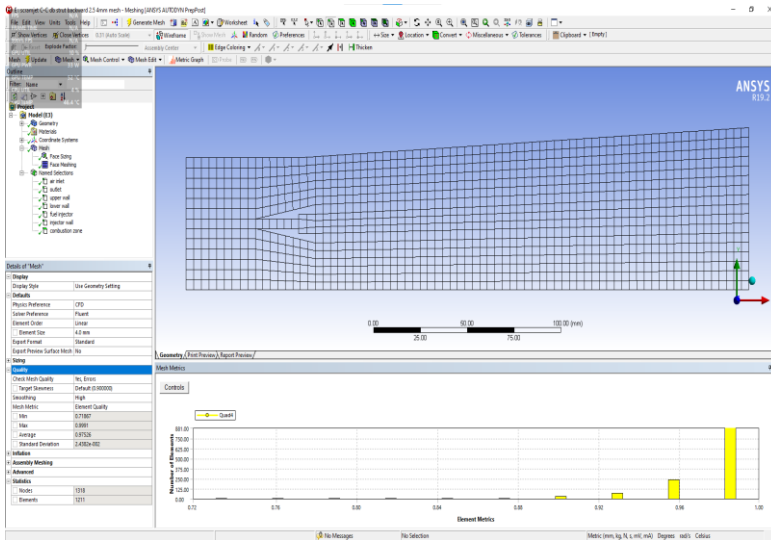

Figure 3-7-2D schematic of scramjet combustor for the double-strut with backward facing steps and a cavity in SpaceClaim.

3.2. <u>**Grid independency analysis :**</u>

The computational simulation is greatly affected by meshing; the grid independence study helps to identify the appropriate grid size for the current simulation to get optimum results. In this paper, three different grids are considered, namely coarse (1211 elements), moderate (18582 elements), and fine grid (1790977 elements).
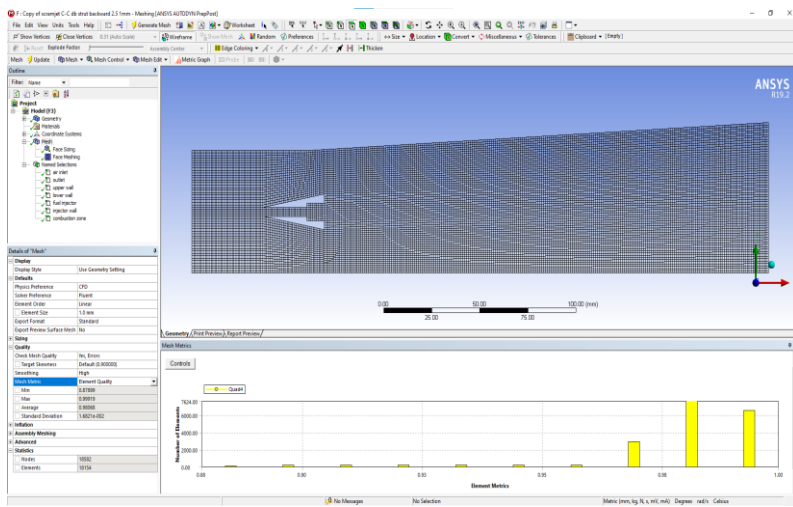
By conducting this study, we can compare our findings with previous research to observe the differences and understand the impact of mesh quality on the results. This comparison will help us identify the influence of various mesh sizes and configurations on the accuracy and efficiency of the simulations. Additionally, we will assess how different boundary conditions and geometric modifications affect the overall performance of the scramjet combustor.

Figure 3-8- (a)Namely coarse mesh, (b)Moderate mesh, (c) fine mesh

Table 3-1-Grid independence table.

	Face Sizing Element Size [mm]	Mesh Elements	Outlet Pressure [Pa]	Outlet Temperature [K]	Outlet Velocity (m/s^{-1})	Outlet Mach Number	Calculation time
DP 3	4	1,211	161,878.3	1,353.468	1,063.545	1.47971	10 min
DP 2	1	18,154	119,313.3	663.27605	1,137.6408	2.3040994	25 min
DP 0	0.1	**1,790,977**	**106,011.42**	**731.7022**	**1,115.0799**	**2.2037163**	**120 min**

The discretization of the computational domain is a crucial and indispensable step for any numerical simulation. It is carried out through an unstructured Cartesian mesh. An optimal grid size is selected through a sensitivity analysis of the mesh cells, as presented in Table 3-1. It is noted that the finer the mesh, the more stable the results. This process ensures that the simulation captures the intricate details of the flow dynamics, which is particularly important in high-speed and turbulent flow regimes such as those found in supersonic combustion. Achieving an optimal balance between mesh resolution and computational efficiency is essential for accurate and reliable simulation outcomes, so we took the 0.1 element size that give us 1,790,977 elements .

3.3. Mesh generation:

In the meshing process and for all the geometries we used an element size of 0.1mm was employed, resulting in a finely resolved computational domain with more accuracy.

o **Double cavity C-C:**

This mesh consisted of 1,060,312 elements and 3,187,133 nodes,
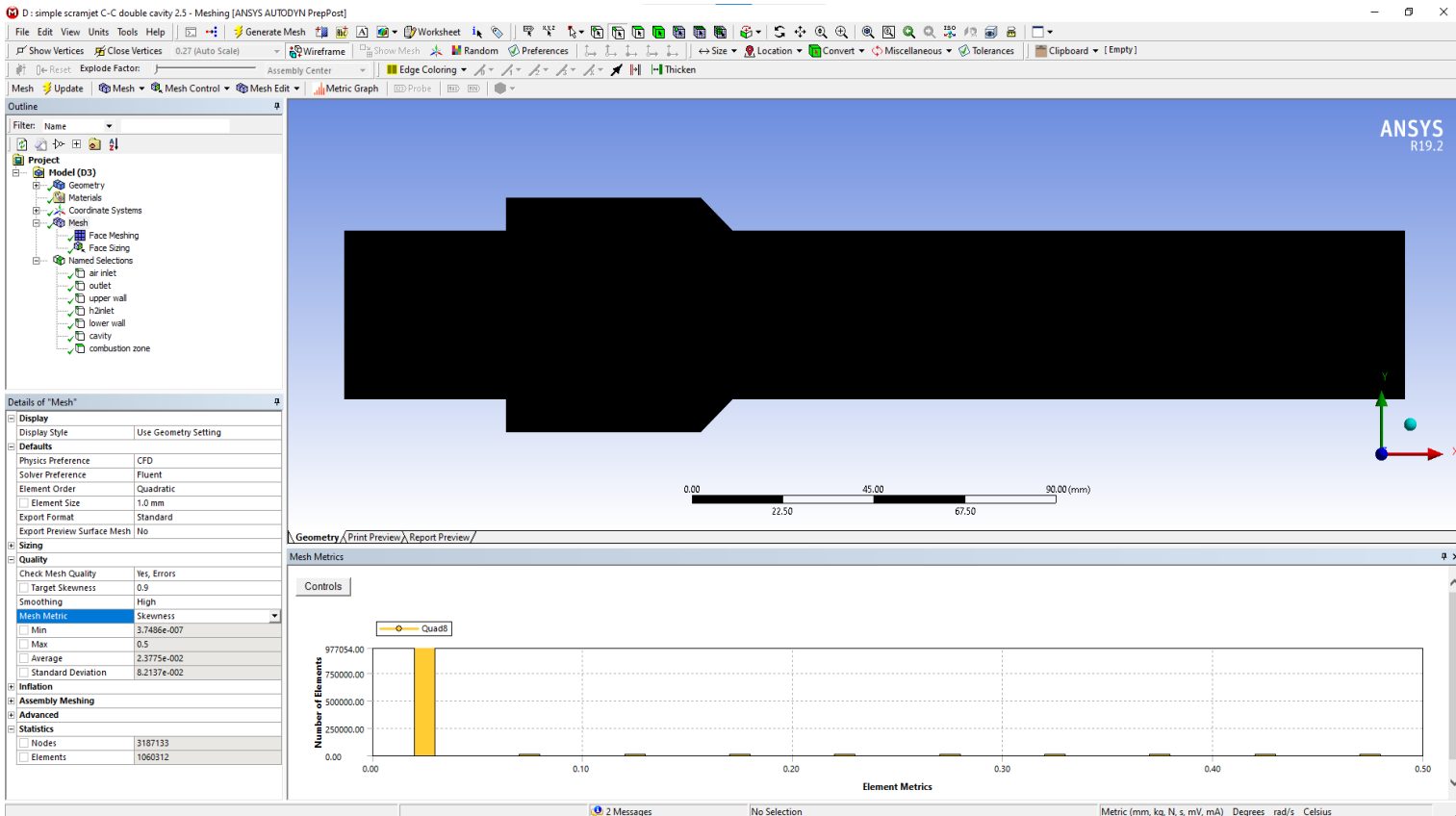
Figure 3-9-Mesh of double-cavity Scramjet combustor.
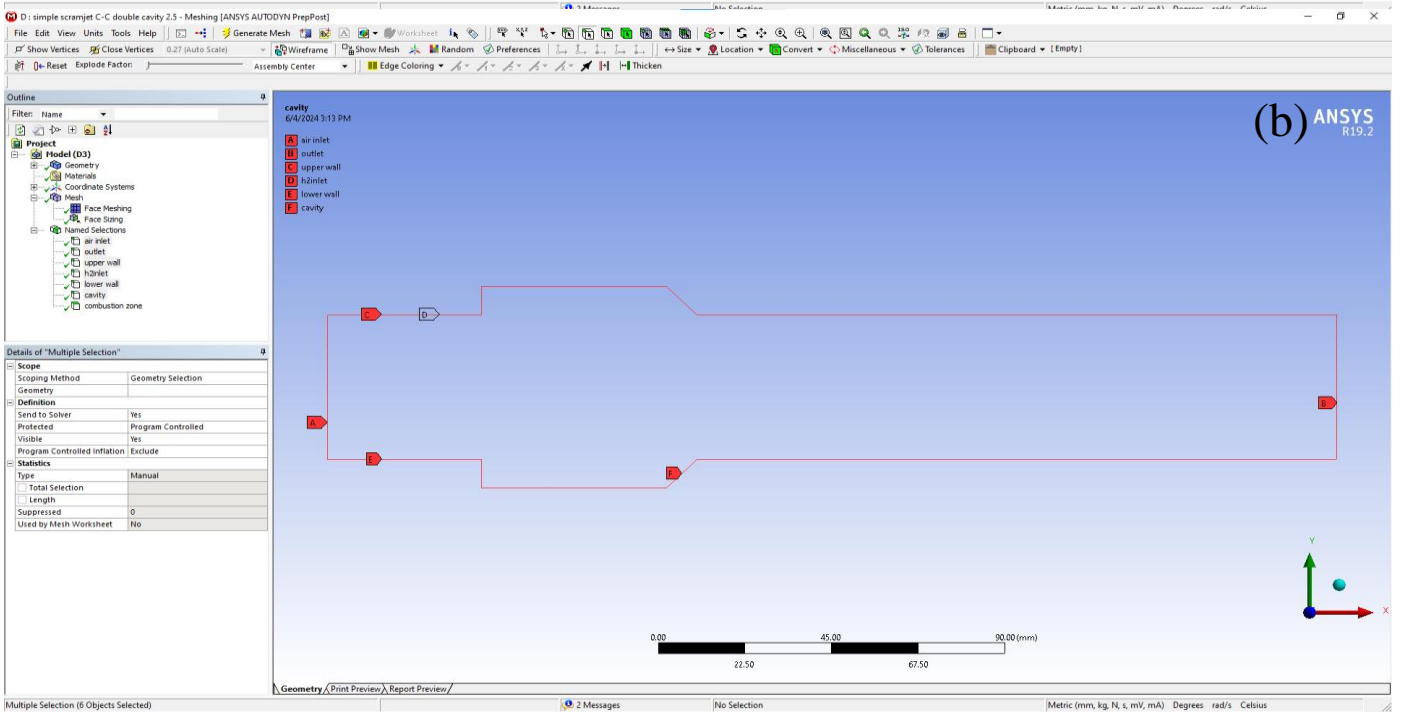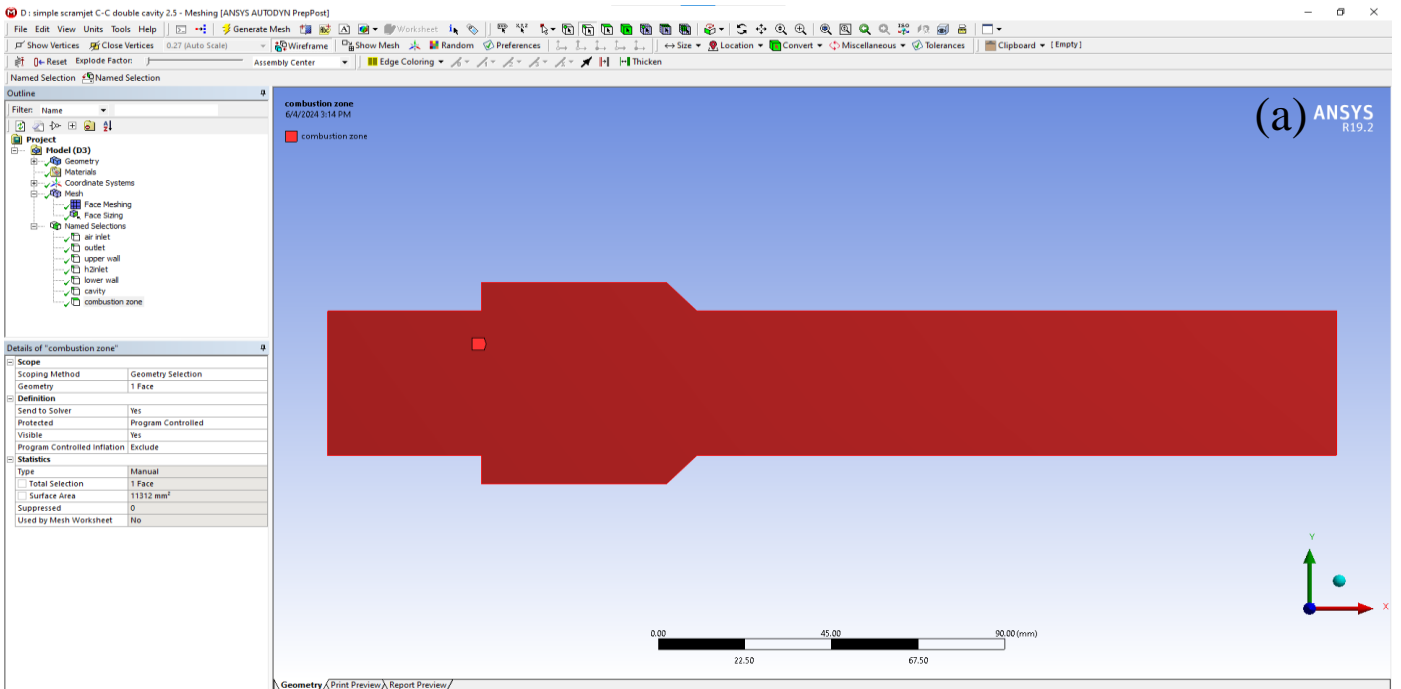
Figure 3-10-inserting the proper names to set boundary condition, (a) combustion zone, (b) inlet, h2 inlet, outlet, walls, cavity.

o **_Single strut C-C:_**

This mesh consisted of 276,309 elements and 279,704 nodes,

Figure 3-11- Mesh of the single strut scramjet combustion chamber, (a) full combustion zone, (b) zoomed view.

o **Double facing backward strut C-C:**

This mesh consisted of 1,611,245 elements and 1,615,222 nodes
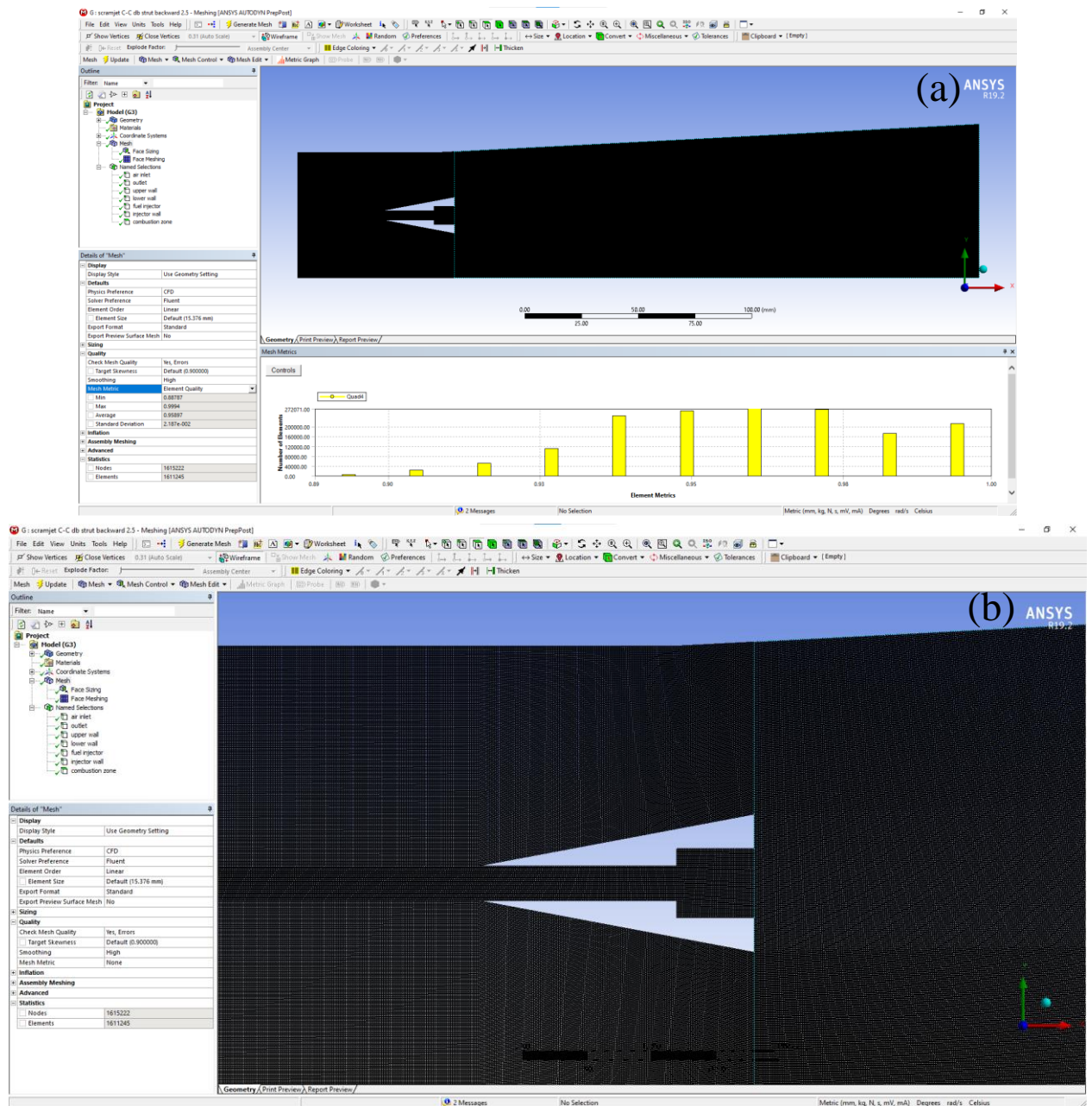
Figure 3-12-Mesh of scramjet combustor for the double-strut with back-ward facing steps(a) full combustion zone, (b) zoomed view.

o **Double facing backward strut C-C with a cavity**

This mesh consisted of 1,060,312 elements and 3,187,133 nodes,

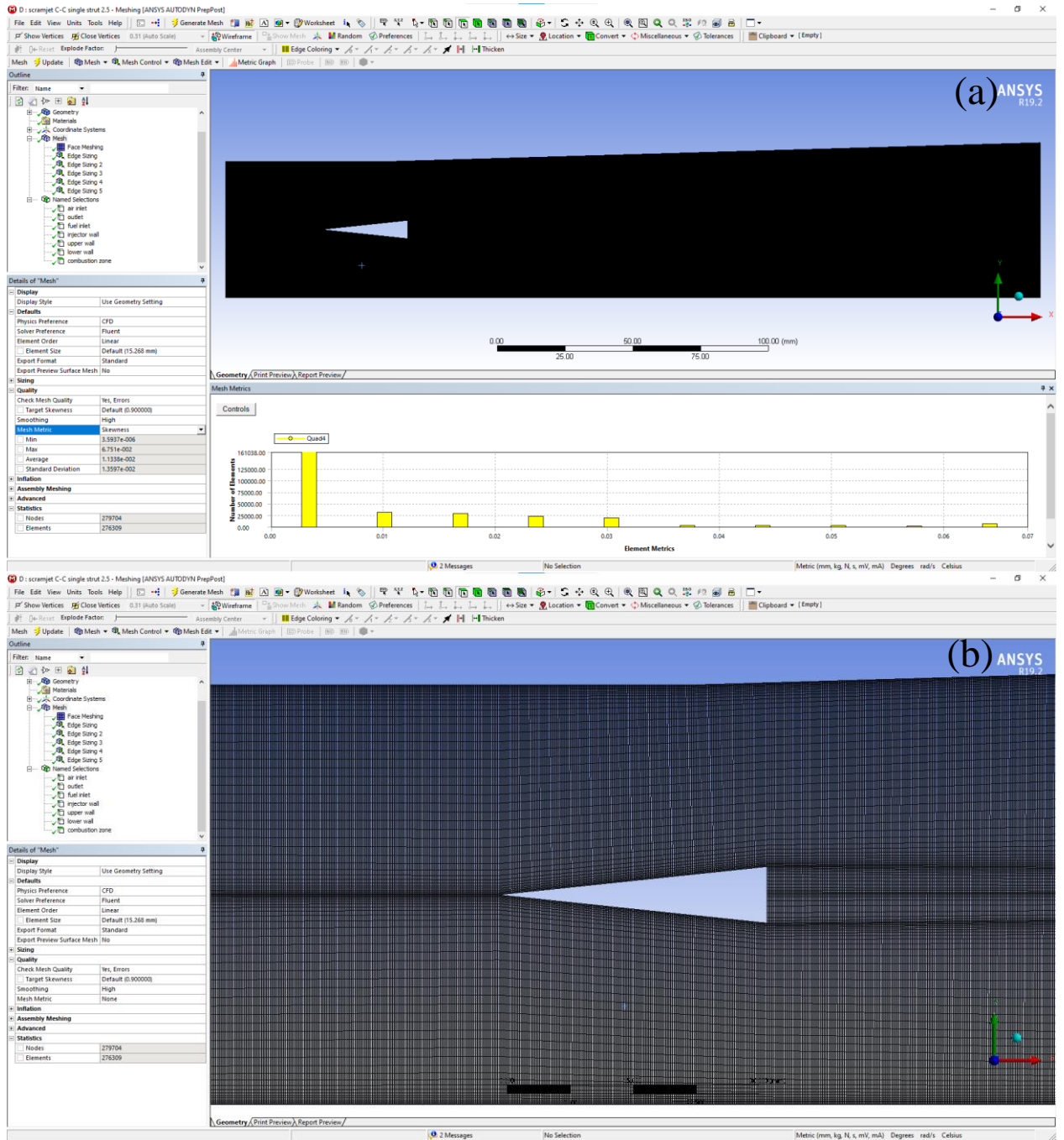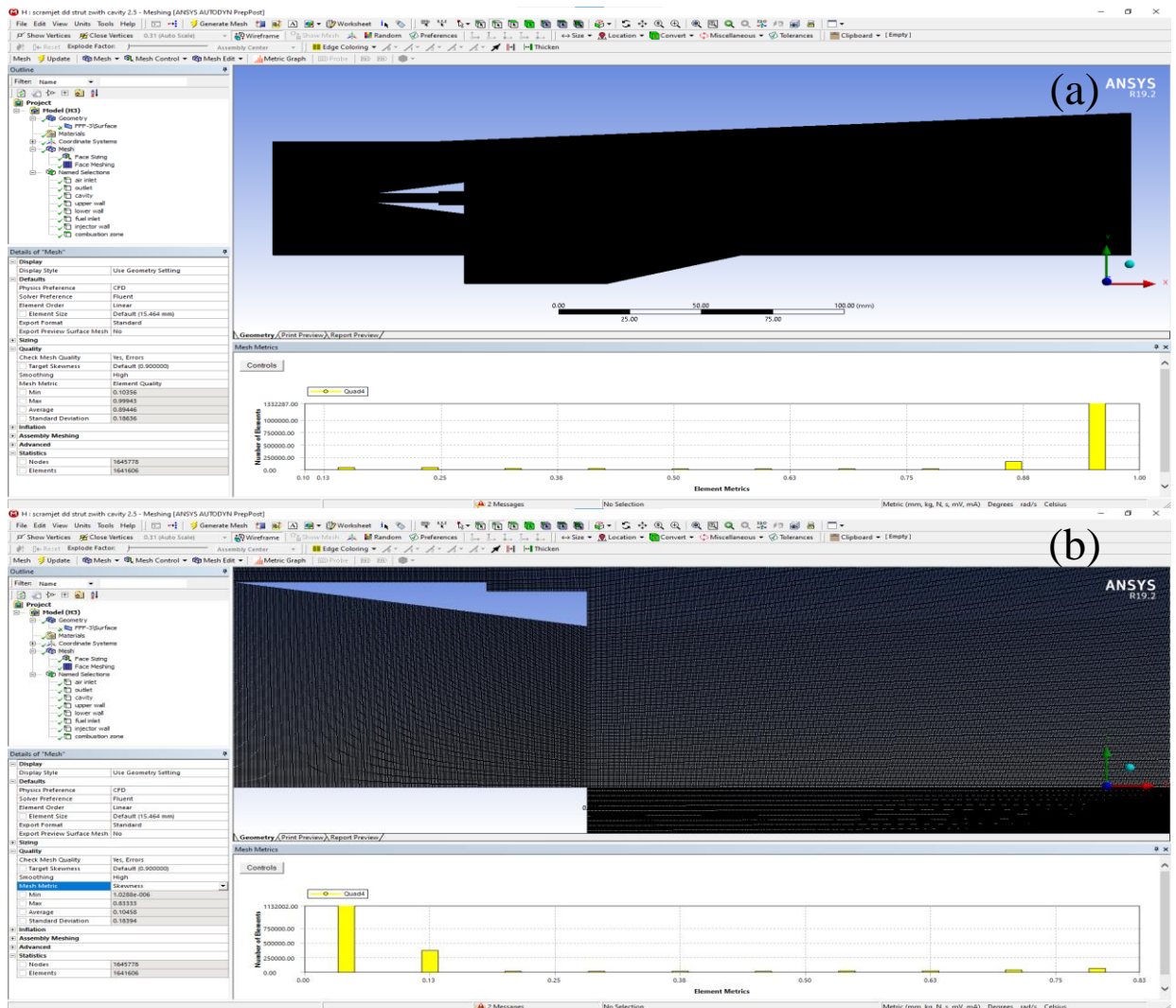*Figure 3-13-Mesh of scramjet combustor for the double-strut with back-ward facing steps with a cavity, (a) full combustion zone, (b) zoomed view*

With this fine mesh it provides a detailed representation of the geometry and flow field. The element quality, a measure of how well-shaped the elements are, was found to be an average of 0.98, indicating that the mesh is of high quality with minimal distortion. Additionally, the skewness of the elements, which describes the deviation of the element shape from an ideal shape, was determined to be an average of 0.03, resulting in a well-balanced mesh with minimal distortion. This high-quality mesh ensures accurate and reliable results for the subsequent simulations.

3.4. Simulation sequences in Fluent and post proccesing:

For all the geometries we use the same setup followed in previous differents researchs.

Assumptions are given as follows:

- Steady-state compressible flow is considered in this paper,
- The 2-dimensional analysis is considered to save computational time,
- The turbulence in the flow field is address by using the standard 2-equation K-ε model,
- Ideal gas laws are assumed.

Chaning the options to "Double Precision" solver, each floating point number is represented using 64 bits in contrast to the single-precision solver, which uses 32 bits. The extra bits increase not only the precision, but also the range of magnitudes that can be represented. The downside of using double precision is that it requires more memory, in this case it used all 8gb of memory (the station has 16gb).

A density-based solver in this simulation ensures that the complex phenomena associated with supersonic combustion, such as shock waves, high-speed flow dynamics, and strong variable coupling, are accurately modeled and resolved.

We also added the gravitational acceleration in the Y axis.
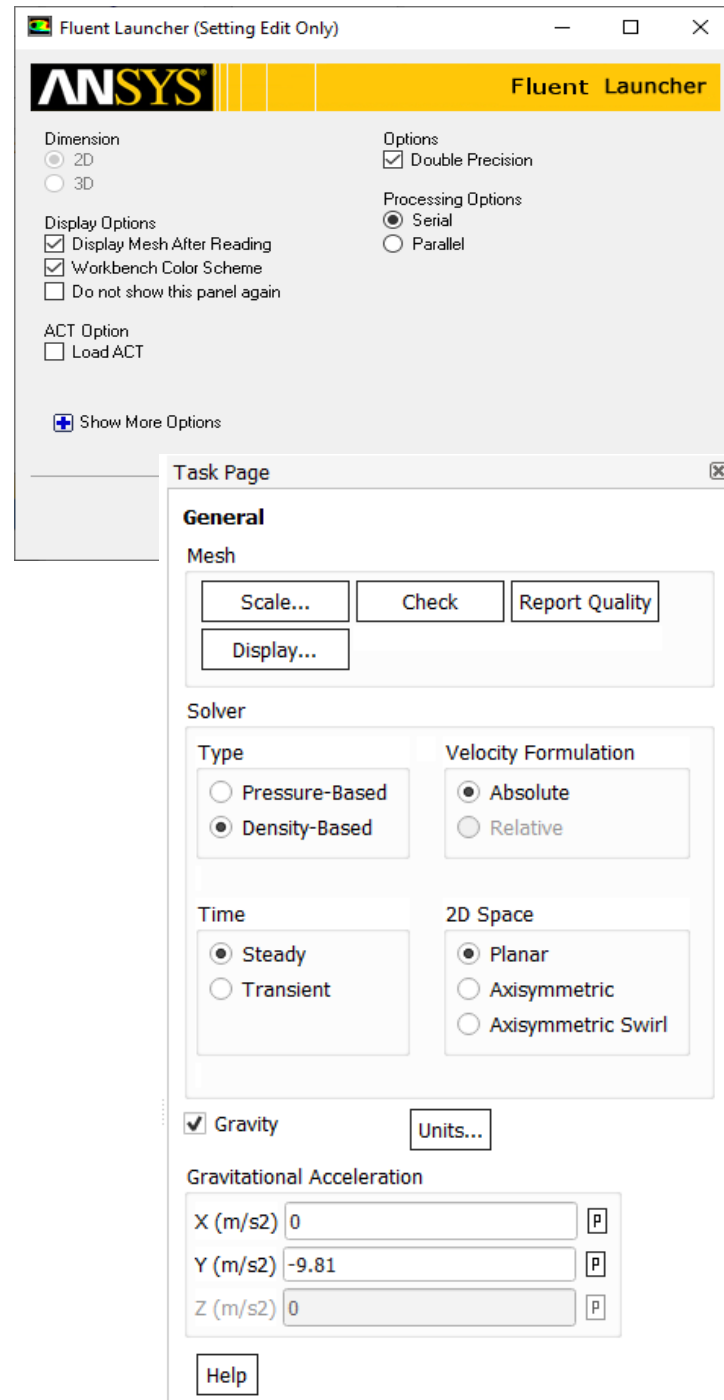
Figure 3-14-choices of precision and the type of solver used

By including the energy equation in the simulation, we ensure that all relevant thermal and energetic interactions are considered, leading to a more accurate and comprehensive understanding of the supersonic combustion process.

Using k-epsilon and realizable model for a more realistic representation of turbulence phenomena, enhancing the simulation's accuracy without significantly increasing computational costs.
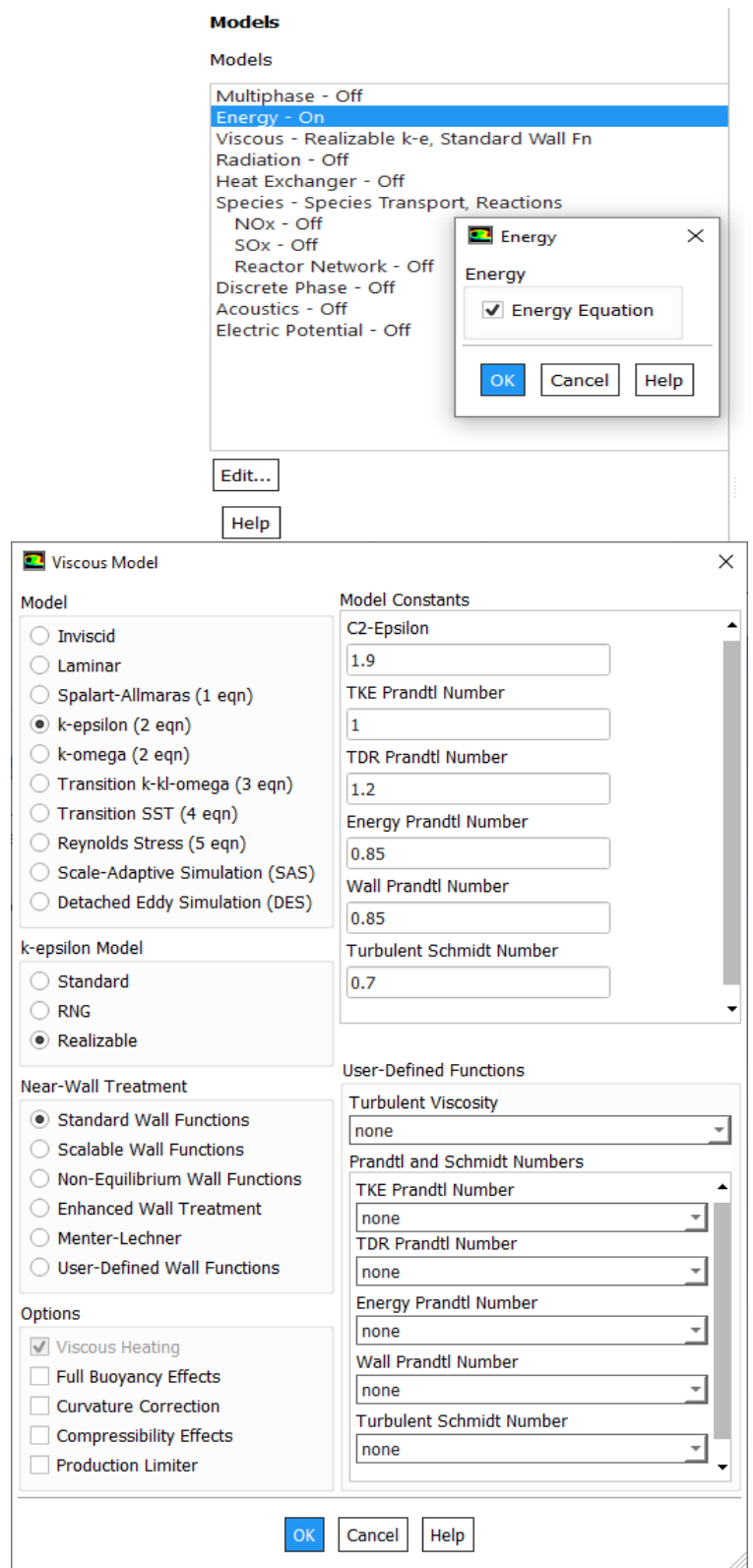
Figure 3-15-Energy equation and turbulence model chosen.

34

The eddy-dissipation model, effectively capture the essential characteristics of hydrogen-air combustion in a supersonic combustor, balancing accuracy with computational feasibility

We used ideal gas in density for both air and hydrogen-air with a viscosity of Sutherland for good accuracy, simplicity and computational efficiency
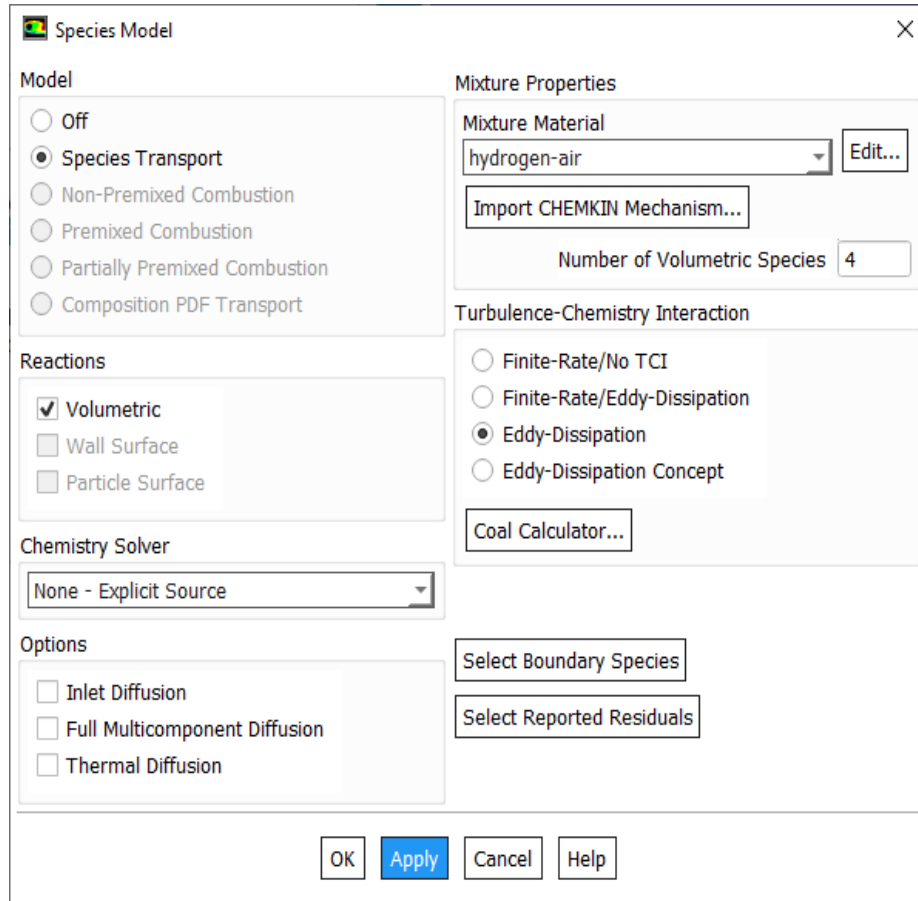
Figure 3-16-species chosen (hydrogen-air).

After some review of the boundary conditions we followed this table we followed the following research [17]
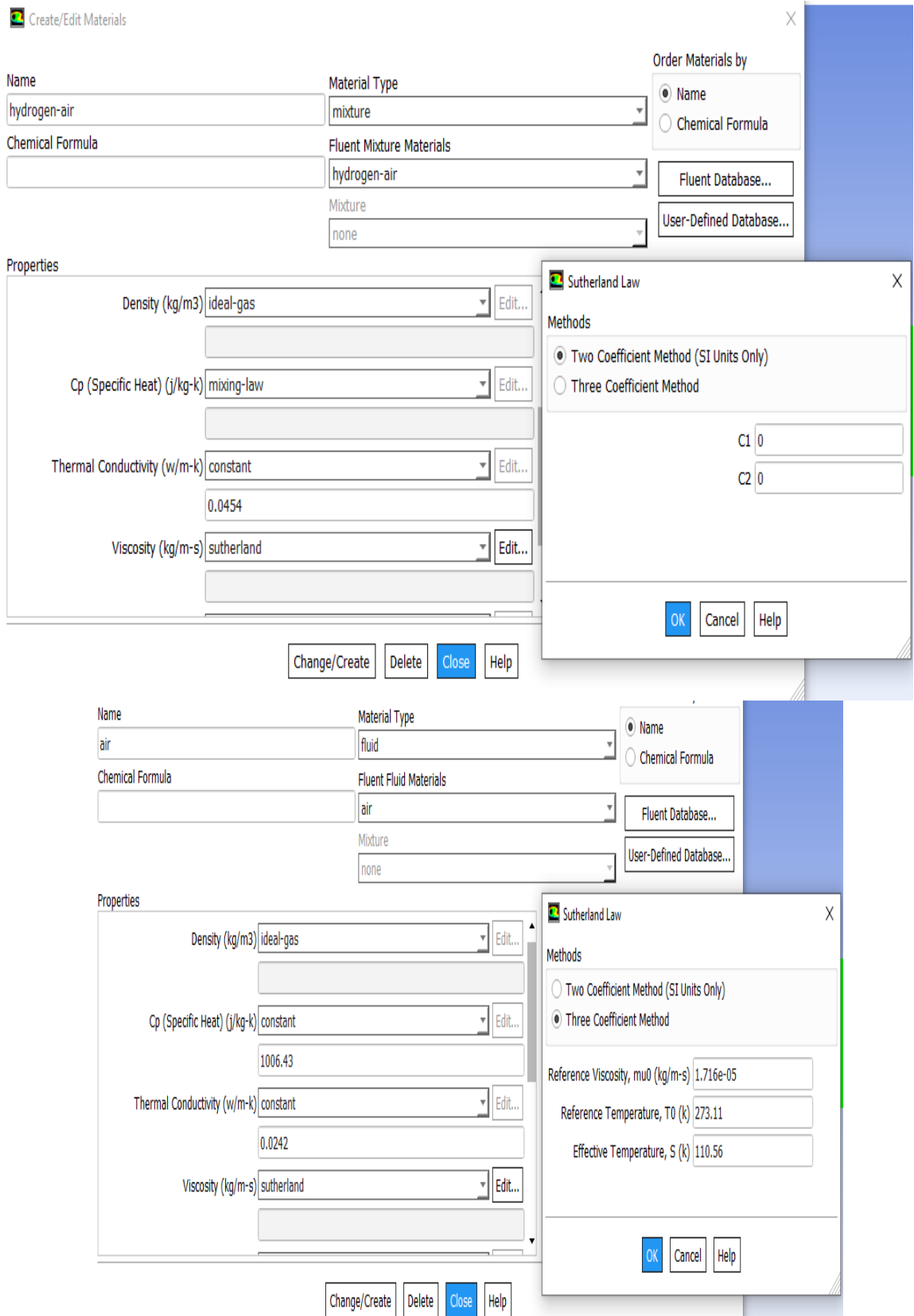
Figure 3-17-properties chosen

Table 3-2- Boundary condition got from previous research [17]

	Variable	Air inlet	Hydrogen fuel inlet
Mach number	Ma	2.5	1
Total Temperature	T (K)	500	300
Total pressure	P (Pa)	110000	110000
Concentration of species			
Oxygen mass fraction	YO2	0.232	0
Nitrogen mass fraction	YN2	0.736	0
Water mass fraction	YH2O	0.032	0
Hydrogen mass fraction	YH2	0	1

We set the parameters:
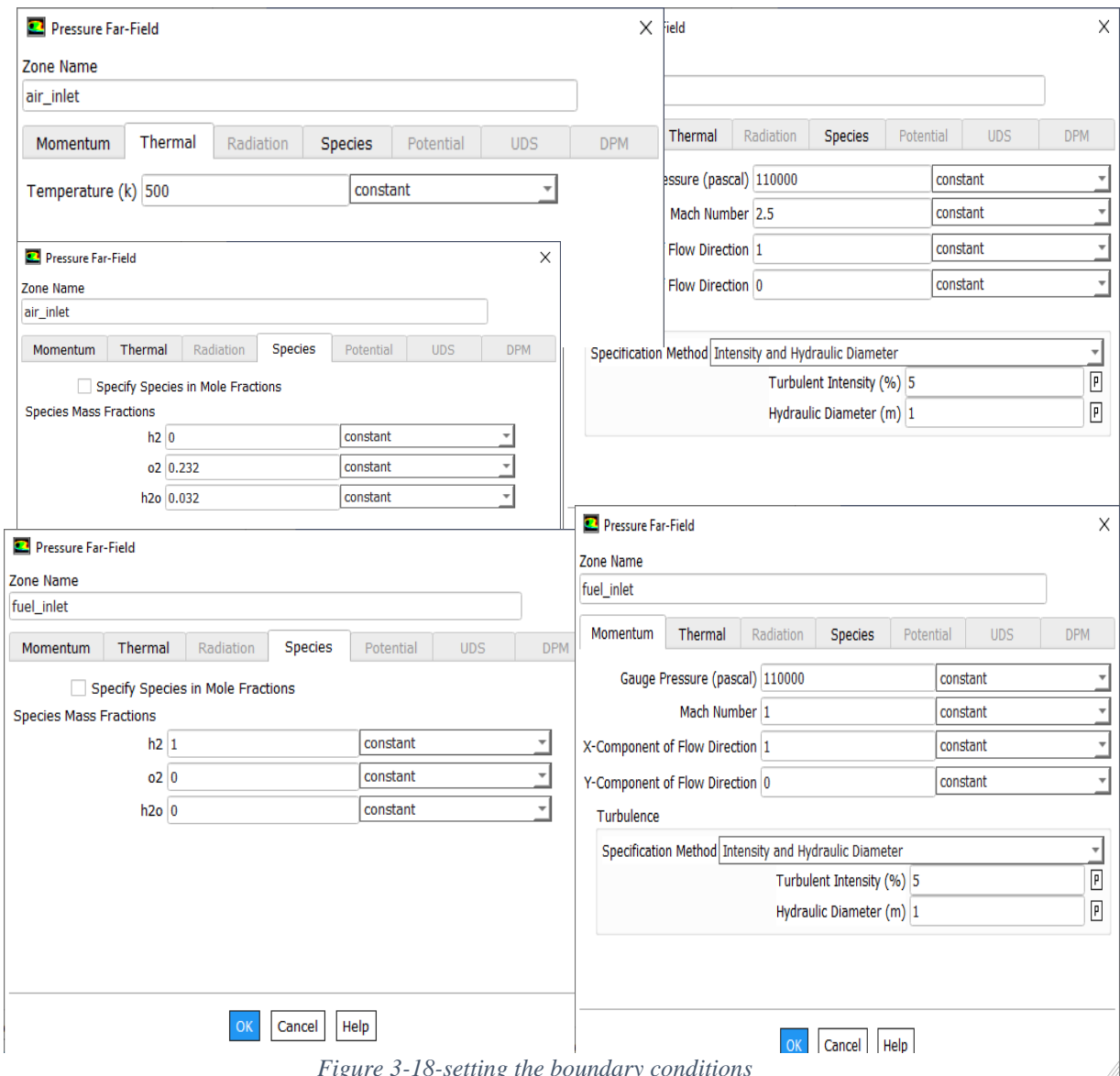
Figure 3-18-setting the boundary conditions

Task Page

Solution Initialization

Initialization Methods
- ○ Hybrid Initialization
- ● Standard Initialization

Compute from
air_inlet

Reference Frame
- ● Relative to Cell Zone
- ○ Absolute

Initial Values

Gauge Pressure (pascal)
110000

X Velocity (m/s)
1124.804

Y Velocity (m/s)
0

Turbulent Kinetic Energy (m2/s2)
4744.443

Turbulent Dissipation Rate (m2/s3)
767117

h2
0

Initialize | Reset | Patch... | Species

Task Page

Run Calculation

Check Case... | Update Dynamic Mesh...

Options

☐ Data Sampling for Steady Statistics

Sampling Interval
1 | Sampling Options...

Iterations Sampled 0

Number of Iterations
500

Reporting Interval
1

Profile Update Interval
1

☑ Solution Steering

Flow Type
supersonic | ☑ Use FMG Initialization

First to Higher Order Blending

100 % ◄ ───────○── ►
First Order   Second Order

More Settings... | Courant Number 5

Data File Quantities... | Acoustic Signals...

Calculate

Help

Task Page

Solution Methods

Formulation
Implicit

Flux Type
Roe-FDS

Spatial Discretization

Gradient
Least Squares Cell Based

Flow
Second Order Upwind

Turbulent Kinetic Energy
Second Order Upwind

Turbulent Dissipation Rate
Second Order Upwind

Transient Formulation

☐ Non-Iterative Time Advancement
☐ Frozen Flux Formulation
☐ Pseudo Transient
☐ Warped-Face Gradient Correction
☐ High Order Term Relaxation | Options...
☐ Convergence Acceleration For Stretched Meshes

Default

Help

Figure 3-19- the choice of resolution method

38

Using the implicit solution method with the second-order upwind scheme ensures stability, accuracy, and efficiency. The implicit method allows for larger time steps and better handles the stiffness of reacting flows, crucial for capturing the rapid changes and complex interactions in supersonic combustion. The second-order upwind scheme reduces numerical diffusion, improving the resolution of sharp gradients and flow features like shock waves and mixing layers. This combination enhances the overall quality of the simulation, making it more robust and reliable for modeling the detailed physics of fuel injection, mixing, and combustion in high-speed flows.

Standard initialization method used where precise initial conditions are critical for capturing the intricate flow dynamics, shock interactions, and combustion processes accurately.

And also we used Full Multi-Grid Initialization and supersonic flow and 500 iteration number for a stable result.

4. **Chapter ɪᴠ:**

Results and discussions

4.1. Presentation of the different contours:

Despite extensive efforts, the simulation did not achieve full convergence. Therefore, we opted for a qualitative convergence criterion, running the simulation for 500 iterations over a duration of 2 hours. This approach allowed us to gather valuable insights and preliminary results, enabling us to analyze the flow characteristics and combustion behavior within the scramjet combustor. The simulations were performed on a workstation equipped with an AMD Ryzen 7 5800X processor and an AMD 6700XT GPU. While the solution did not fully converge, the qualitative data provided a basis for understanding the performance trends and identifying areas for further investigation and optimization.

4.1.1. Single strut scramjet combustion chamber:

For the single strut configuration, the oblique shocks generated at the strut's tip interact with the boundary layers on the upper and lower walls. This interaction causes the formation of separation zones due to the oblique shocks and boundary layers on the lower wall. the upper shock is reflected off the upper wall, while a shock wave forms from the boundary layers and separation zones on the lower wall. There is no separation zone on the upper wall in the single strut case. The upper oblique shock generated by the strut tip interacts with the expansion wave created by the divergent angle on the upper wall, which diminishes the oblique shock's intensity. So the interaction between the weakened oblique shock and the boundary layer does not produce a separation region, as depicted in Fig. 9.
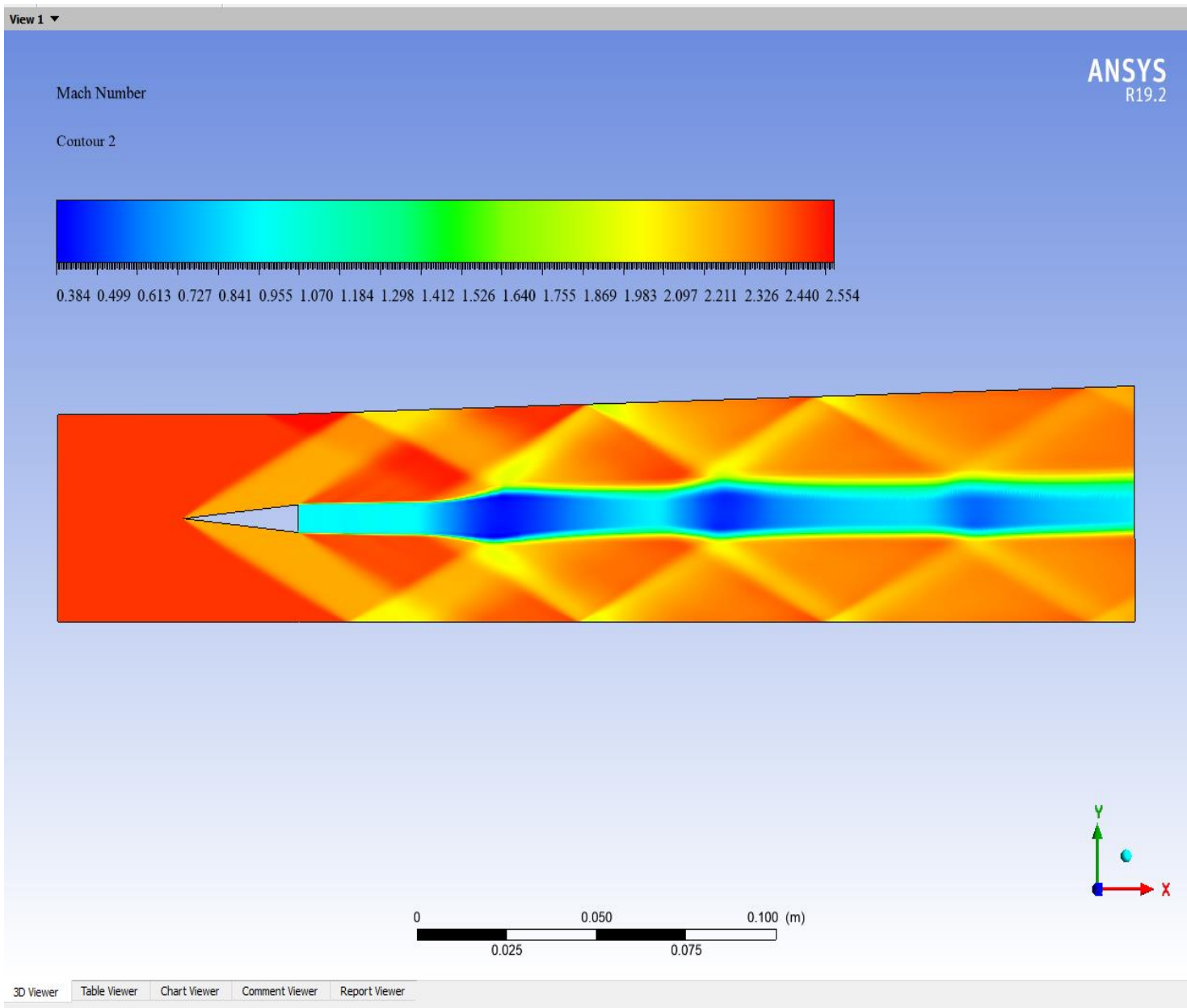
Figure 4-1-Mach number contour, $Ma_{air\ inlet} = 2.5$, $P_{air\ inlet} = 110\ Kpa$, $T_{air\ inlet} = 500K$.
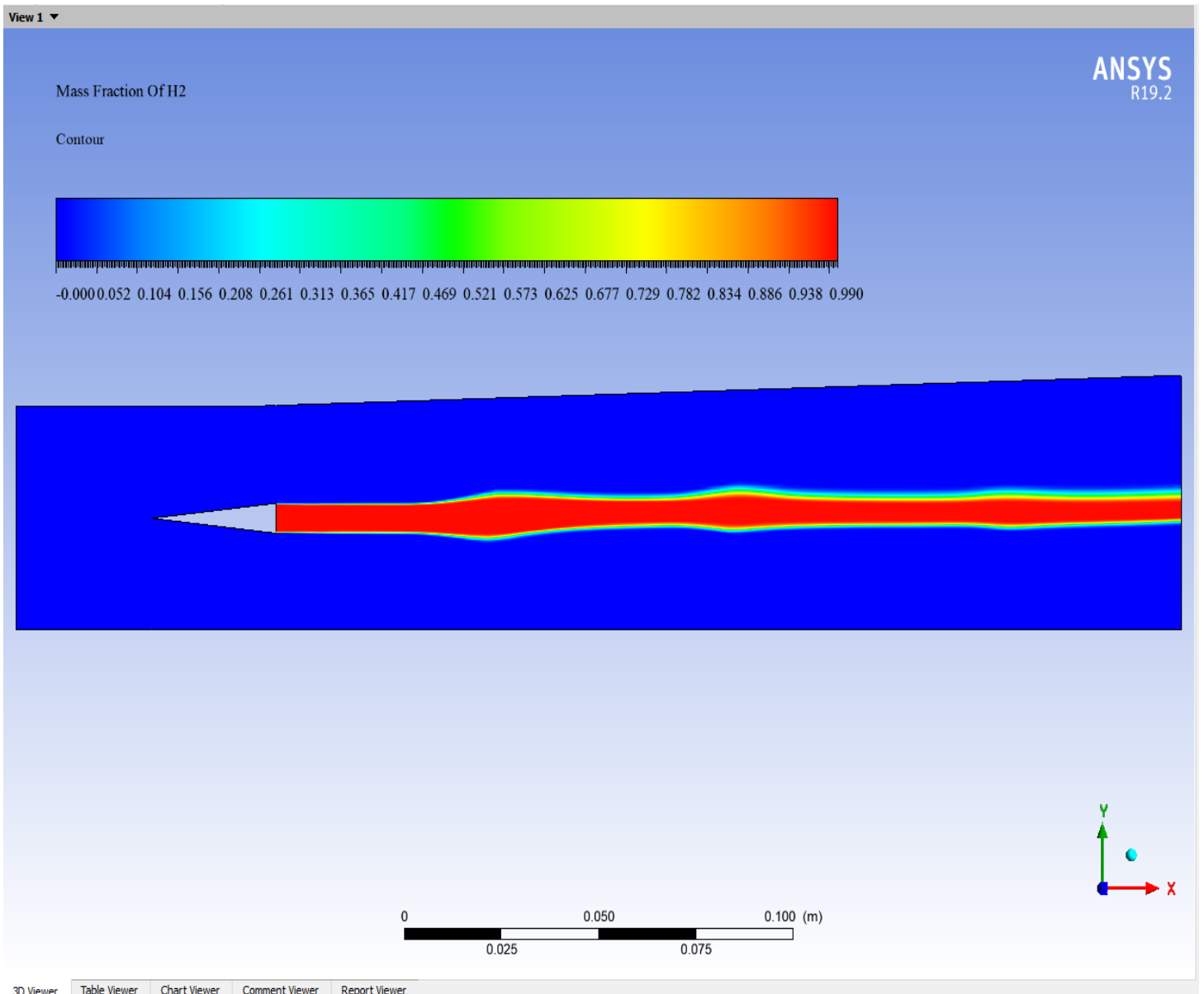
Figure 4-2-H2 mass fraction contour, $Ma_{h2\ inlet} = 1,\ T_{h2\ inlet} = 300K, Y_{H_2} = 1.$

The H2 mass fraction contour shows in this single strut combustion chamber shows that along the center line in this case the H2 is present more than the outer part of the combustion chamber and it keeps going untill the outlet part that's cause of the supersonic airflow.

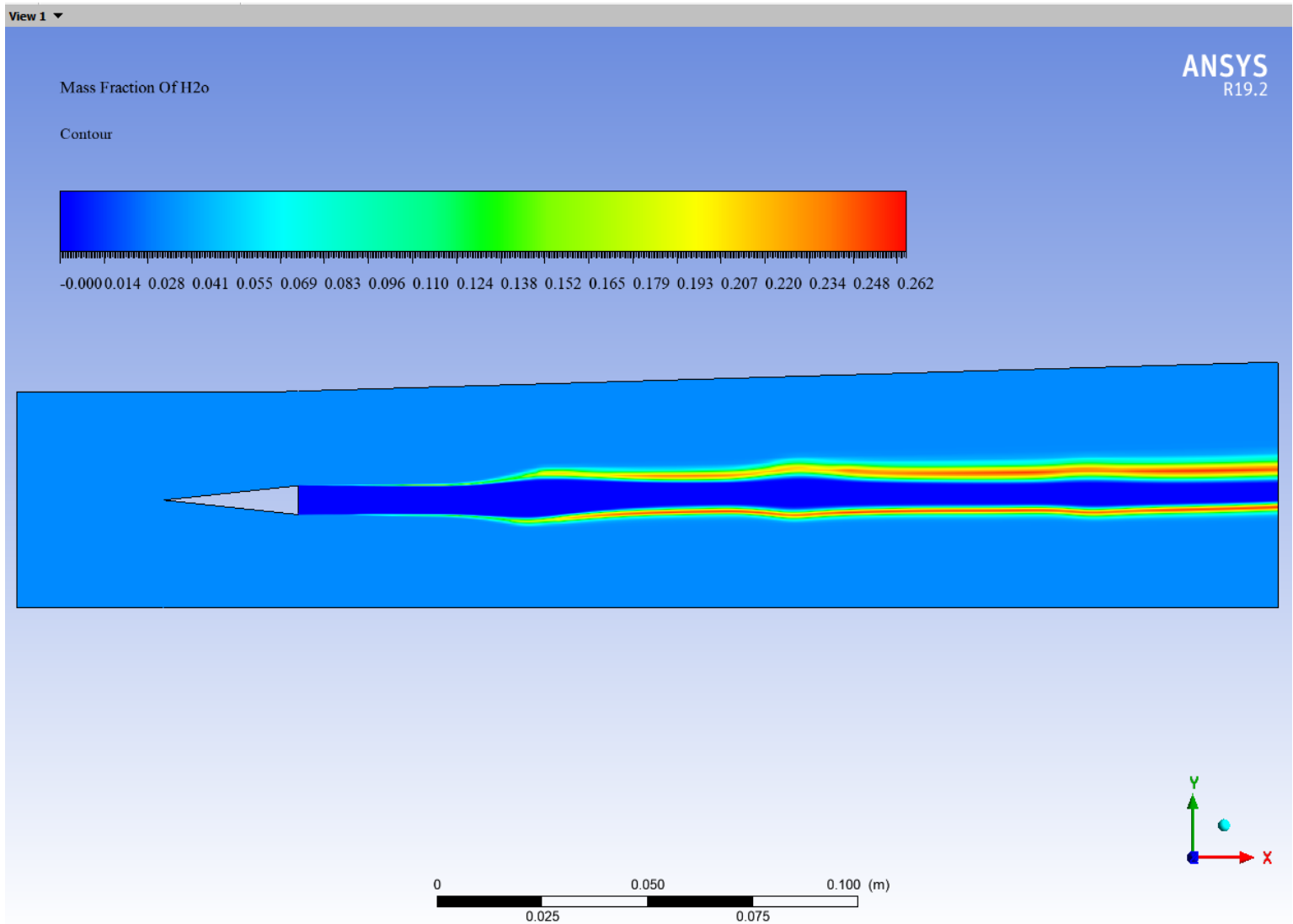*Figure 4-3-H2O mass fraction contour, $Ma_{h2\ inlet} = 1$, $P_{h_2\ inlet} = 110\ Kpa$, $T_{h2\ inlet} = 300K$, $Y_{H_2} = 1$, $Y_{h_2o} = 0.032$, $Ma_{air\ inlet} = 2.5$, $P_{air\ inlet} = 110\ Kpa$, $T_{air\ inlet} = 500K$.*

This figure of the H2O mass fraction contour it is the fuel/air mixture it show the combustion happened when the hydrogen makes contact with the oxygen.
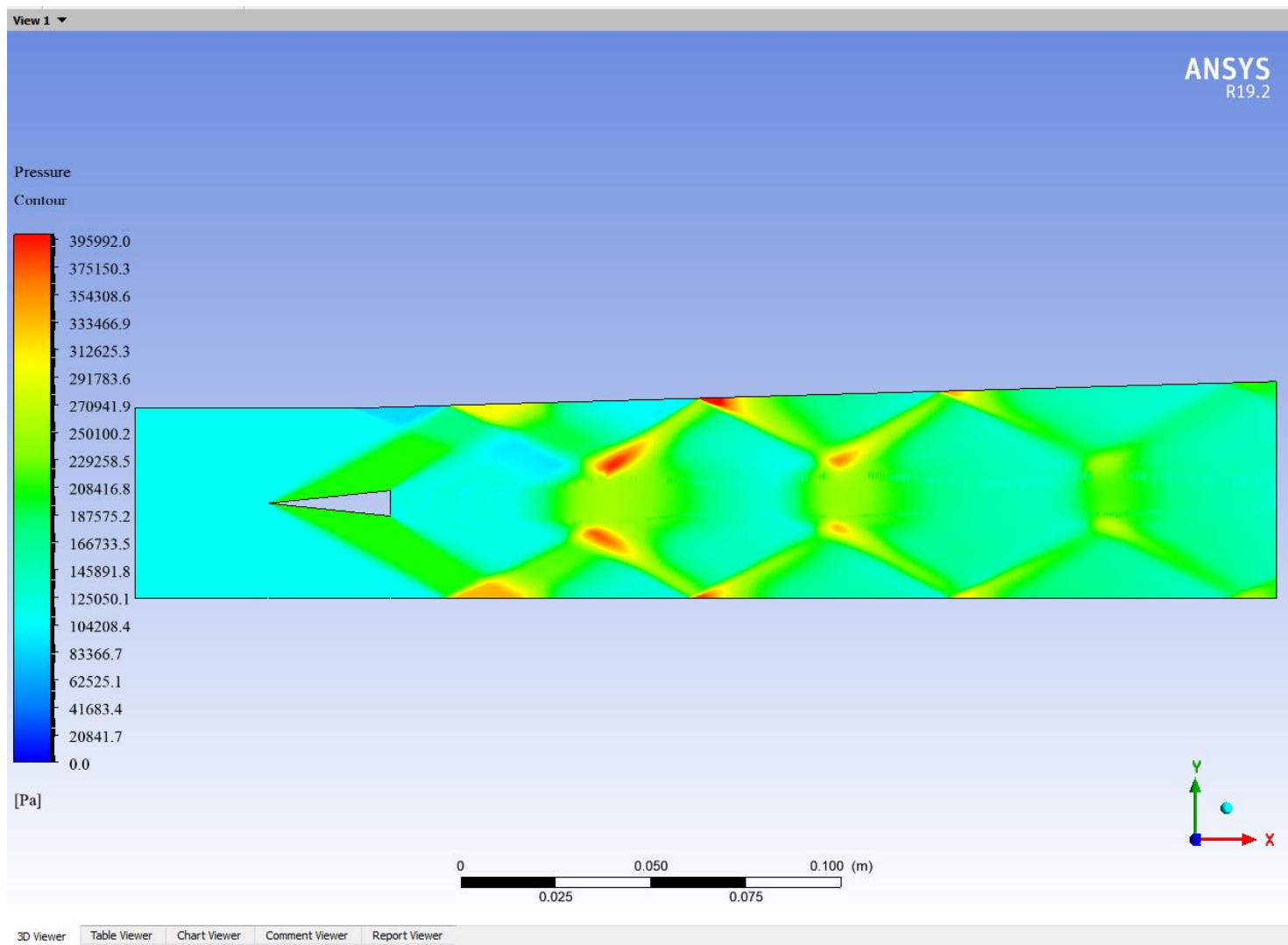
Figure 4-4-Pressure contour, $P_{air\ inlet} = 1100000$ pa, $P_{h_2\ inlet} = 110$ Kpa.

45
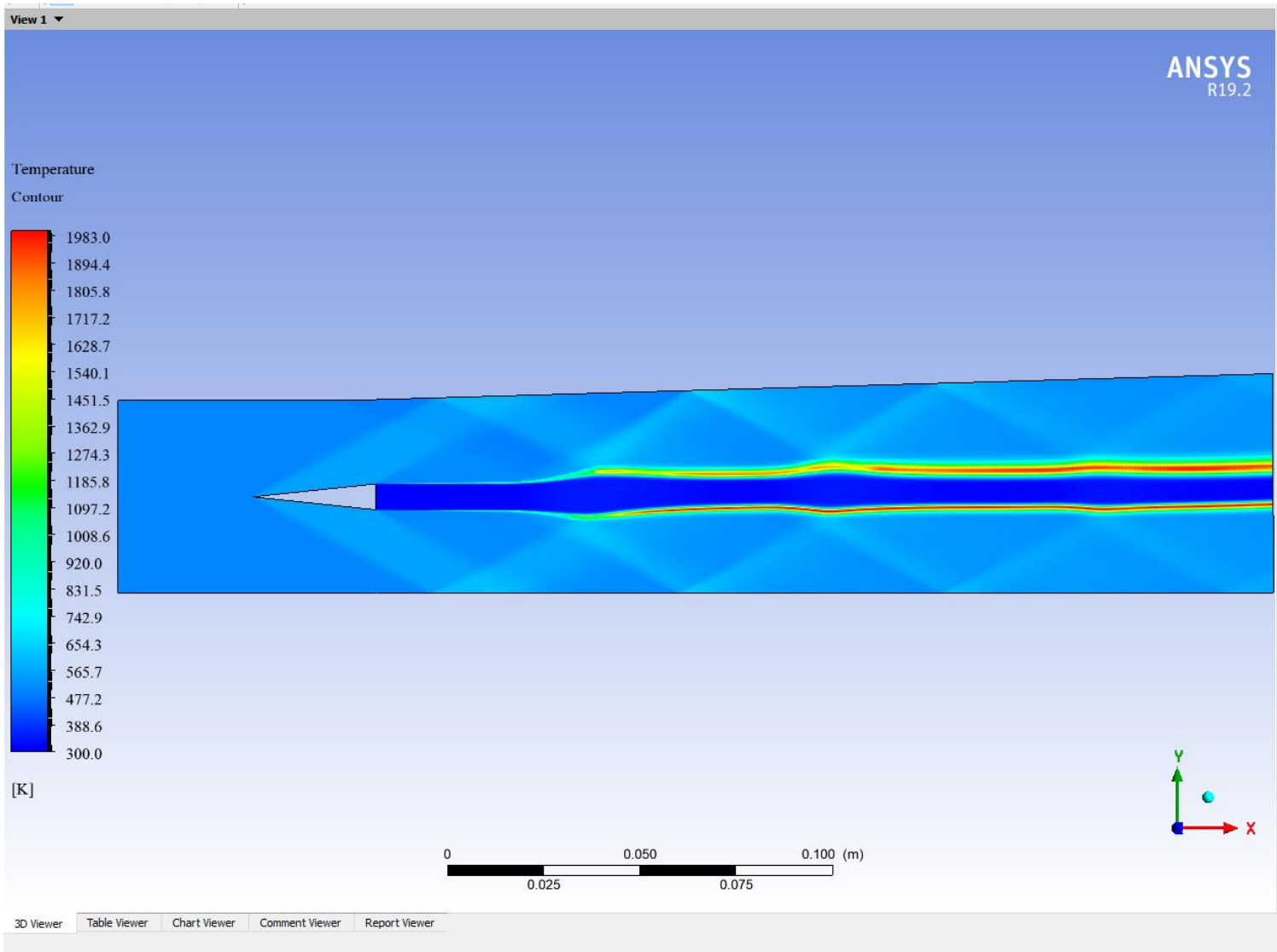
Figure 4-5-Temperature contour, $T_{air\ inlet} = 500K, T_{h2\ inlet} = 300K.$
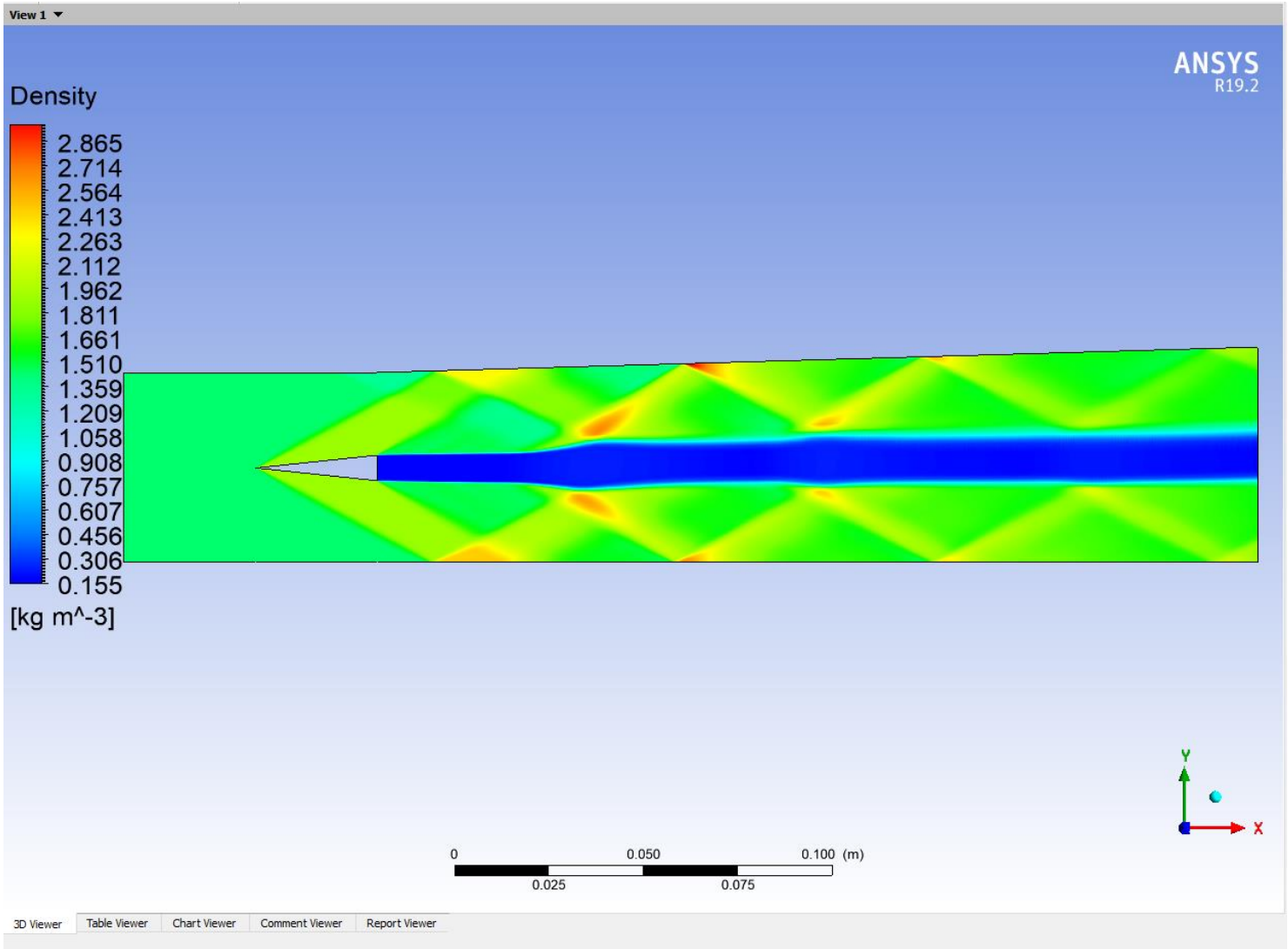
Figure 4-6-Density contour.

4.1.2. Double strut facing backward steps :

Figure 4-7--Mach number contour, $Ma_{air\ inlet} = 2.5$, $P_{air\ inlet} = 110\ Kpa$, $T_{air\ inlet} = 500K$.
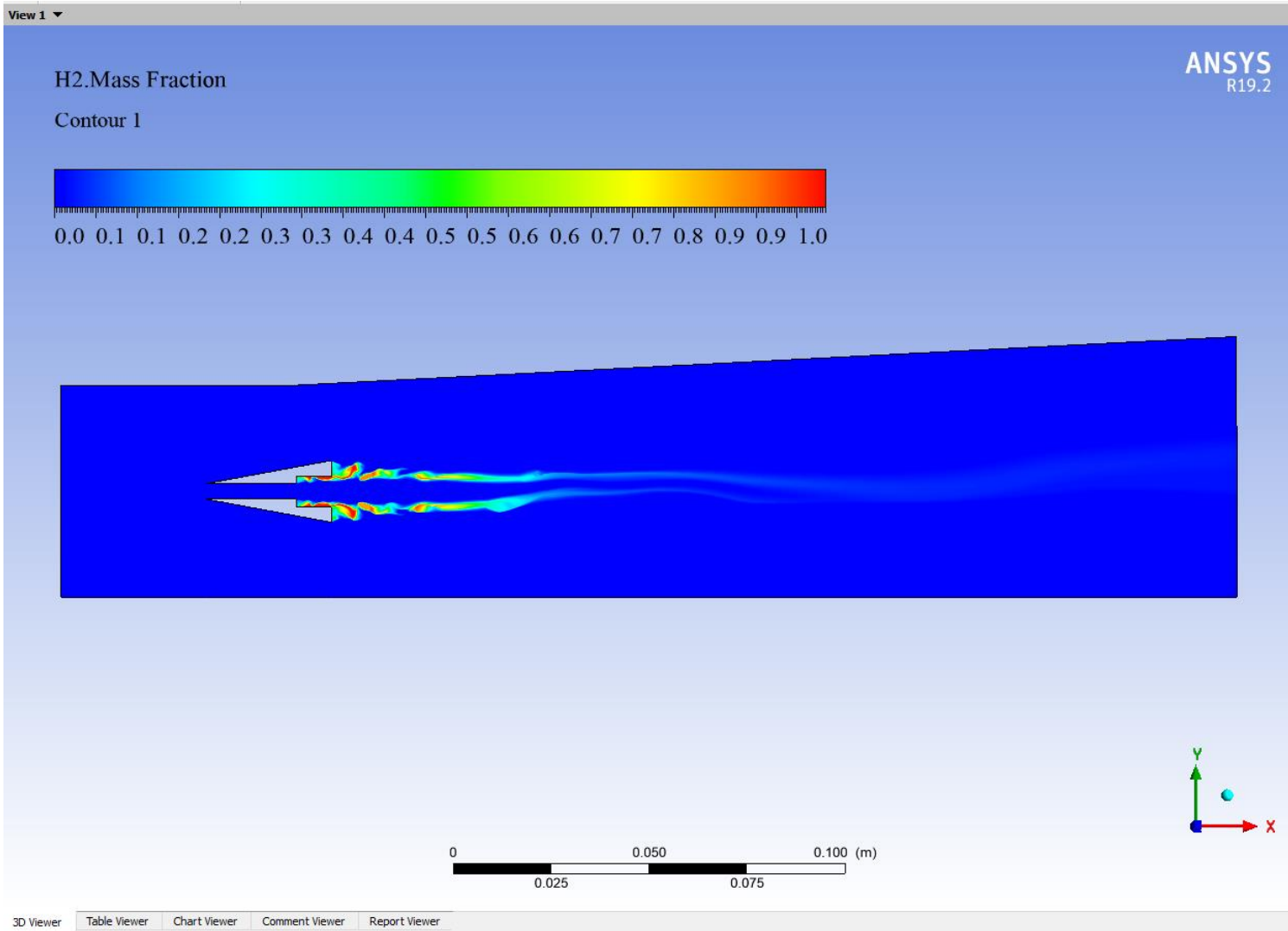
Figure 4-8-H2 mass fraction contour, $Ma_{h2\ inlet} = 1,\ T_{h2\ inlet} = 300K, Y_{H_2} = 1$

In this case we see the H2 faded along the combustion chamber that the evedience of a good mixure.
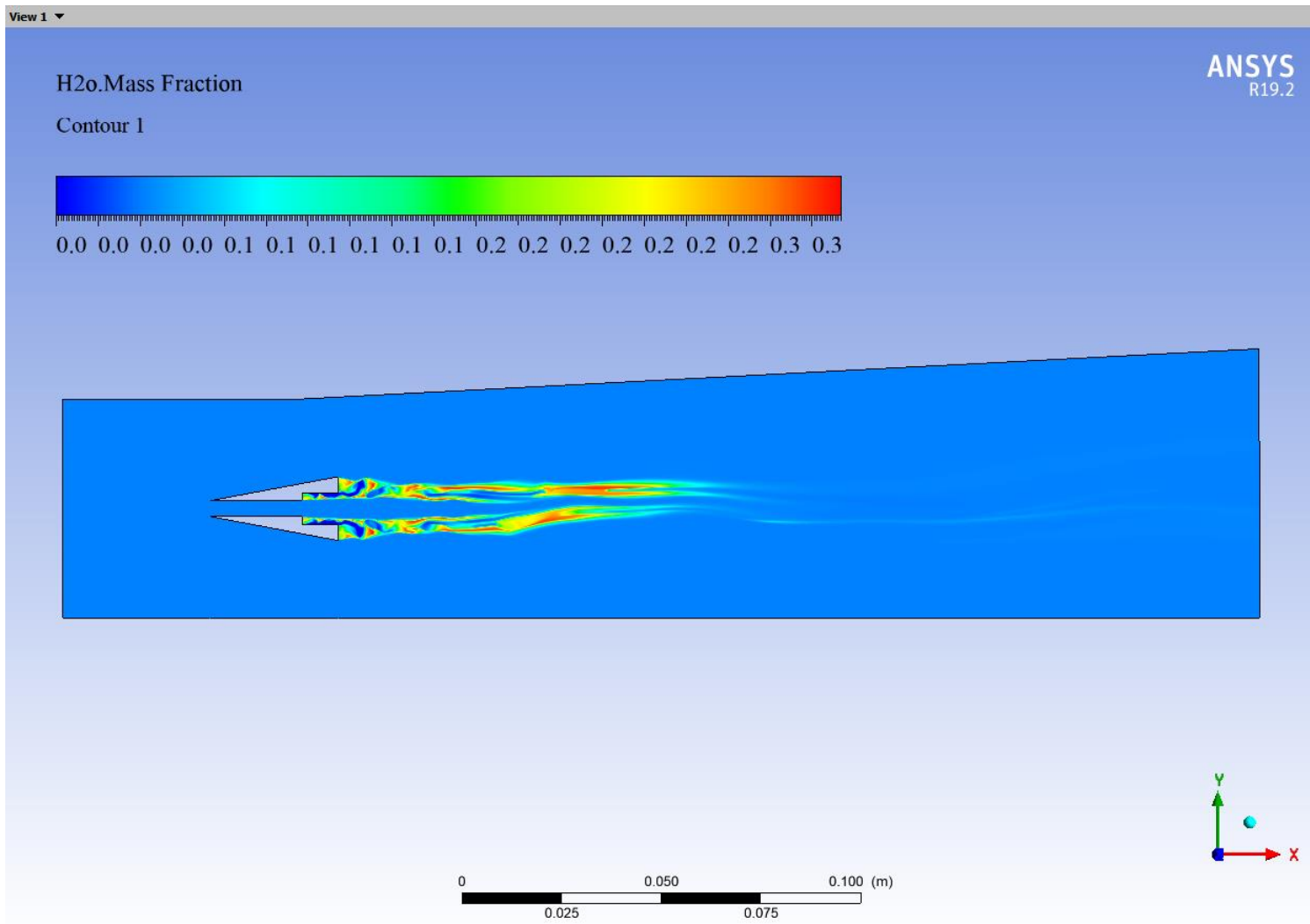
Figure 4-9 H2O mass fraction contour, $Ma_{h2\ inlet} = 1$, $P_{h_2\ inlet} = 110\ Kpa$, $T_{h2\ inlet} = 300K$, $Y_{H_2} = 1$, $Y_{h_2o} = 0.032$, $Ma_{air\ inlet} = 2.5$, $P_{air\ inlet} = 110\ Kpa$, $T_{air\ inlet} = 500K$

we can notice the H2O goo mixture because the geometry proposed.

Figure 4-10-Pressure contour, $P_{air\ inlet} = 1100000\ pa, P_{h_2\ inlet} = 110\ Kpa.$
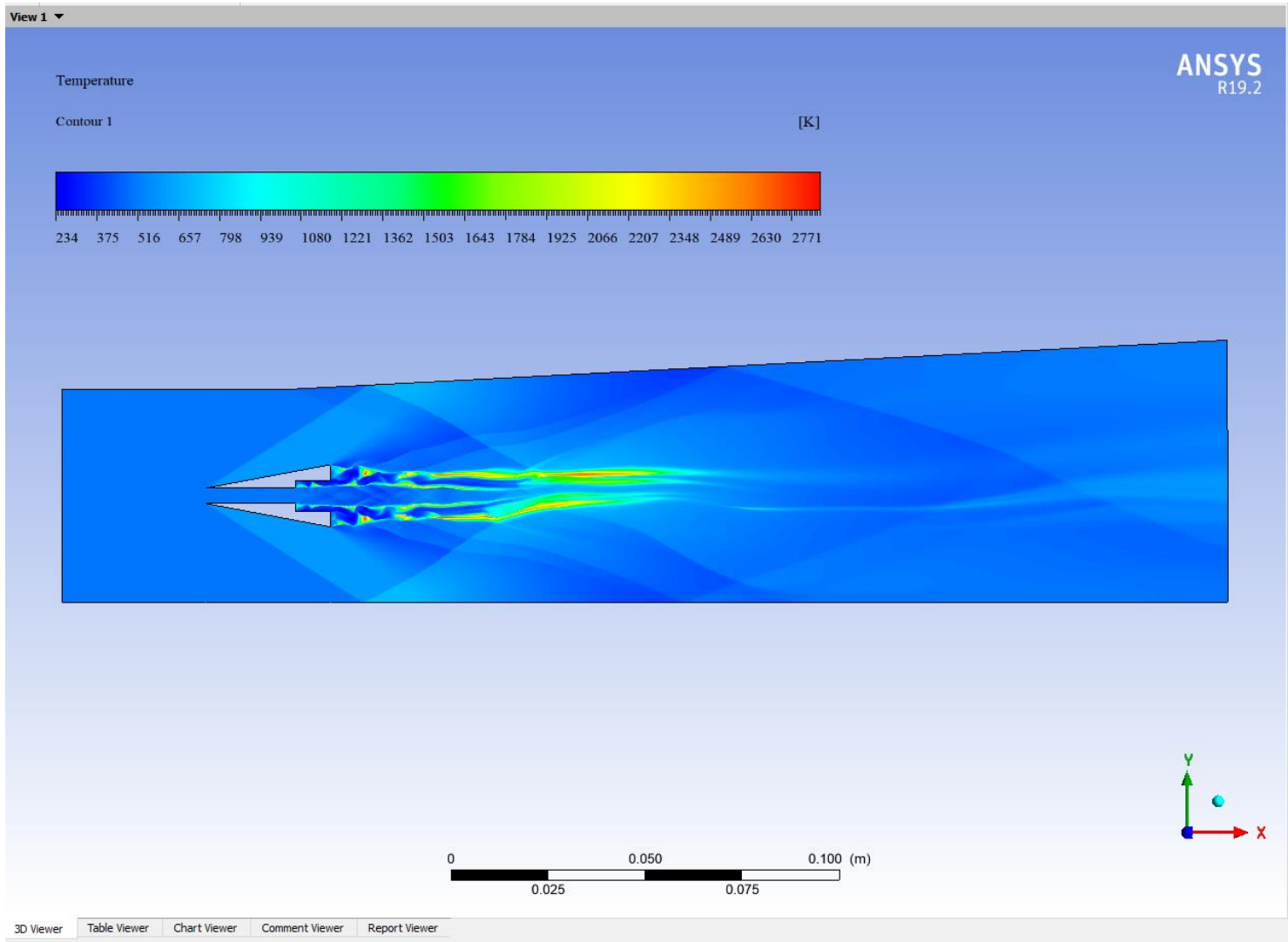
*Figure 4-11-Temperature contour, $T_{air\ inlet} = 500K, T_{h2\ inlet} = 300K$.*

Comment on the single and double strut configuration contour:

The double-strut design with backward-facing steps significantly outperformed the single-strut configuration. The double-strut setup created additional shear layers and recirculation zones, which further enhanced the mixing of fuel and air. This design not only improved combustion efficiency but also resulted in a more uniform temperature distribution within the combustor. The increased interaction between the fuel jets and the high-speed airflow in the double-strut configuration led to better combustion characteristics and higher overall efficiency.
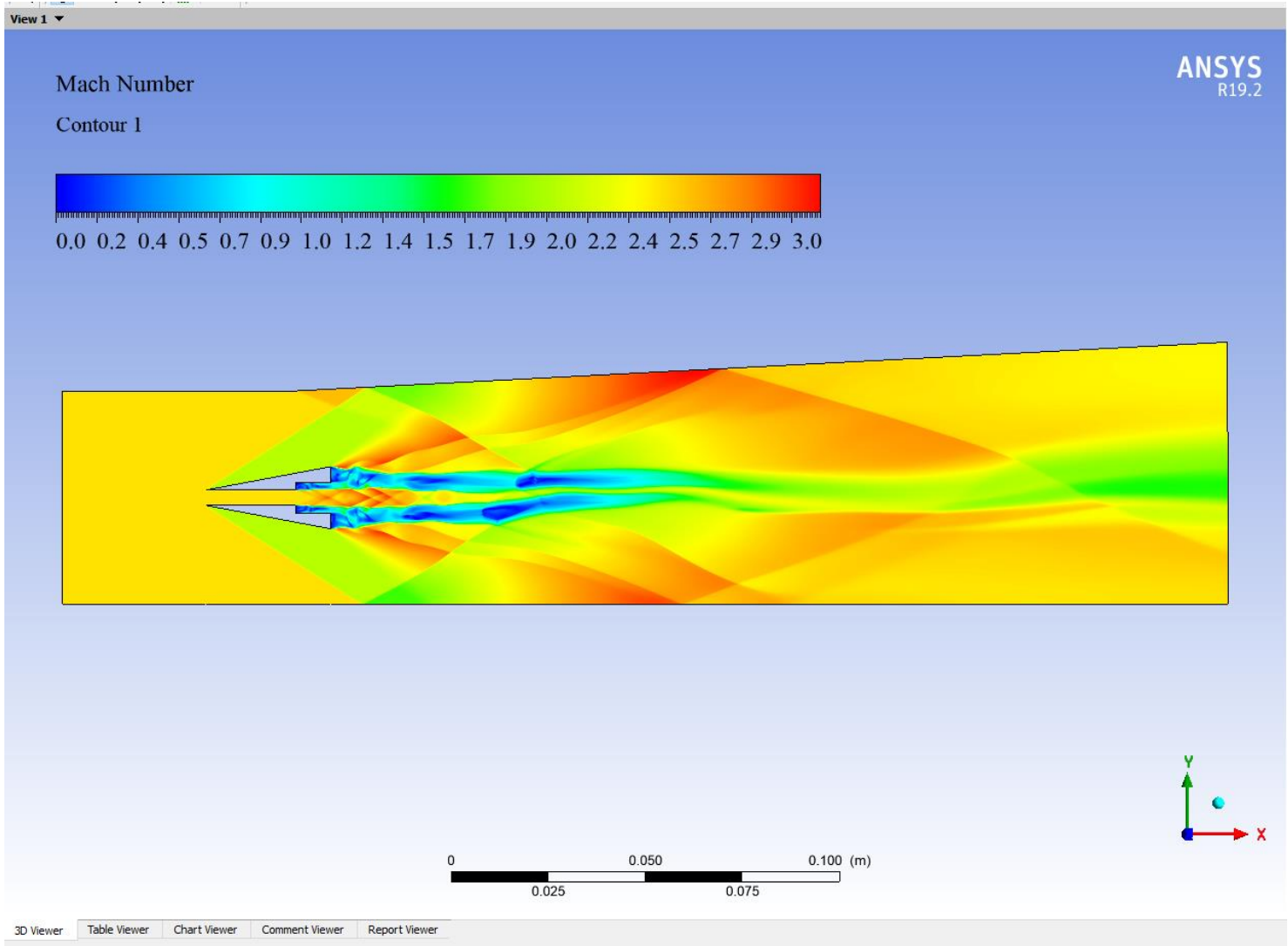
4.1.3. Double-strut with cavity :
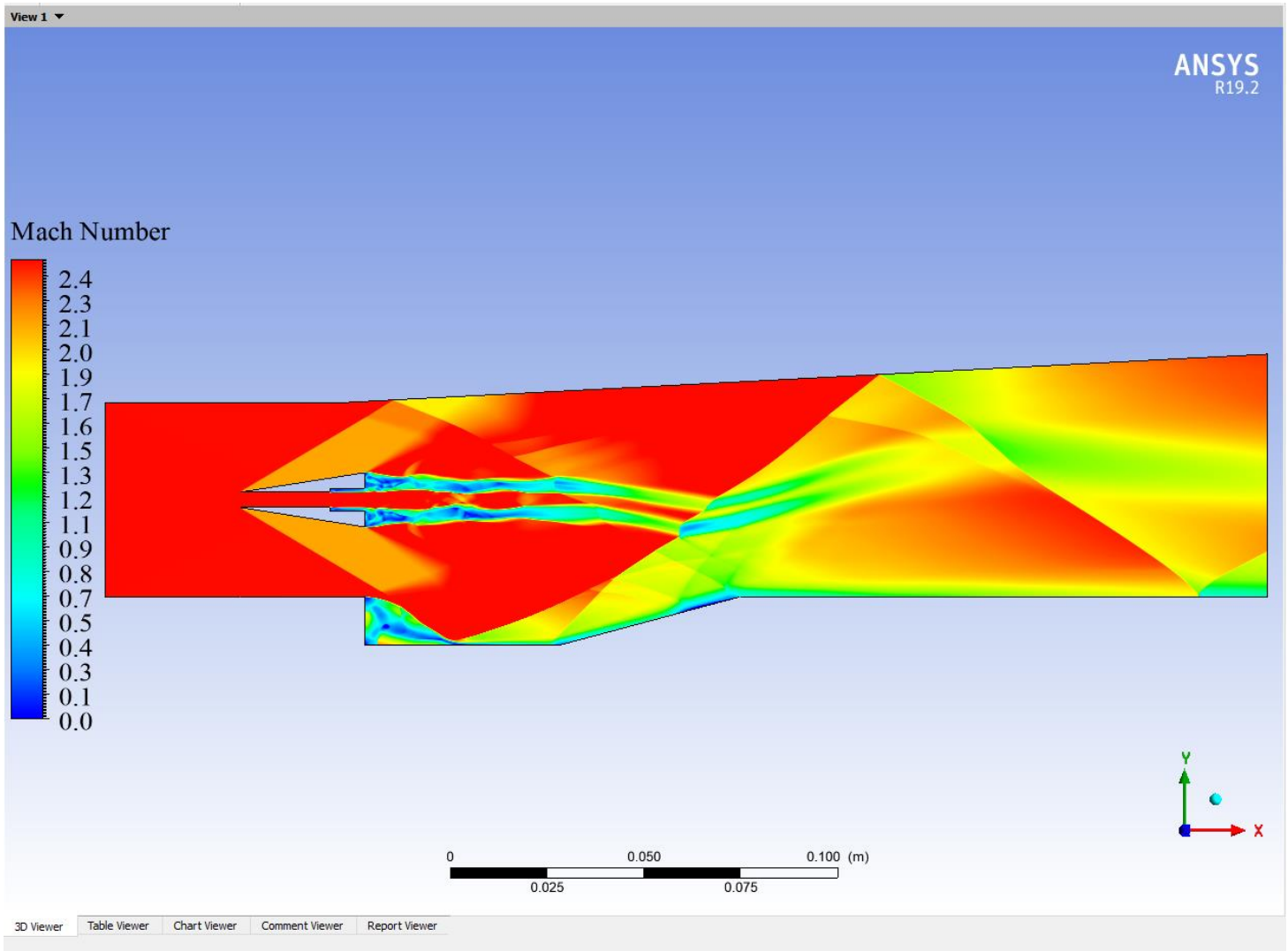
*Figure 4-12 Mach number contour* $Ma_{air\ inlet} = 2.5,\ P_{air\ inlet} = 110\ Kpa,\ T_{air\ inlet} = 500K.$
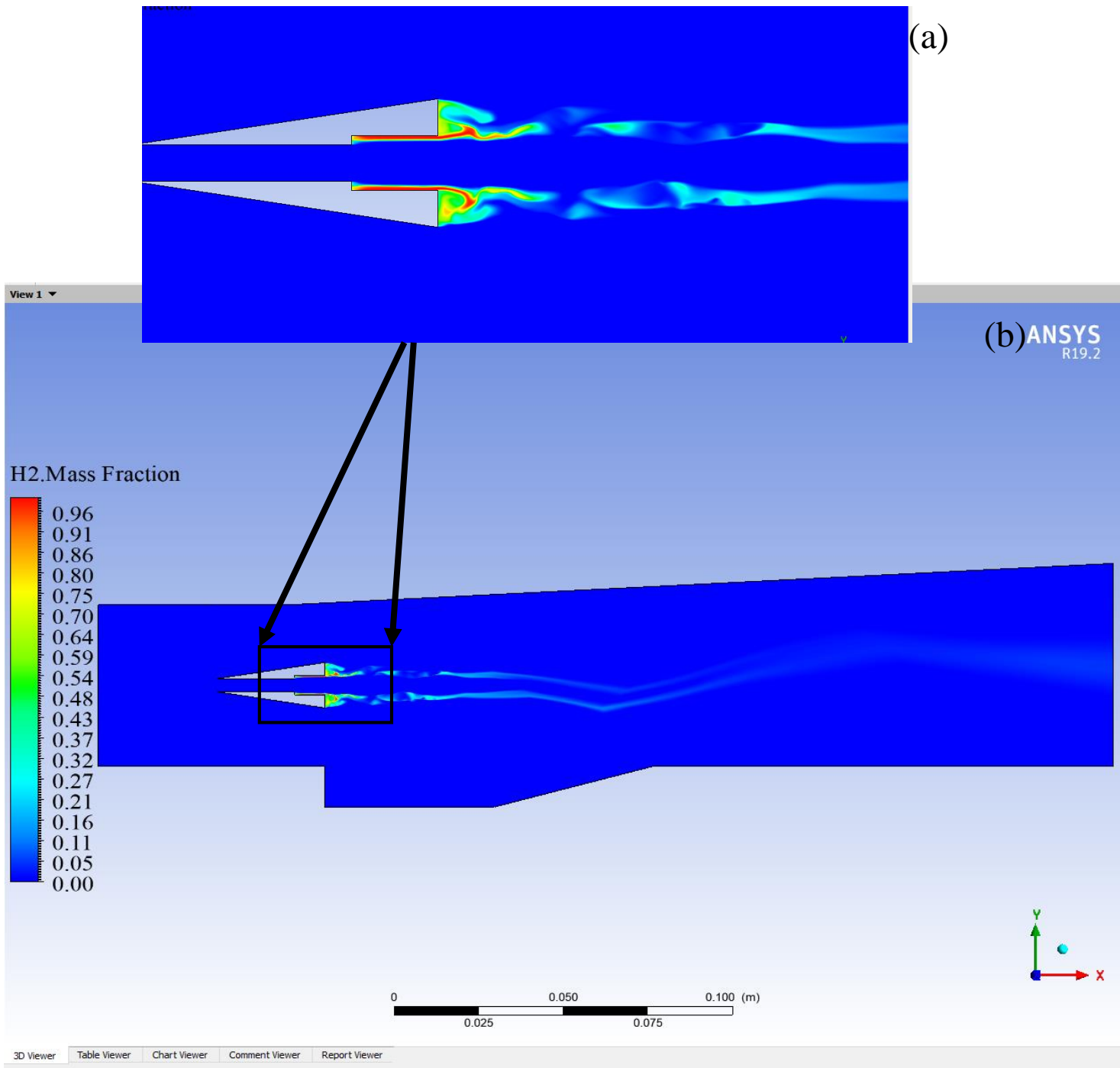
Figure 4-13-H2 mass fraction contour (a) default rainbow contour, (b) zebra contour.,
$$Ma_{h2\ inlet} = 1,\ T_{h2\ inlet} = 300K, Y_{H_2} = 1$$

55
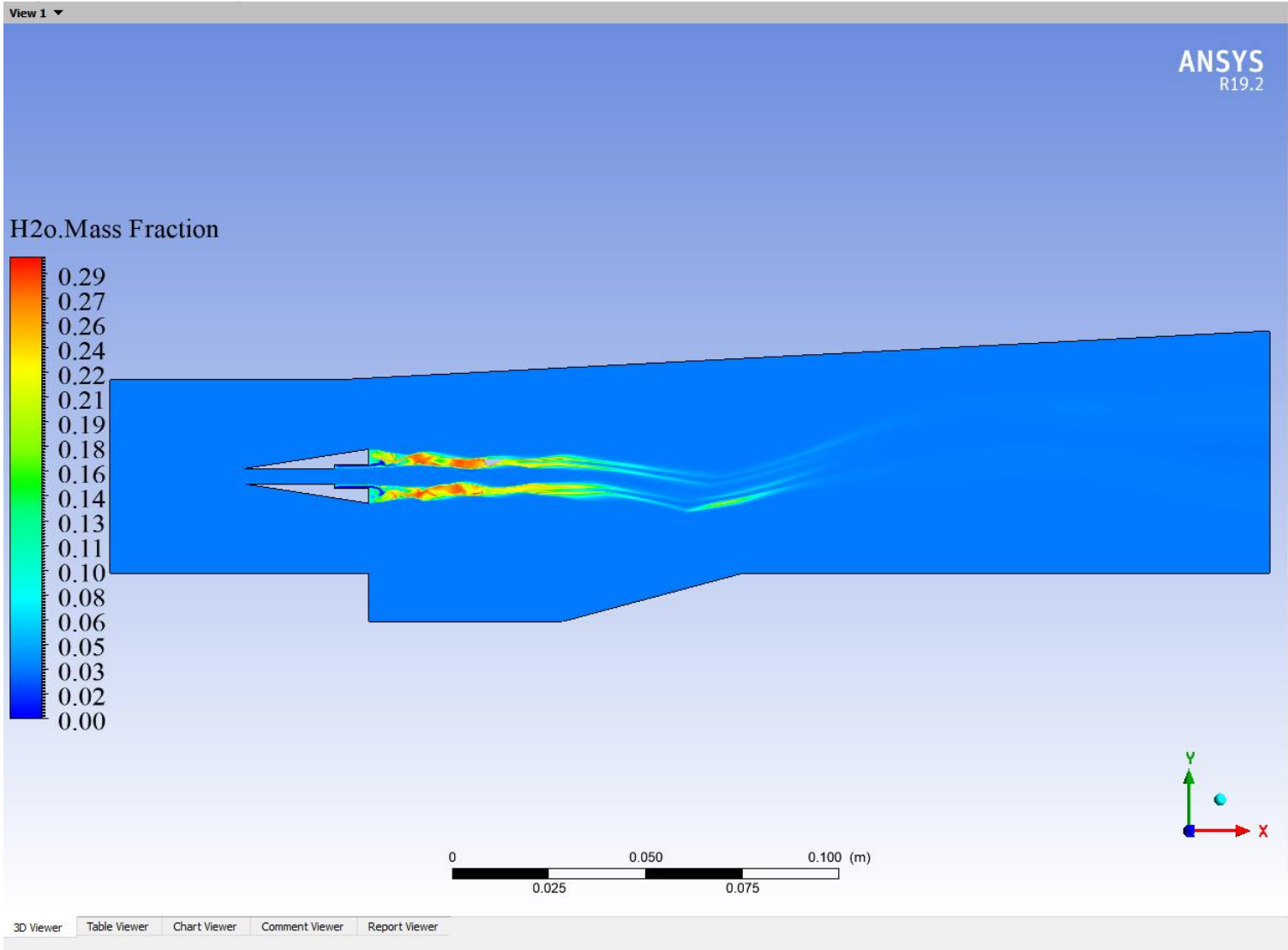
Figure 4-14-H2O mass fraction contour, $Ma_{h2\ inlet} = 1,\ P_{h_2\ inlet} = 110\ Kpa,\ T_{h2\ inlet} = 300K, Y_{H_2} = 1,\ Y_{h_2o} = 0.032,\ Ma_{air\ inlet} = 2.5,\ P_{air\ inlet} = 110\ Kpa,\ T_{air\ inlet} = 500K$
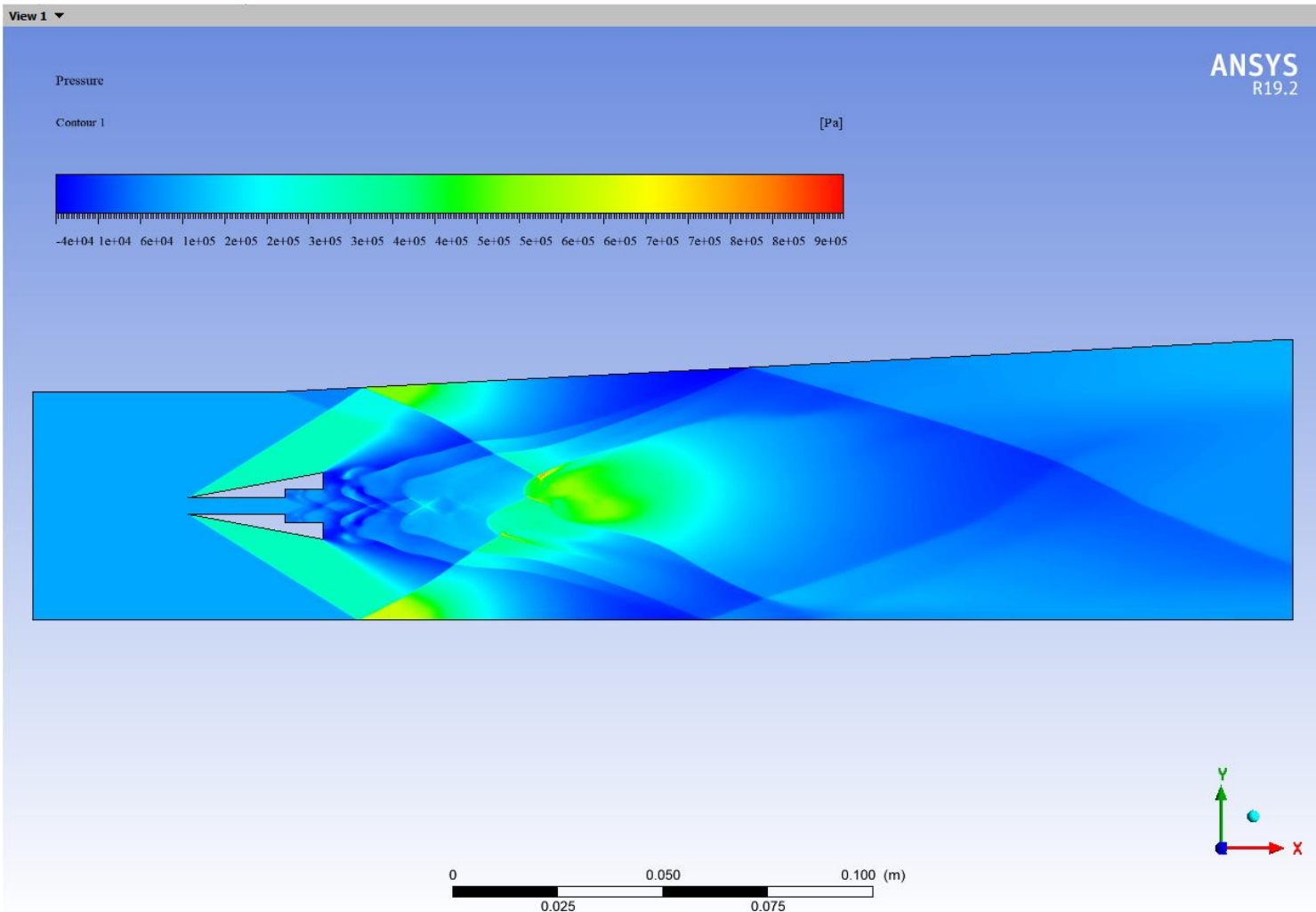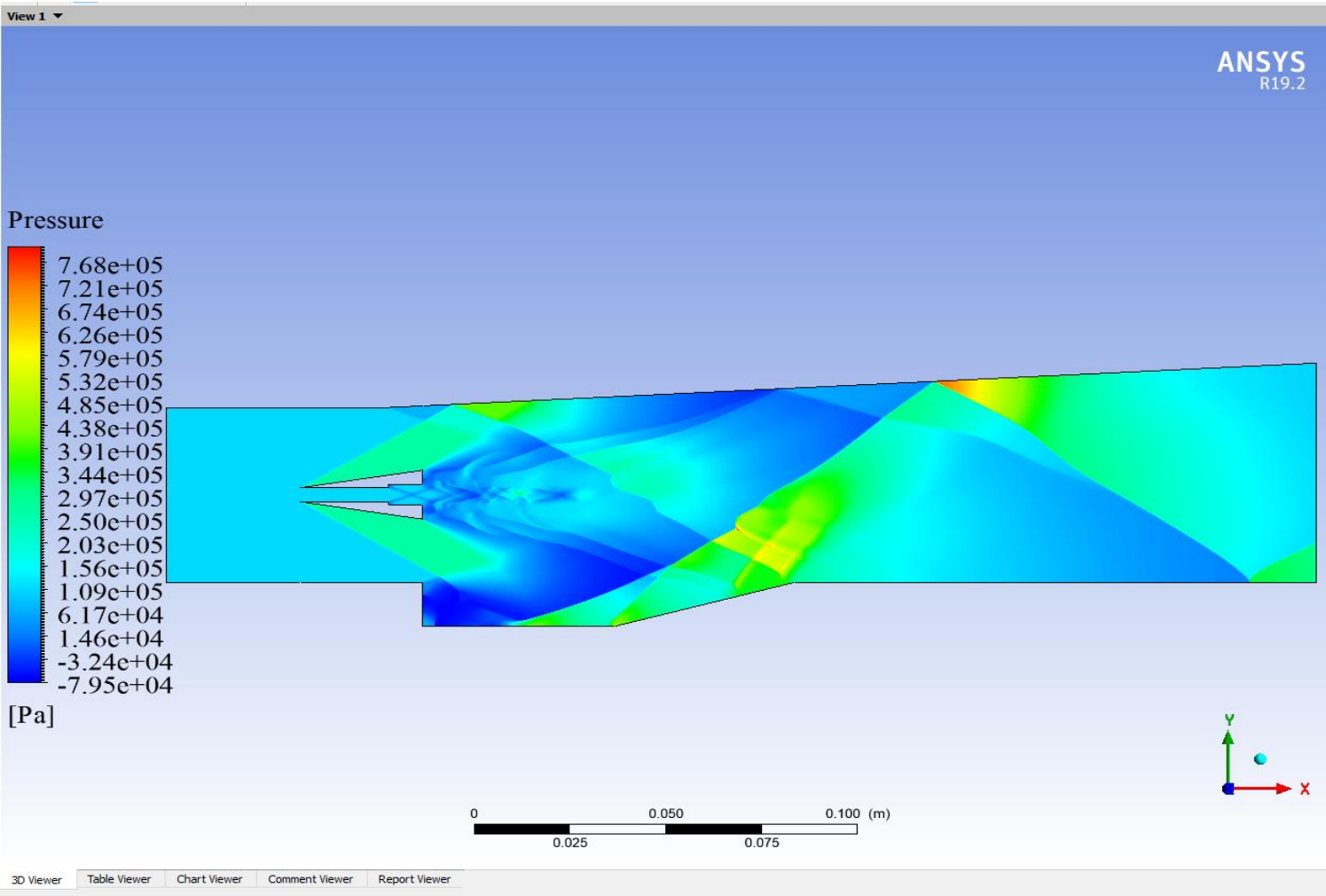
Figure 4-15-Pressure contour, $P_{air\ inlet} = 1100000\ pa, P_{h_2\ inlet} = 110\ Kpa.$
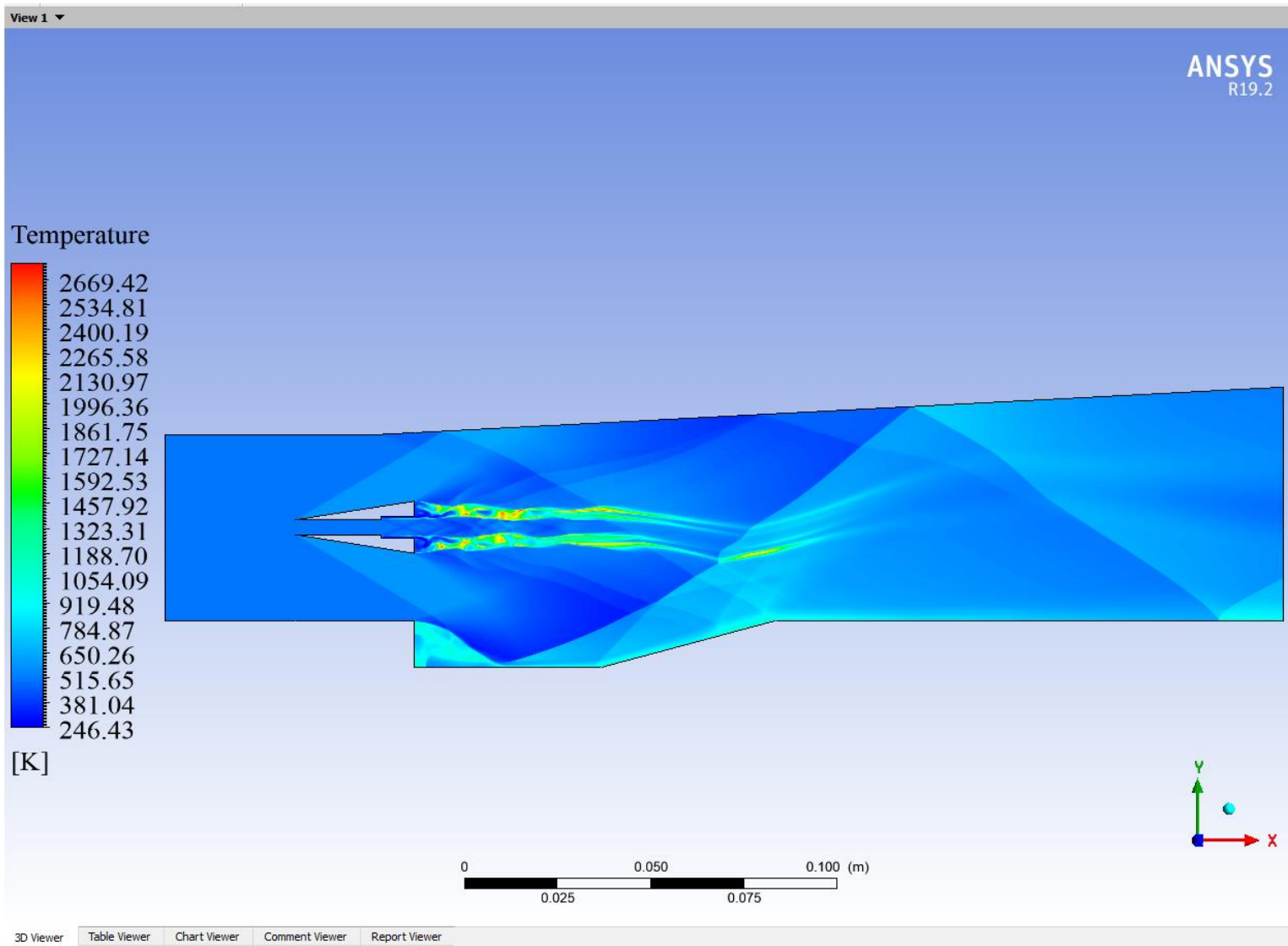
Figure 4-16-Temperature contour, $T_{air\ inlet} = 500K, T_{h2\ inlet} = 300K$.
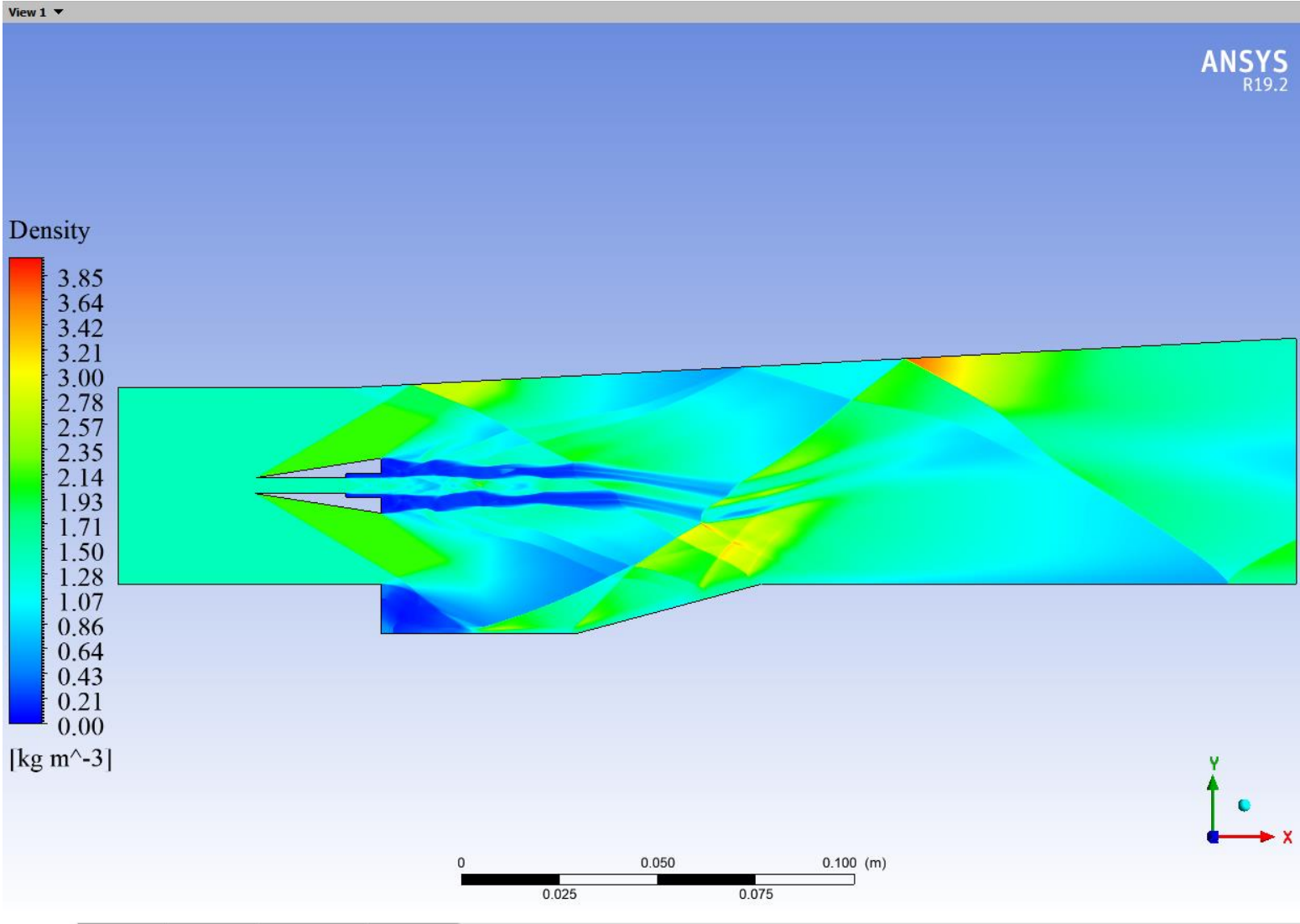
Figure 4-17-Density contour

4.1.4. Double cavity scramjet
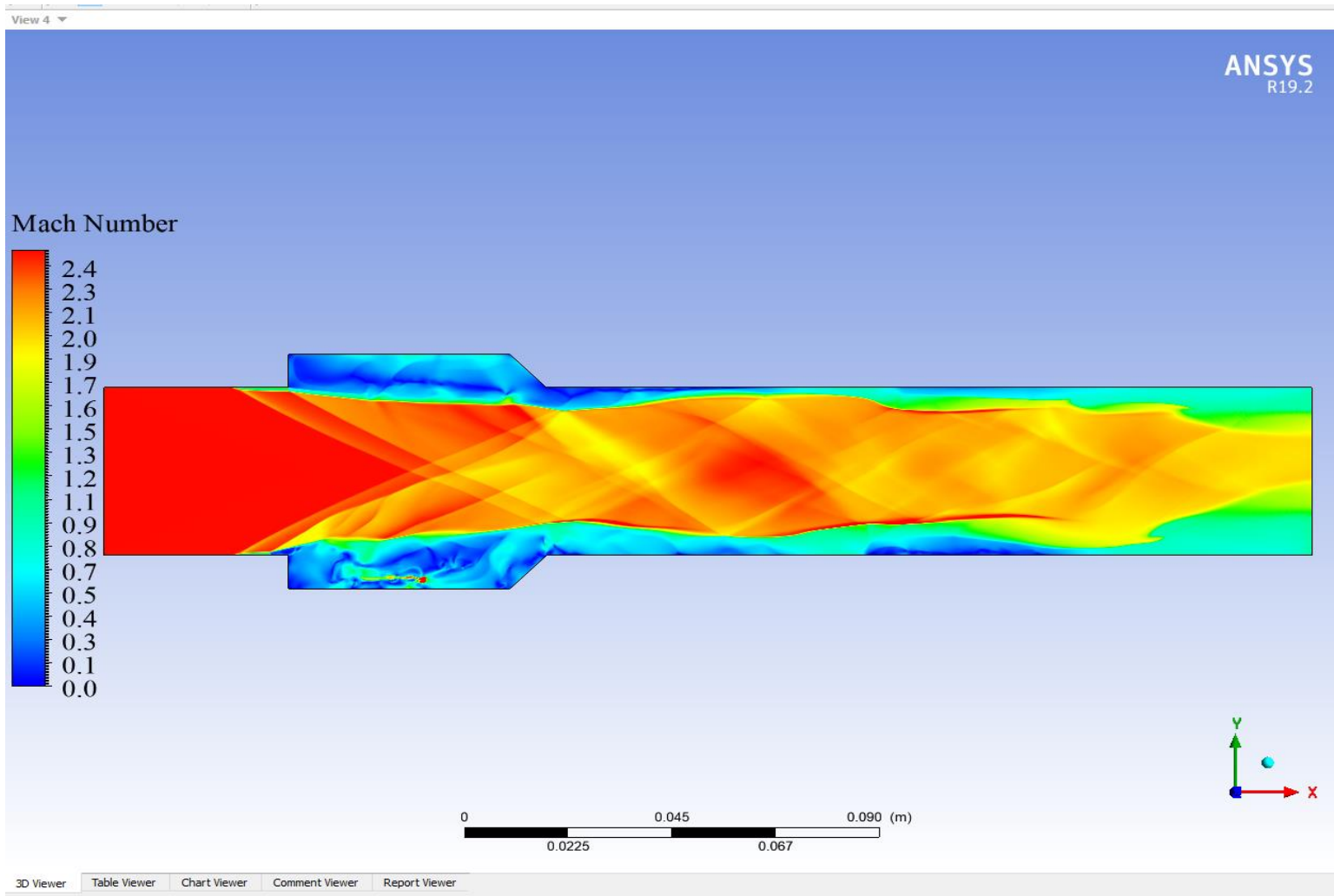
Figure 4-18-Mach number contour $Ma_{air\ inlet} = 2.5,\ P_{air\ inlet} = 110\ Kpa,\ T_{air\ inlet} = 500K$
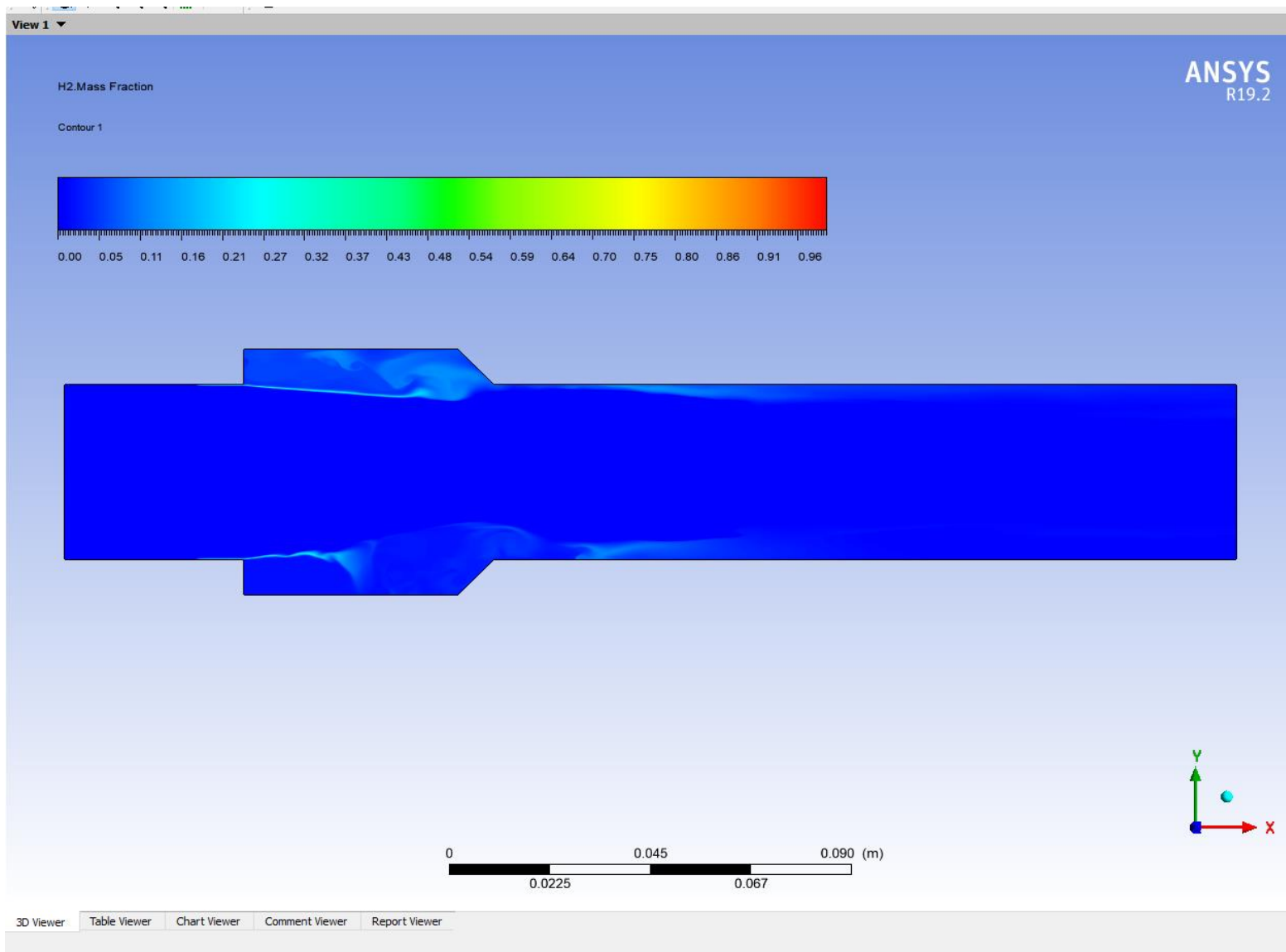
Figure 4-19-H2 mass fraction contour, $Ma_{h2\ inlet} = 1,\ T_{h2\ inlet} = 300K, Y_{H_2} = 1.$
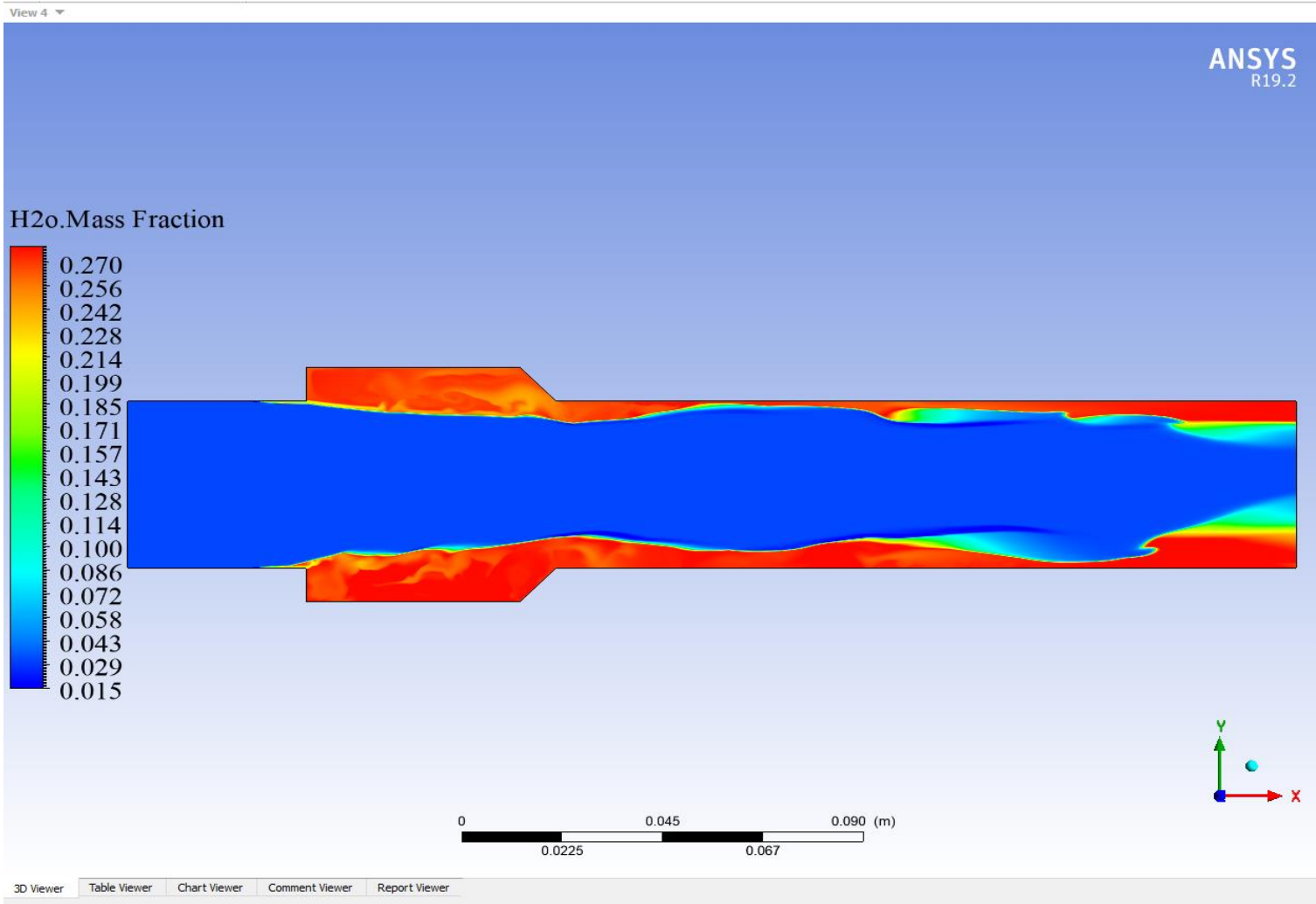
Figure 4-20-H2O mass fraction contour, $Ma_{h2\ inlet} = 1,\ P_{h_2\ inlet} = 110\ Kpa,\ T_{h2\ inlet} = 300K, Y_{H_2} = 1,\ Y_{h_2o} = 0.032,\ Ma_{air\ inlet} = 2.5,\ P_{air\ inlet} = 110\ Kpa,\ T_{air\ inlet} = 500K$
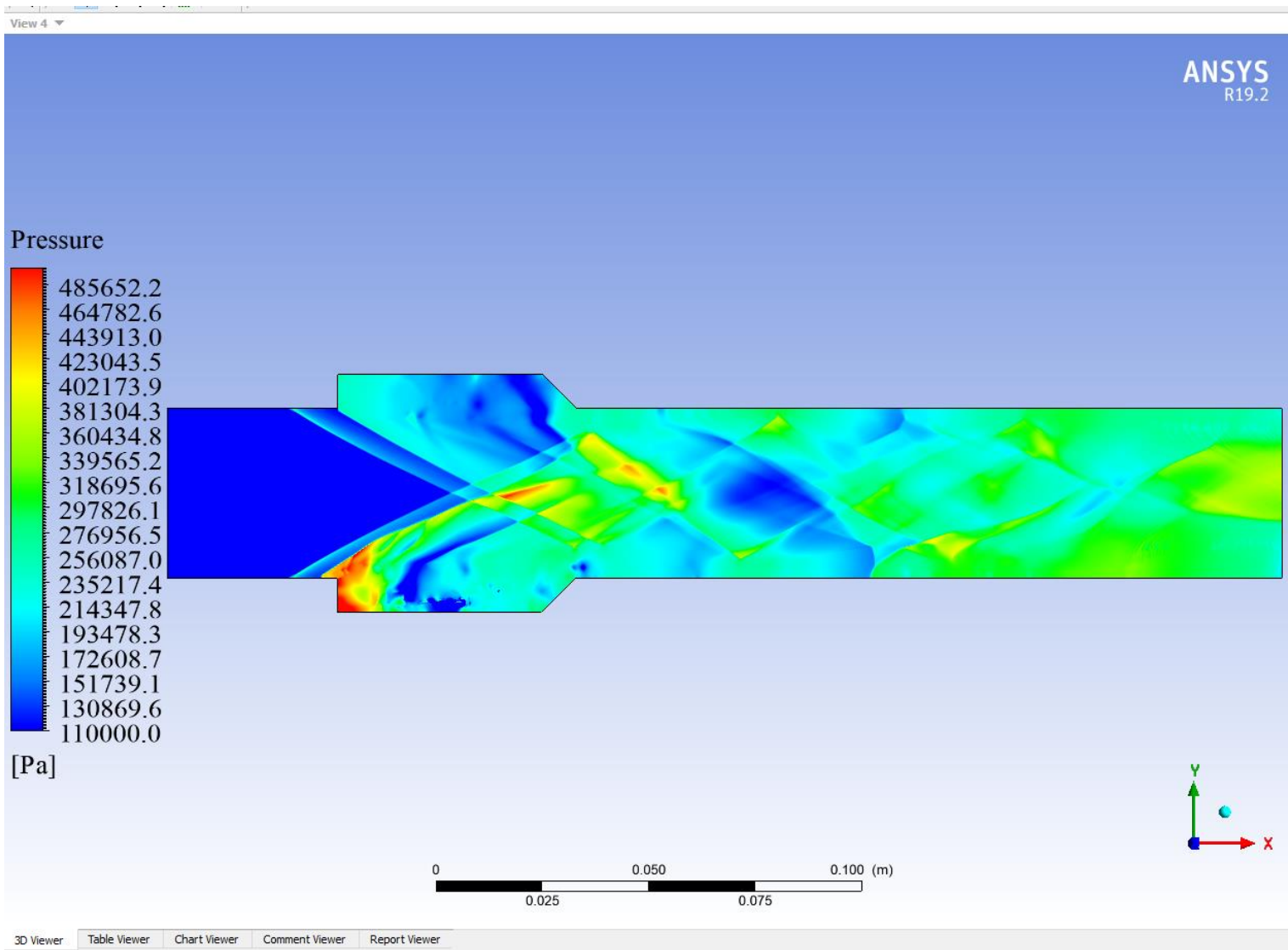
Figure 4-21-Pressure contour, $P_{air\ inlet} = 1100000\ pa, P_{h_2\ inlet} = 110\ Kpa.$

The pressure contours follow the density contours very closely. The contours indicate the generation of shock waves and the mixing of fuel and air. The e static pressure contours of the combustor are shown in Figure 4-21. The contours show asudden rise in pressure after injection of fuel irrespective of Mach number. The generation of bow shock leads to anincrease in the pressure which is due to the transverse fuel injection technique. This results in air compression, which leads to high-pressure creation. The shock waves interaction generates regions of high pressure at the center of the combustor. The high-pressure region results in the creation of immense gradients of pressure that knocks the fuel to-wards the

wall of the combustor. Towards the downstream of the combustor, reattachment shock waves and their inter-action with the bow and initial shock waves are visible in the contours.
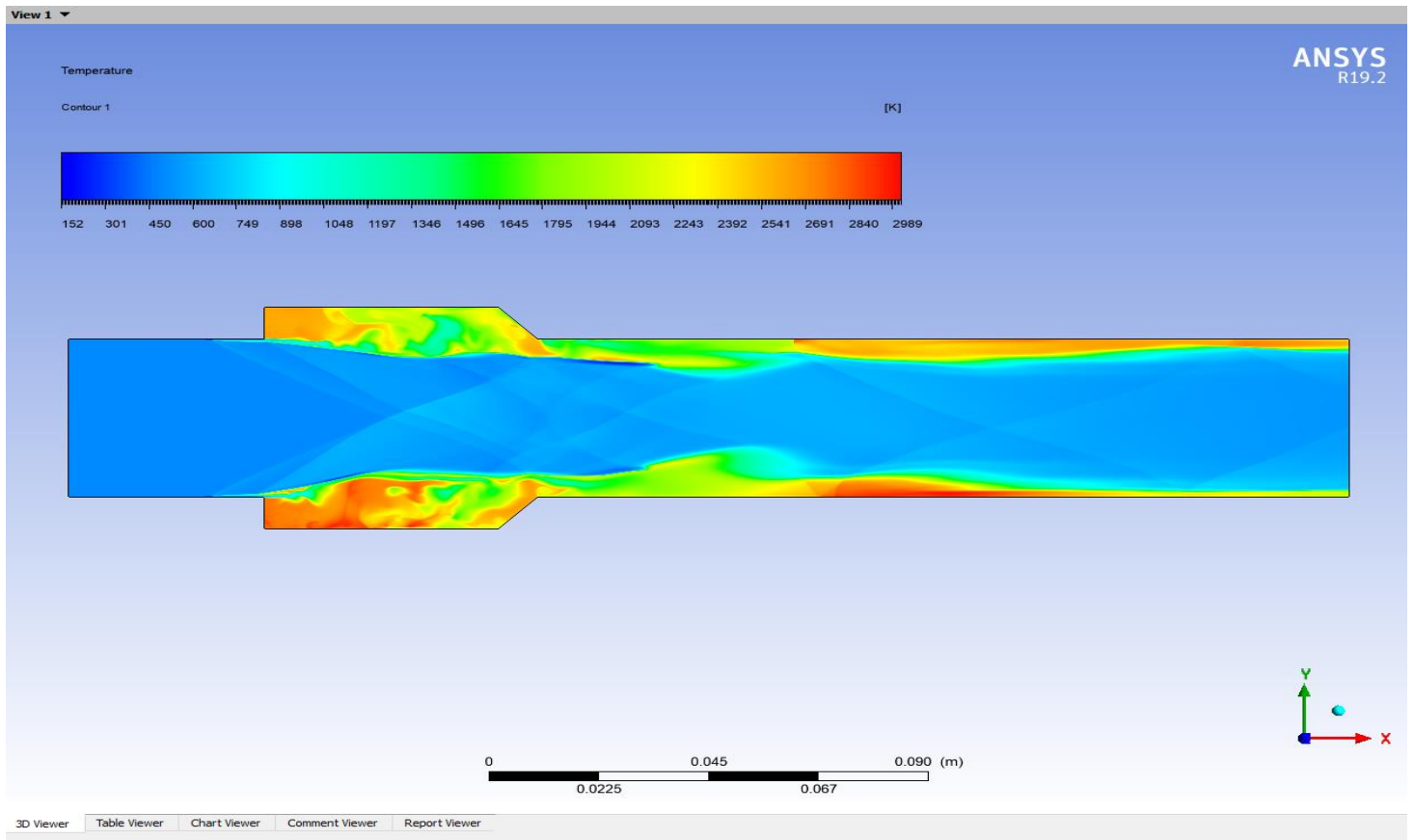
Figure 4-22-Temperature contour, $T_{air\ inlet} = 500K, T_{h2\ inlet} = 300K$.

Density

2.2
2.1
2.0
1.8
1.7
1.6
1.5
1.4
1.2
1.1
1.0
0.9
0.7
0.6
0.5
0.4
0.2
0.1
0.0

[kg m^-3]

0   0.045   0.090 (m)
    0.0225   0.067

3D Viewer   Table Viewer   Chart Viewer   Comment Viewer   Report Viewer

(a)

(b)

0.050   0.100 (m)
    0.075
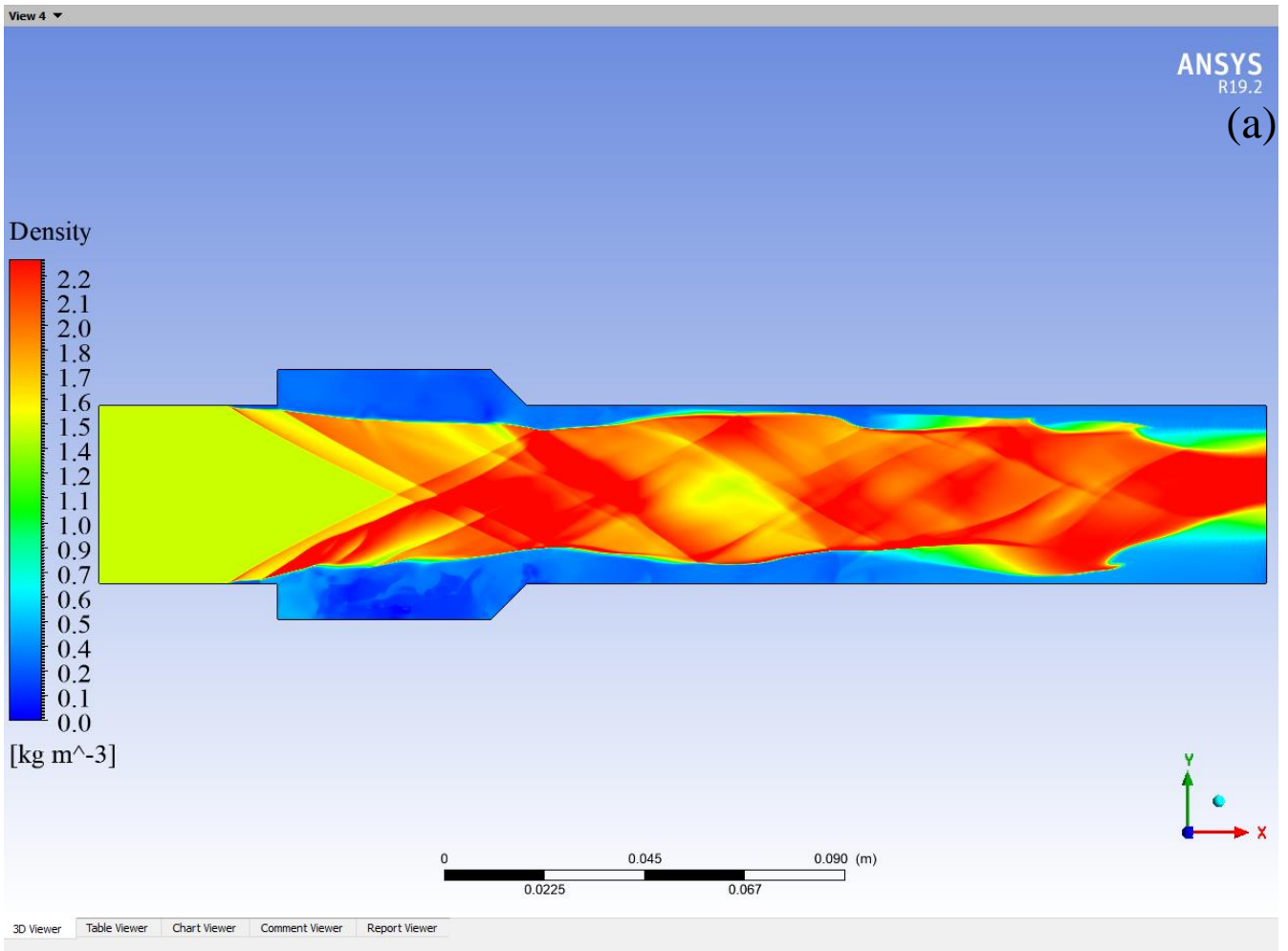
Figure 4-23-Density contour, (a) default rainbow contour, (b) zebra contour.

4.1.5. Comparison between the experimantal results and expirement of all the combustion chamber :
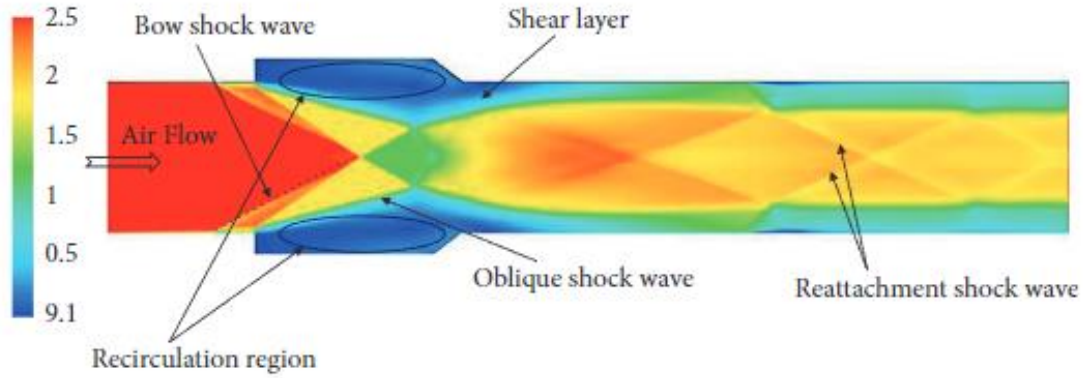
Figure 4-24-Mach number contour showing the nomenclature of the shock waves and their interactions experimental [15].
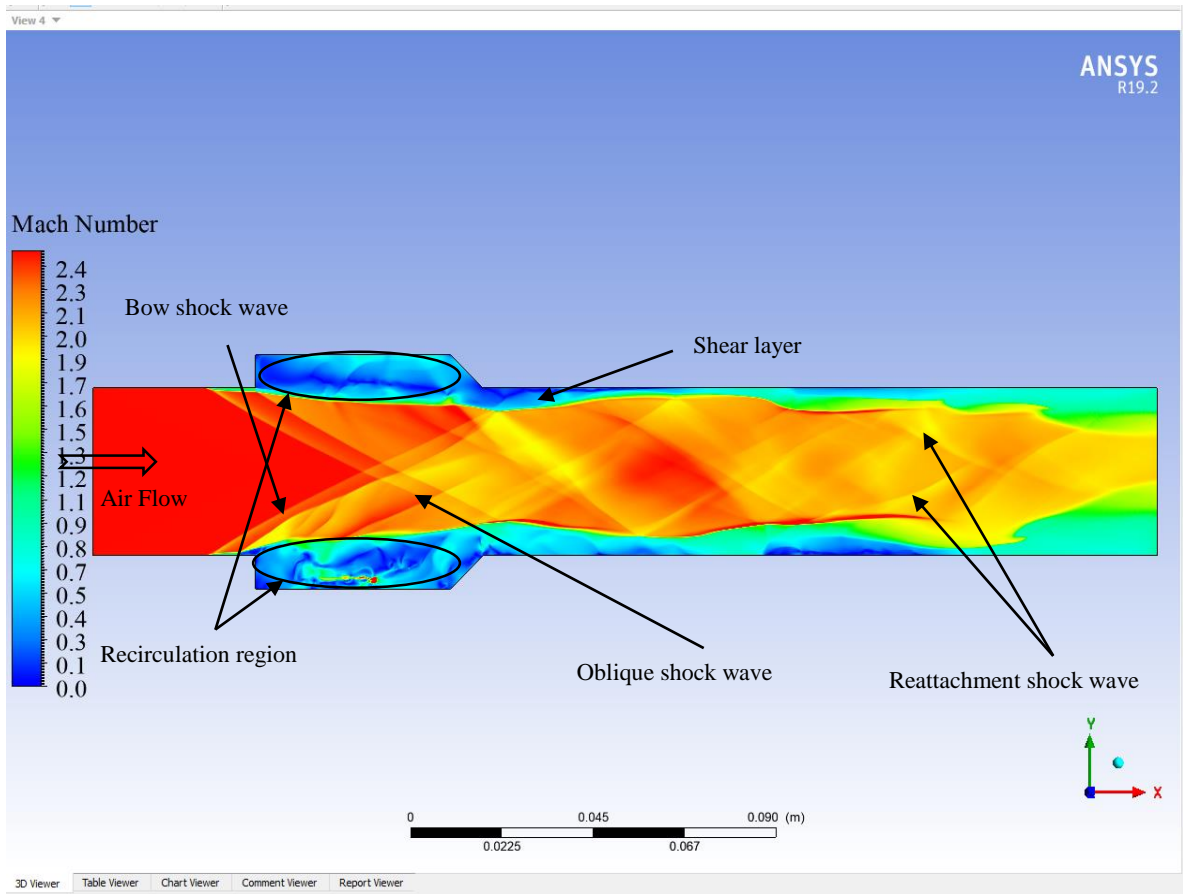
Figure 4-25-Mach number contour for our simulation to show the nomenclature of the shock waves and their interactions

For numerical simulation problems, validation and grid independence study are very important aspects of the study. The selection of the appropriate computational model for better accuracy and reliability of the computational results for a certain application is very necessary. Therefore, a comparison of the experimental and simulation results and close visualization of the obtained results justify the reliability of the selected computational code. In this paper, the Ansys Fluent 19.2 is selected as the computational software to carry out the simulations. The present research work is validated from two different experimental scramjet configurations.

First, the results of the present simulations are compared with the combined experimental and numerical work operated by Yang et al [18].The experiments were conducted at the National University of Defence Technology. The setup consists of a combustor inlet.

Secondly, the validation of supersonic combustion flow has not been carried out yet. Therefore, we chose the DLR case as the verification example. The accuracy and reliability of the numerical algorithm were validated by comparing its results with the DLR experimental results. Comparison between the DLR experimental shadowgraph available in open literature and the DLR computational density gradient contour is demonstrated in Fig. 4.26. The global structure of the reacting flow shows a relatively wider combustion zone compared with the experimental image.

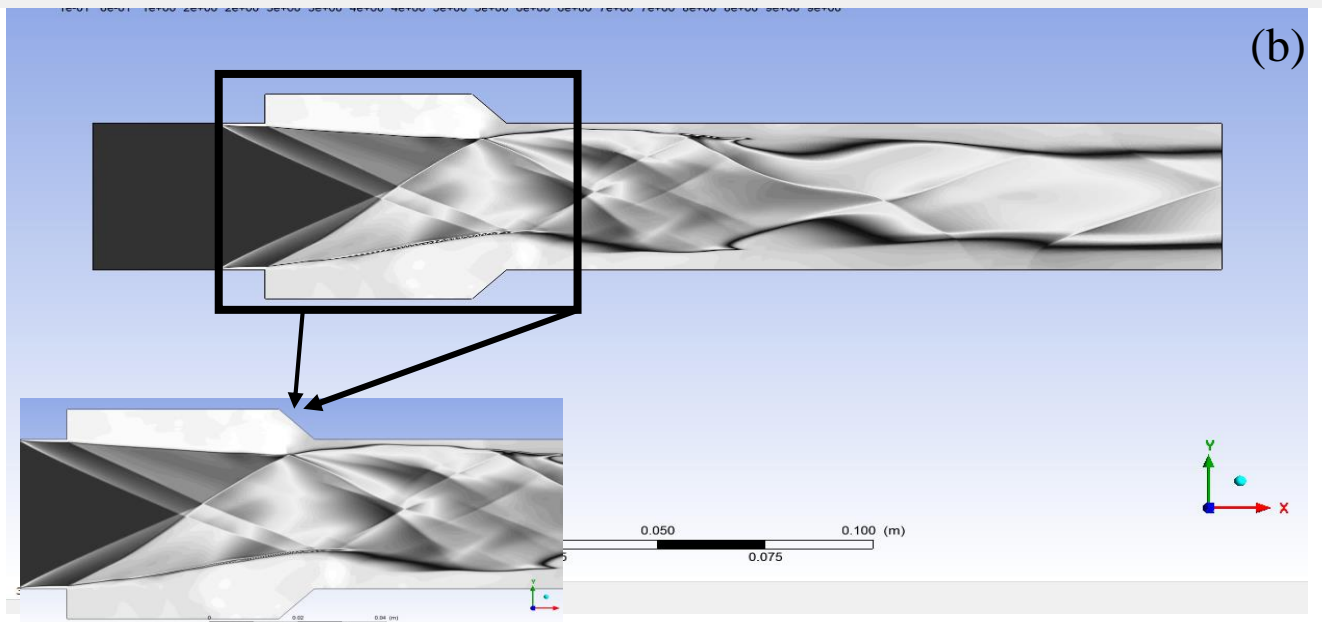The qualitative validationof the simulation results is done by comparing the shadow images and the density and pressure contours obtained from Oevermann [19] simulation, as shown in Figures 4-26 and 4-27. The flow characteristics and generation of shock waves of thescramjet combustor for both configurations are in good agreement with the experimental results.

Two shock waves form at the strut's point and reflect off the upper and lower combustor walls. These reflected shocks interact with shear layers between the fuel jet and supersonic flow. Additionally, weak shock waves, originating at the strut corners, intersect with the reflected shocks. The upper weak shock wave also intersects an expansion wave from the combustor's divergent angle. Both experimental and computational results show the combustion zone widening immediately after the strut.
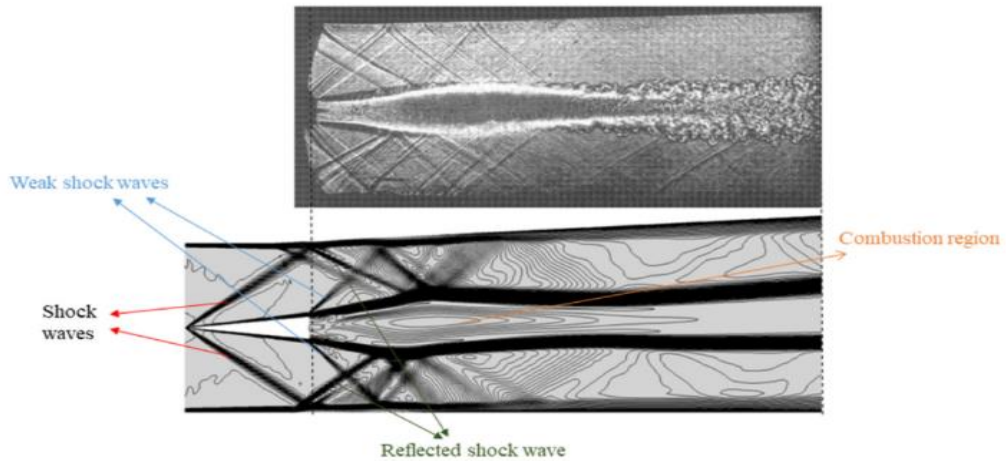
Figure 4-26-Top: Schlieren image of the chemical reaction flow. Bottom: computational contours of density gradient of reacting flow [17].
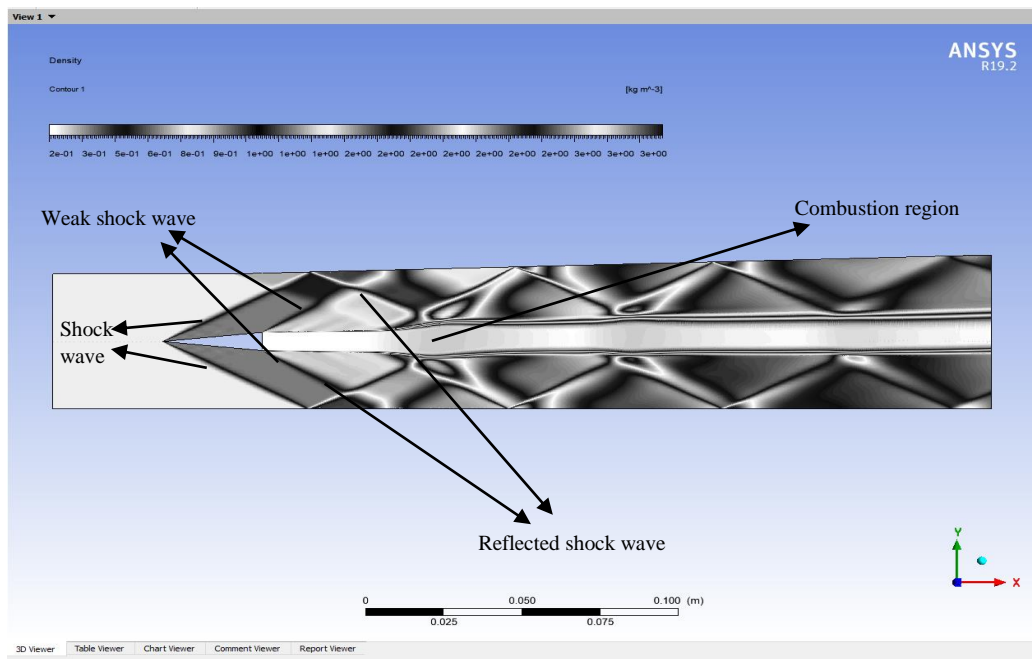
Figure 4-27-Density contour for our simulation

4.2. Effect of the mach on combustion efficiency:

We varied the mach number between 2.5 and 3 for both the double-strut backward steps with the cavity designs and the typical double cavity combustor :
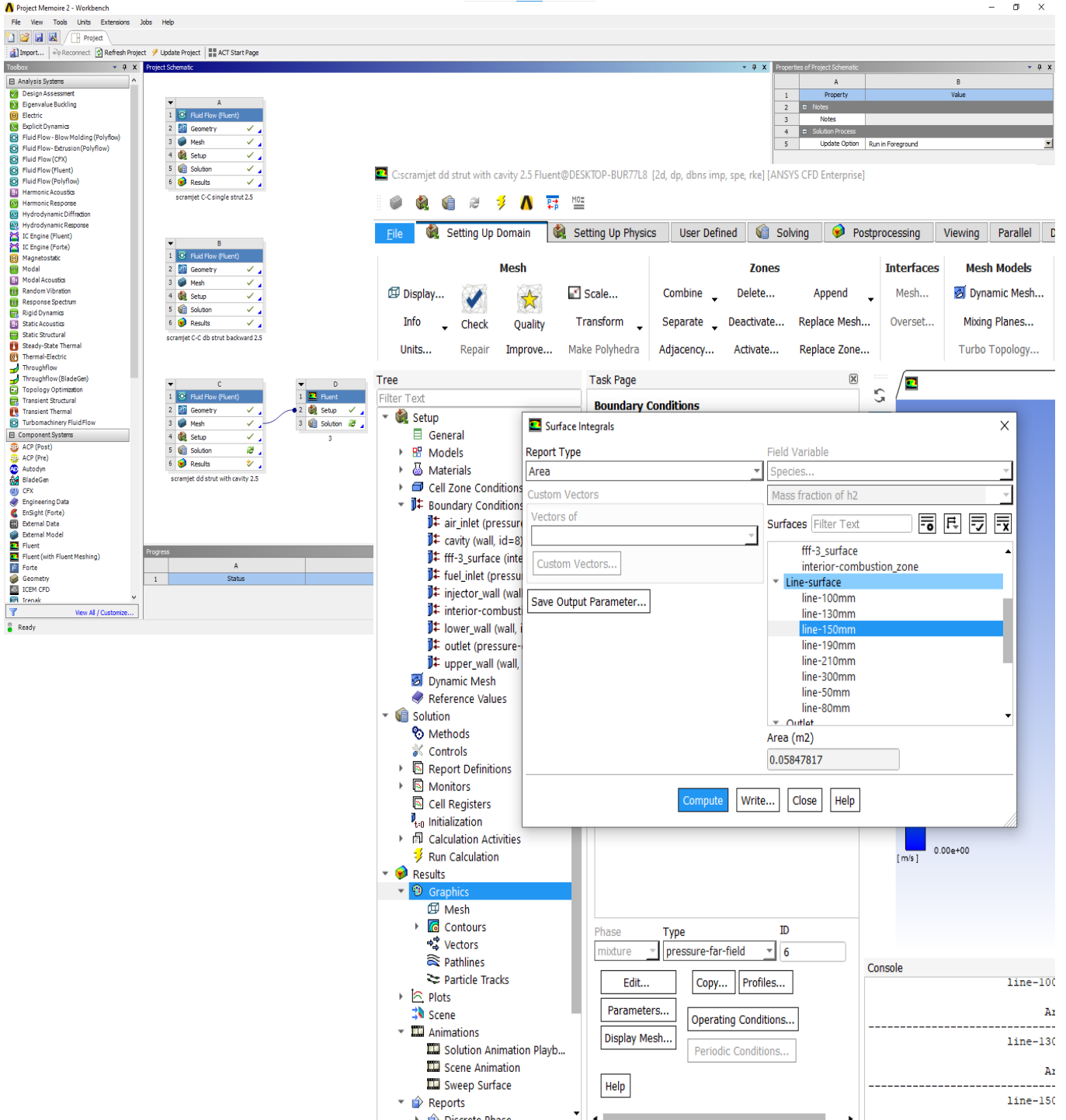
Figure 4-28-Adding Mach variation and lines to calculate the combustion efficiency.

4.3. __Observing the Combustion Efficiency:__

Combustion efficiency "η_c" is one of the parameters selected for the estimation of the combustion process and it is particularly challenging yet crucial for effective propulsion. Supersonic combustion, as utilized in scramjet engines, involves fuel combustion at velocities greater than the speed of sound. The rapid airflows and the extremely short residence time of the air-fuel mixture in the combustion chamber make it difficult to achieve complete combustion [18]

$$\eta_{c(x)} = \frac{\dot{m}_{H2(in)} - \int \rho u A(x) Y_{H2} dA}{\dot{m}_{H2(in)}} = 1 - \frac{\int \rho u Y_{H2} dA}{\dot{m}_{H2(in)}} \tag{4.8}$$

$$= 1 - \frac{\dot{m}_{H2}}{\dot{m}_{H2(in)}} \tag{04.9}$$

4.3.1. Double-strut with cavity mach 2 :

Table 4-1-results proprieties for case 1

X(mm)	Density (Kg/m^3)	Velocity (m/s)	Mass fraction of Yh2	Area (m²)	Mass fraction of Yh2 (inlet)	Combustion efficiency (%)	Static Pressur (Pa)	T(K)
80	1.230588	1029.704	0.003721253	0.06365273	0.9963815	9.96E-01	106556.7	673.2968
100	1.165934	1101.282	0.0052609	0.06470066	0.9963815	9.95E-01	91459.22	583.379
130	1.227255	1057.495	0.006193272	0.06470066	0.9963815	9.94E-01	152091.9	778.125
150	1.550926	1002.866	0.00599873	0.05847817	0.9963815	9.94E-01	249833.6	739.5696
190	1.480864	1007.072	0.004378011	0.05691637	0.9963815	9.96E-01	183481.1	620.7858
210	1.473923	1003.912	0.005450503	0.0579643	0.9963815	9.95E-01	177692.2	598.8202
300	1.312815	1006.942	0.01034323	0.06268	0.9963815	9.90E-01	147215.6	575.9773

Figure 4-29-The combusting effciency for case 1 a long side the line

71

Figure 4-30-The pressure for case 1 a long side the line

Figure 4-31-The temperature for case 1 a long side the line

72

4.3.2. <u>Double-strut with cavity mach 3 :</u>

Table 4-2-results proprieties for case 2

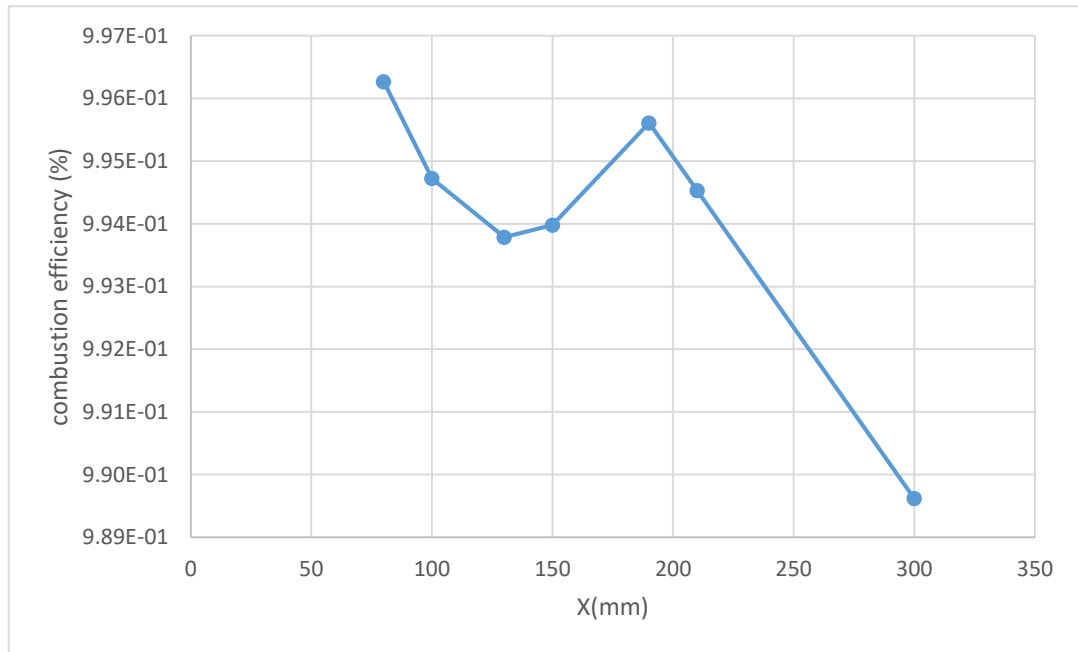| X(mm)	Density (Kg/m^3)	Velocity (m/s)	Mass fraction of Yh2	Area (m²)	Mass fraction of Yh2 (inlet)	Combustion efficiency (%)	Static Pressur (Pa)	T(K)
80	1.192717	1206.806	0.008826224	0.06365273	0.9972607	0.991149532	101130.2	663.1136
100	181436	1283.941	0.008812612	0.06470066	0.9972607	0.991163181	99642.38	588.3102
130	1.242575	1264.187	0.004134052	0.06278922	0.9972607	0.995854592	131192.7	689.3954
150	1.517446	1135.206	0.001961229	0.05847817	0.9972607	0.998033384	237612.8	903.7725
190	1.449286	1191.4	0.001858548	0.05691637	0.9972607	0.998136347	258882	1006.577
210	1.481719	1281.838	0.001708284	0.0579643	0.9972607	0.998287024	275813.3	1087.232
300	1.291856	1233.548	0.00357991	0.06268	0.9972607	0.996410257	149289.1	624.7767

Figure 4-32-The combusting effciency for case 2 a long side the line
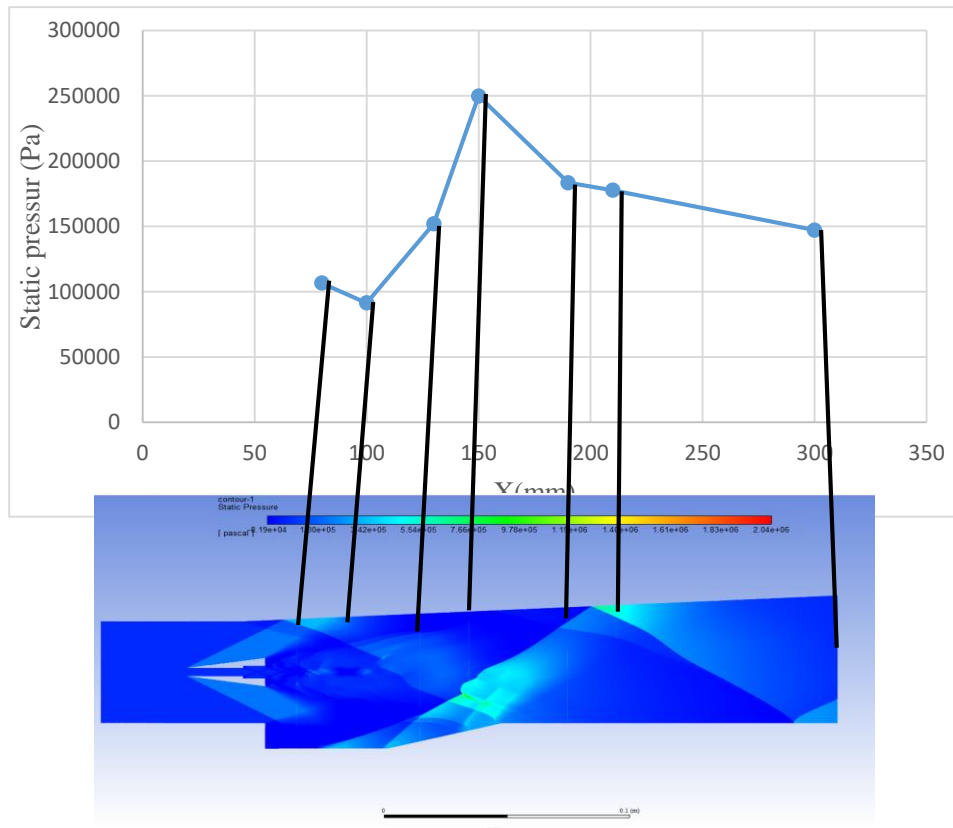
Figure 4-33-The pressure for case 2 a long side the line

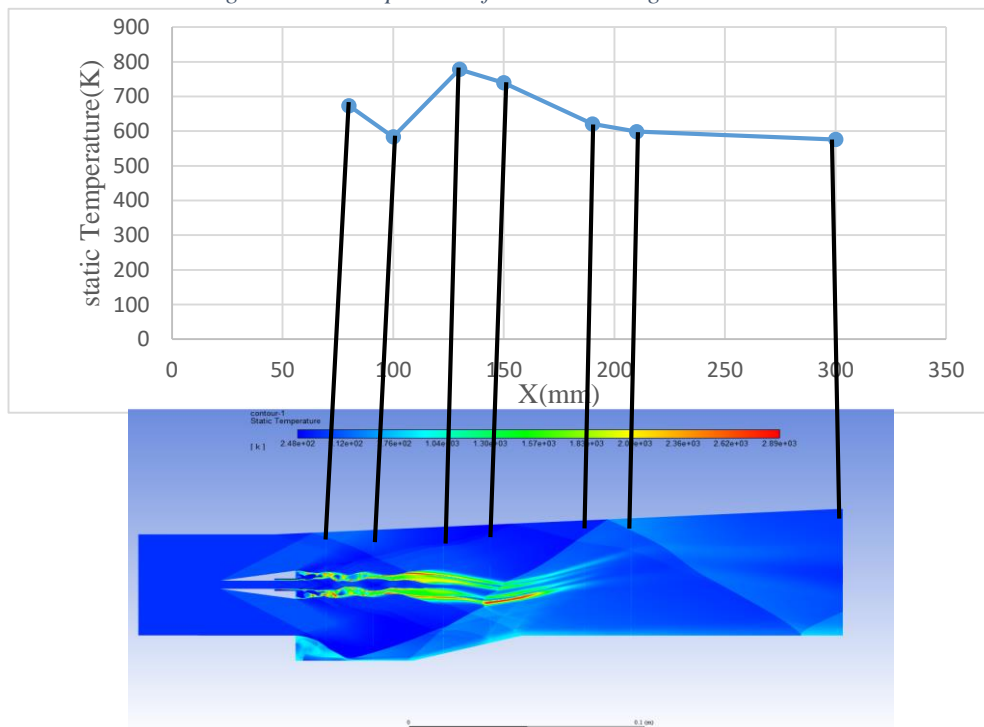*Figure 4-34-The temperature for case 2 a long side the line*

4.3.3. Typical double cavity mach 2 :

Table 4-3-results proprieties for case 1.2

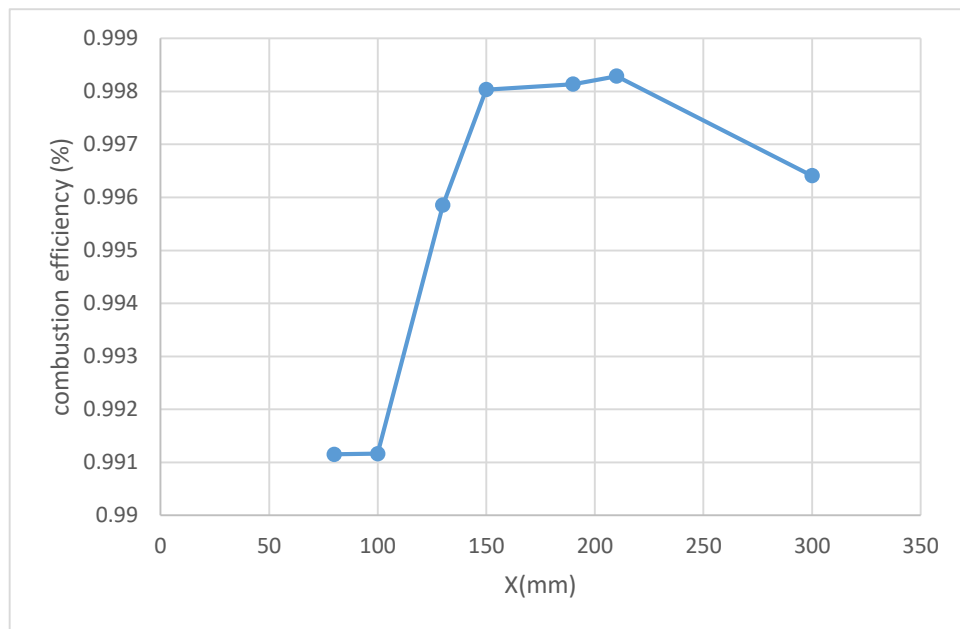| X(mm)	Density (Kg/m^3)	Velocity (m/s)	Mass fraction of Yh2	Area (m²)	Mass fraction of Yh2 (inlet)	Combustion efficiency (%)	Static Pressure (Pa)	T(K)
50	1.142191	829.7916	0.01659615	0.056	0.851194	0.980502506	168118.7	1128.141
80	1.536322	811.8105	0.02802303	0.056	0.851194	0.967077975	222136.2	1281.468
100	1.680006	1011.823	0.01007955	0.04	0.851194	0.98815834	228123.6	1029.631
130	1.680006	1018.458	0.01292788	0.04	0.851194	0.984812064	236758.3	794.2541
150	1.547401	970.6835	0.01200462	0.04	0.851194	0.985896729	278938.4	1039.35
190	1.751593	1117.131	0.005690741	0.04	0.851194	0.993314402	352741.4	1211.442
240	1.639486	1090.805	0.005226041	0.04	0.851194	0.993860341	333479.9	1236.261

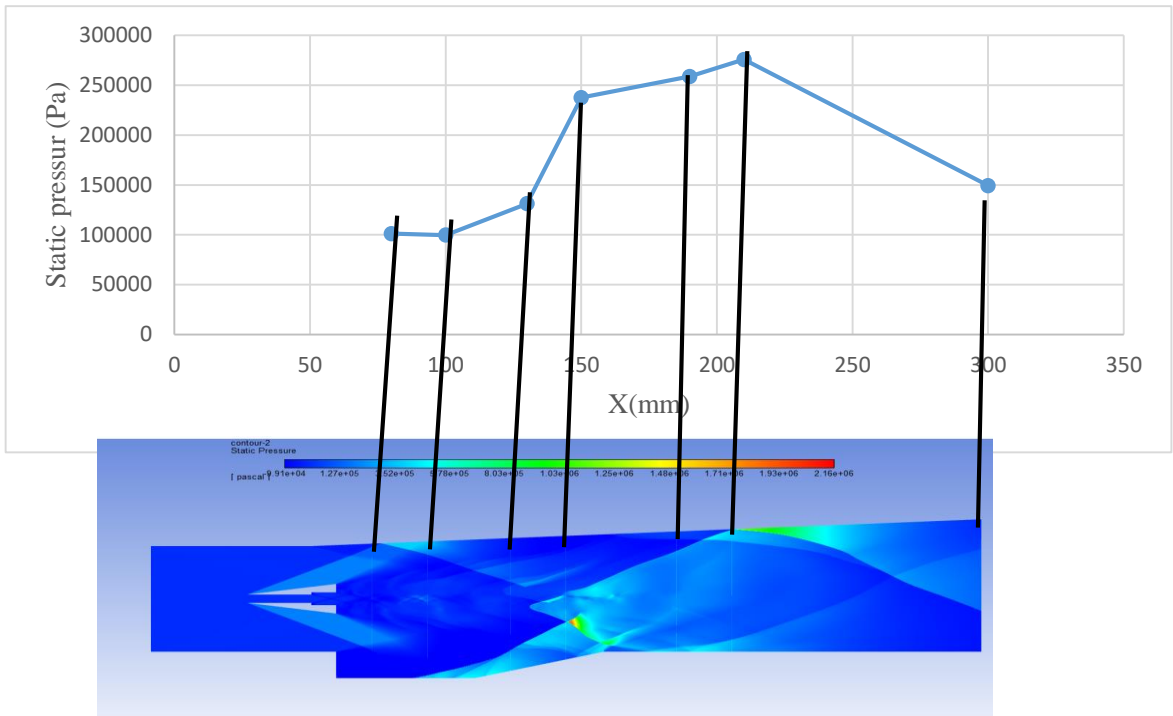*Figure 4-35-The combusting efficiency for case 1.2 a long side the line*

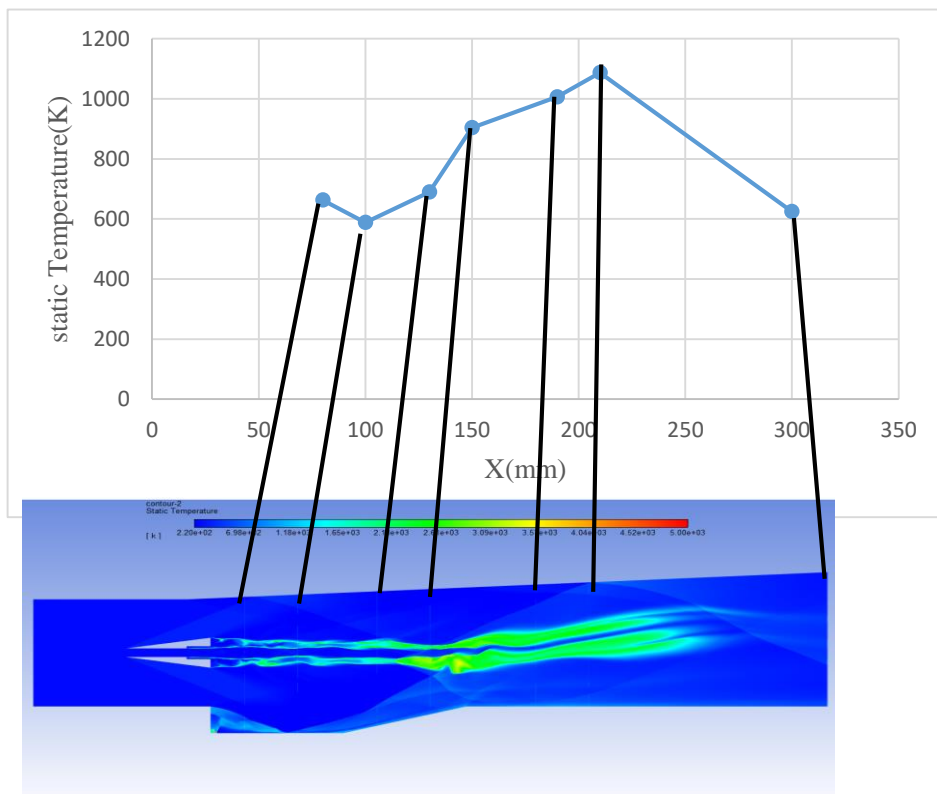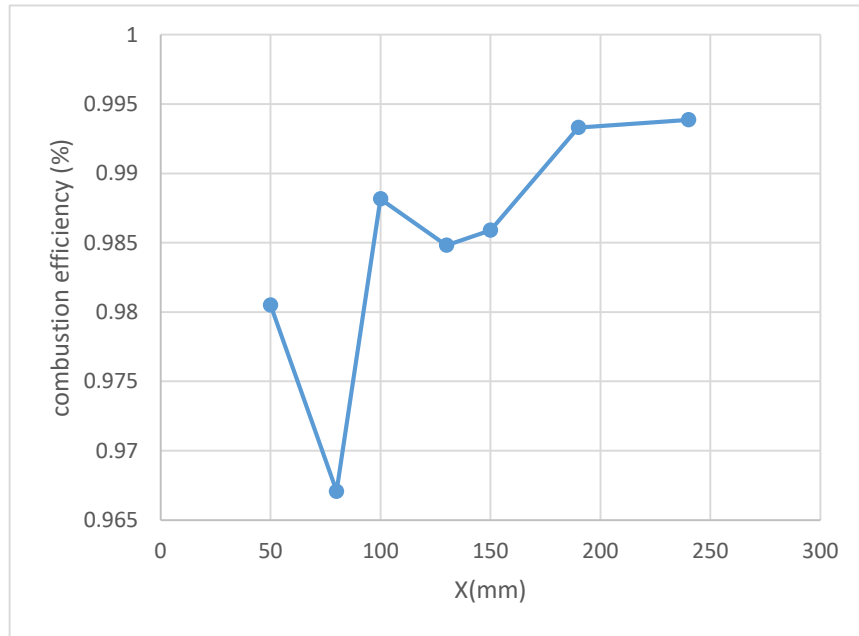Figure 4-36-The pressure for case 1.2 a long side the line
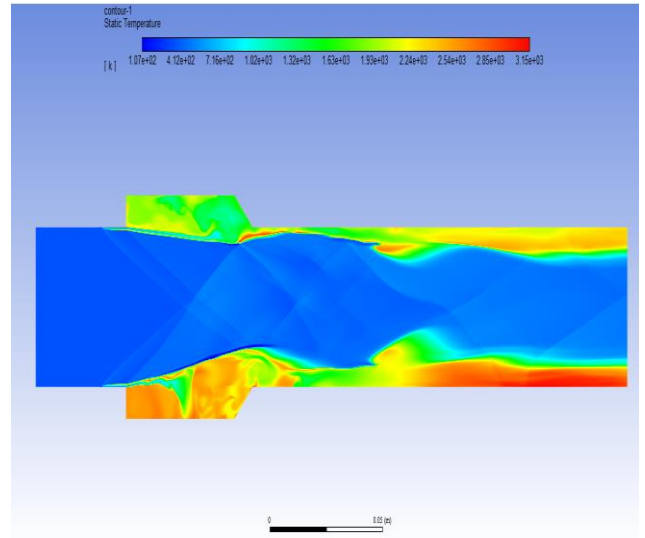
Figure 4-37-The temperature for case 1.2 a long side the line

4.3.4. Typical double cavity mach 3 :

Table 4-4-results proprieties for case 2.2

X(mm)	Density (Kg/m^3)	Velocity (m/s)	Mass fraction of Yh2	Area (m²)	Mass fraction of Yh2 (inlet)	Combustion efficiency (%)	Static Pressure (Pa)	T(K)
50	1.145866	1007.054	0.01827309	0.056	0.8435053	0.978336722	180852.7	1150.71
80	1.14748	1049.061	0.02131073	0.056	0.8435053	0.974735511	197412	1334.171
100	1.554763	1253.716	0.004239207	0.04	0.8435053	0.994974297	215937.8	1010.521
130	1.494721	1223.984	0.01321445	0.04	0.8435053	0.984333886	241580.2	1042.181
150	1.475801	1315.197	0.009306016	0.04	0.8435053	0.988967448	292375	1186.06
190	1.538759	1275.399	0.00475222	0.04	0.8435053	0.994366105	304713.8	1231.489
240	1.547013	1286.929	0.004547309	0.04	0.8435053	0.994609033	251087.4	1027.461

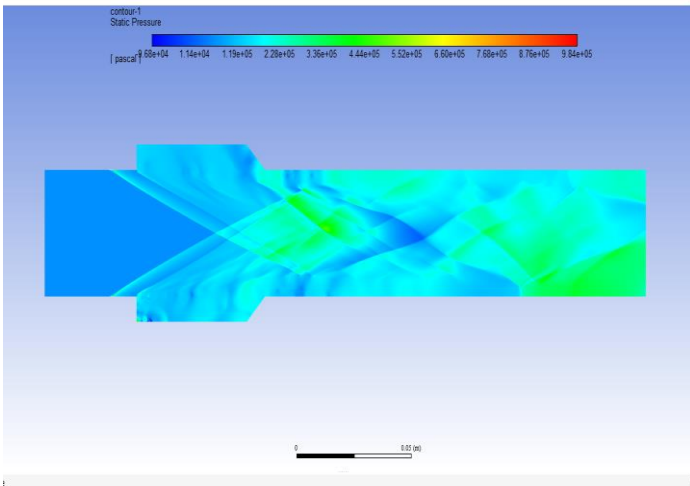*Figure 4-38-The combusting effeciency for case 2.2 a long side the line*
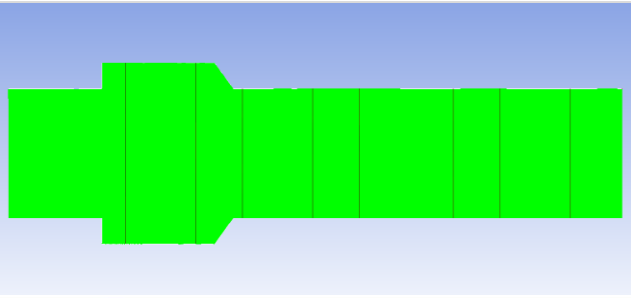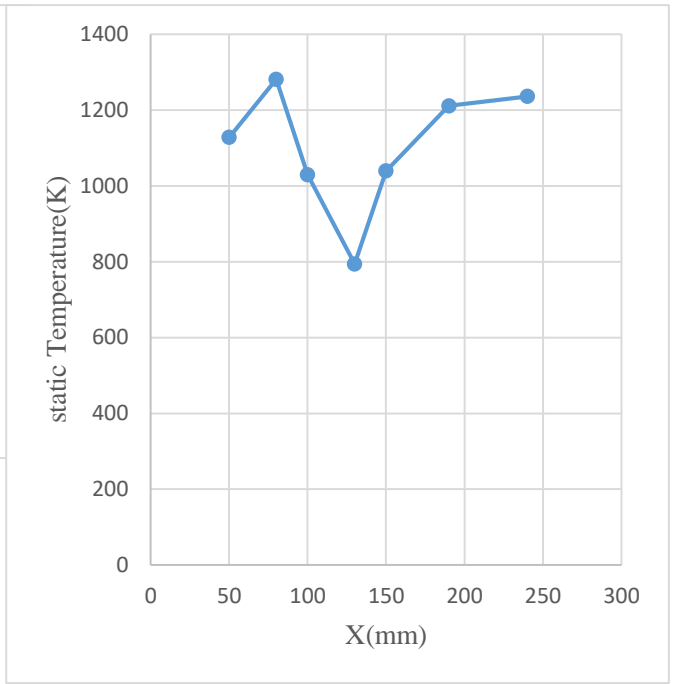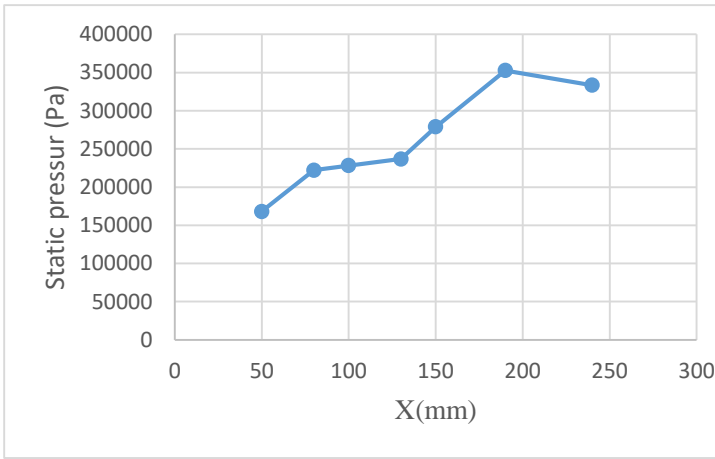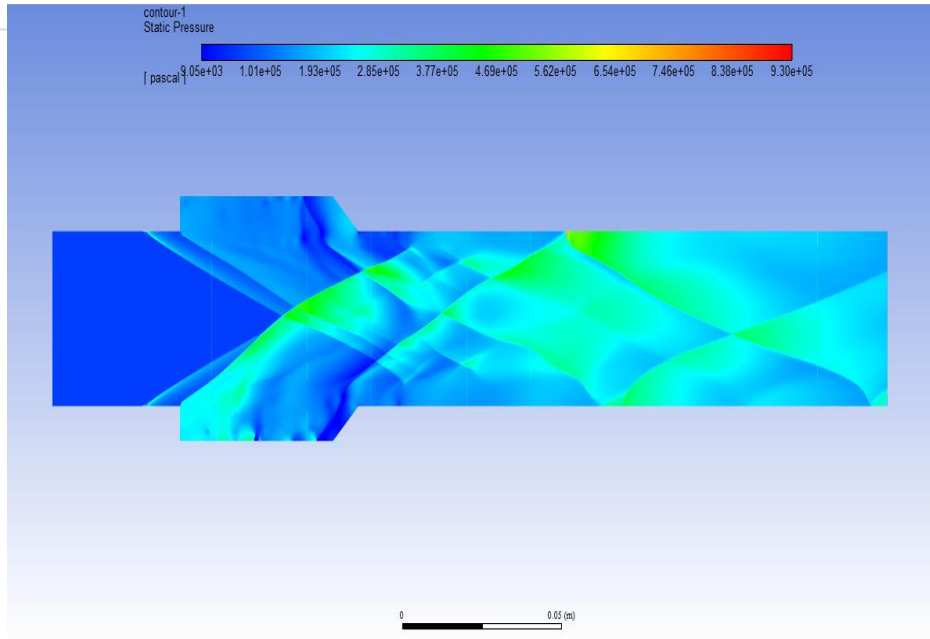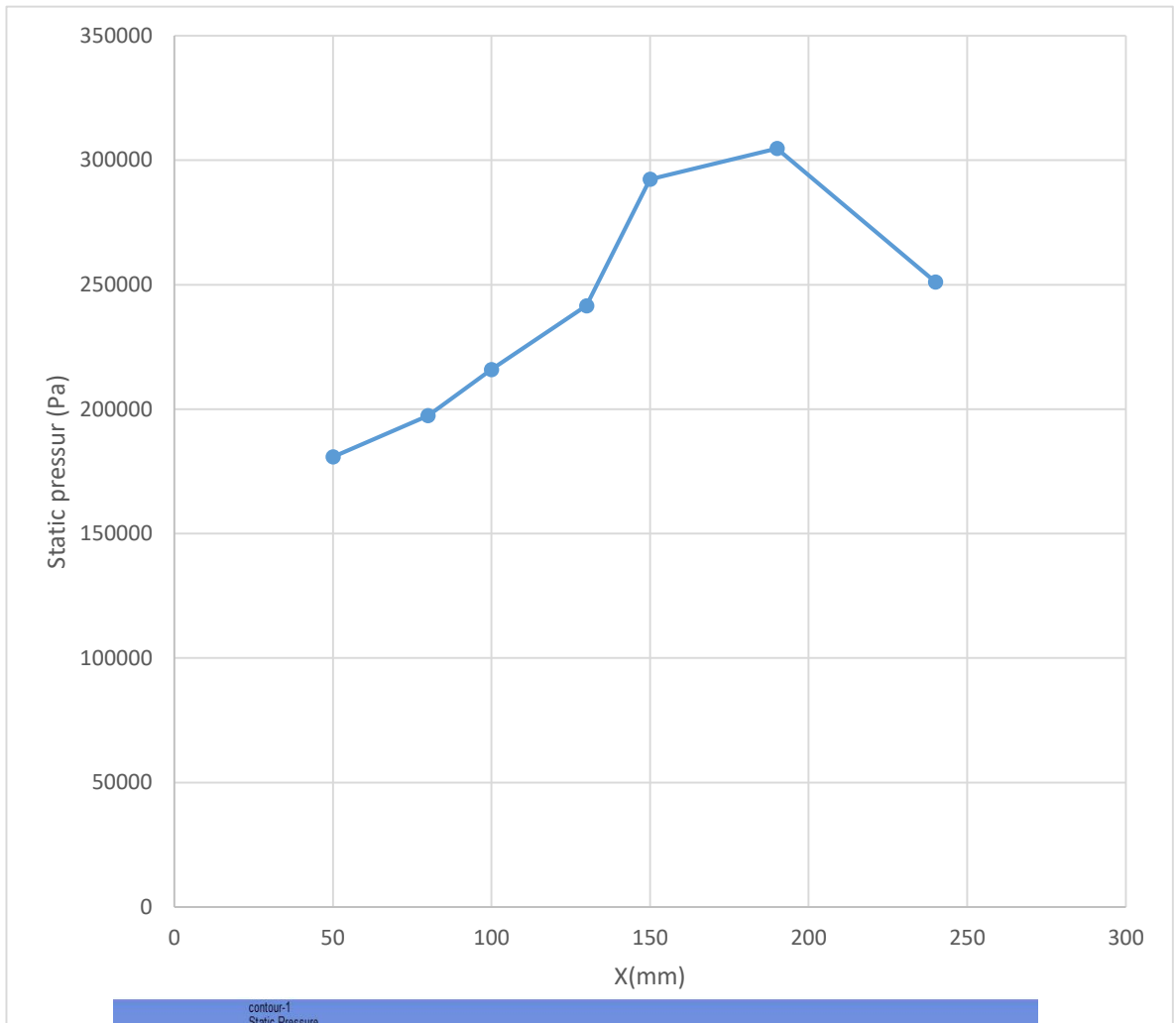
Figure 4-39-The pressure for case 2.2 a long side the line

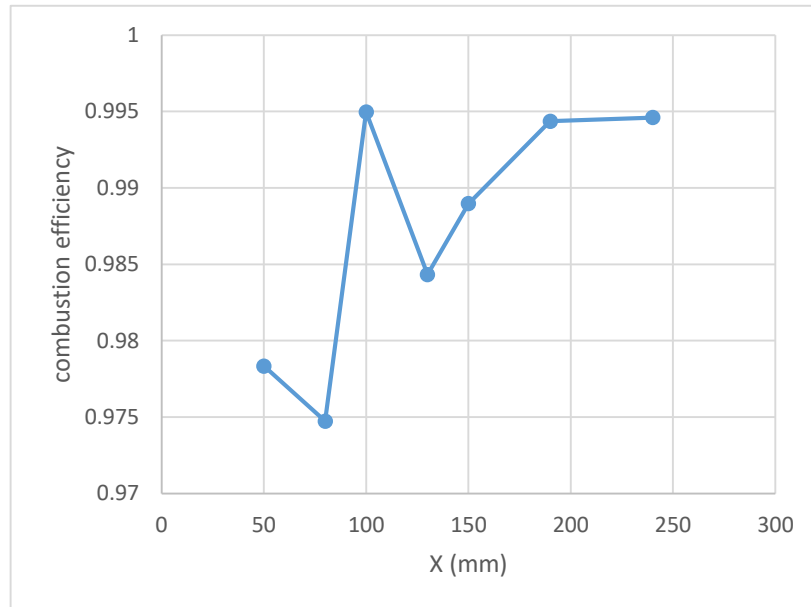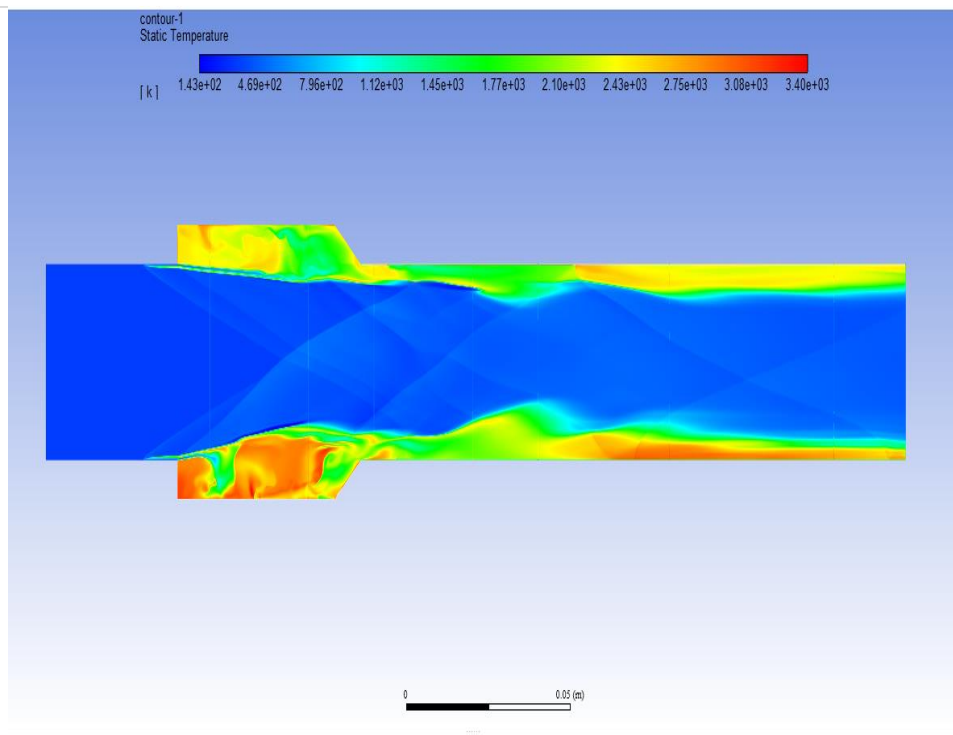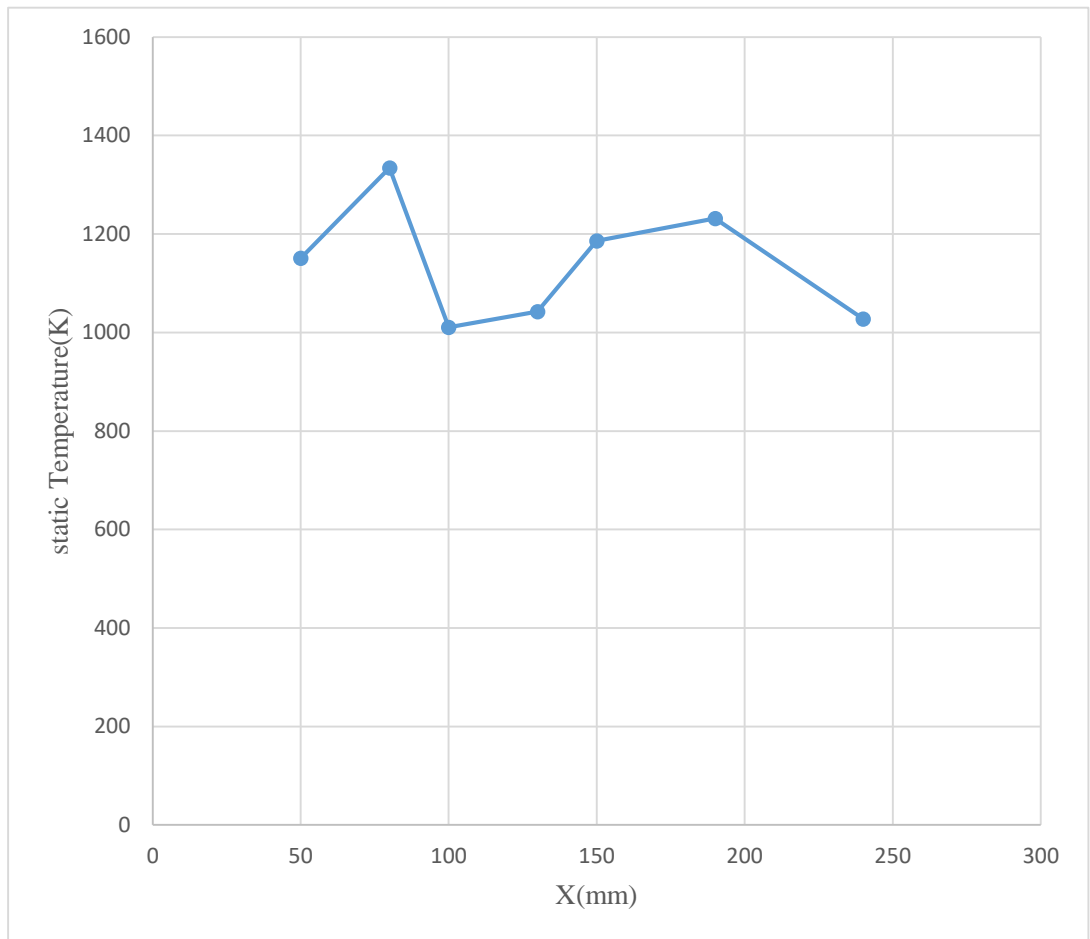*Figure 4-40-The temperature for case 2.2 a long side the line*

4.3.5.   Observation for the effect variation of Mach number on different parameters:

At Mach 2, the combustion process exhibited stable flame characteristics with moderate pressure and temperature distributions. The introduction of cavities significantly enhanced the shear-mixing layer, which improved the mixing of fuel and air. This resulted in a more efficient combustion process. However, despite the stability and improved mixing, the overall combustion efficiency was lower compared to the higher Mach number case.

In contrast, at Mach 3, the higher inlet velocity intensified shock interactions and increased turbulence within the combustor. This enhanced turbulence promoted better fuel-air mixing, leading to a more complete and efficient combustion process. The higher Mach number also resulted in higher temperature regions and increased thrust. Nevertheless, the elevated thermal and mechanical stresses on the combustor walls required advanced cooling techniques and materials capable of withstanding such harsh conditions.

The addition of cavities at both Mach numbers played a crucial role in enhancing the mixing and combustion efficiency. The cavities created recirculation zones that prolonged the residence time of the fuel-air mixture, promoting more complete combustion. At Mach 3, the benefits of the cavity configuration were even more pronounced, as the increased turbulence further amplified the mixing efficiency facilitated by the cavities.

Conclusion:

This study specifically focuses on the numerical simulation and analysis of supersonic combustion chambers using Ansys Fluent. It examines the performance of hydrogen-fueled cavity SCRAMJET combustors under different Mach numbers and cavity configurations. The objective is to determine how various design elements impact combustion efficiency, pressure, and temperature profiles. The study utilizes the standard k-epsilon turbulence model and Reynolds-averaged Navier-Stokes (RANS) equations with a finite-rate/eddy dissipation species reaction model. It compares the effects of single-strut and double-strut designs with backward-facing steps, as well as the impact of cavity configurations on the mixing and combustion process. The results provide valuable insights into optimizing SCRAMJET combustor designs for improved performance, highlighting the critical role of turbulence and recirculation zones in achieving efficient supersonic combustion.

The study include:

- o **Stable Combustion at Mach 2.5:** The flame exhibited stability with moderate pressure and temperature distributions.
- o **Cavity Impact:** Introducing cavities had a significant positive effect on the shear mixing layer, enhancing fuel and air mixing.
- o **Improved Mixing Efficiency:** Despite lower overall combustion efficiency at Mach 2.5, the cavities resulted in a more efficient combustion process.
- o **Intensified Shock Interactions at Mach 3:** The higher inlet velocity at Mach 3 increased turbulence within the combustor, promoting better fuel-air mixing.
- o **Higher Temperature Regions:** The higher Mach number led to increased thrust, but advanced cooling techniques were necessary to manage the higher temperature.
- o **Recirculation Zones:** The cavities created recirculation zones, extending the residence time of the fuel-air mixture and promoting more complete combustion.
- o **Enhanced Turbulence at Mach 3:** The benefits of the cavity configuration were more pronounced due to increased turbulence at Mach 3.
- o **Double-Strut Design Superiority:** The double-strut design with backward-facing steps significantly outperformed the single-strut configuration.
- o **Additional Shear Layers:** The double-strut setup created additional shear layers and recirculation zones, further enhancing fuel and air mixing.
- o **Uniform Temperature Distribution:** The overall result was a more uniform temperature distribution within the combustor, leading to better combustion characteristics and higher efficiency.

Finally, implementing cavity configurations and the double-strut design with backward-facing steps enhances combustion performance at both Mach numbers. Optimizing the combustor design to balance these factors is crucial for achieving optimal performance in practical applications. This study underscores the importance of advanced cooling techniques and materials to manage the increased thermal and mechanical stresses at higher Mach numbers, paving the way for more efficient and robust SCRAMJET designs.

Outlooks

The outlooks highlight strategic areas for advancing SCRAMJET technology, emphasizing the need for precise engineering solutions to optimize performance and reliability in high-speed aerospace applications.

1. **Advanced Cooling Strategies**: Future research should focus on developing robust cooling techniques to manage the high temperatures encountered during high-speed SCRAMJET operations. This effort aims to enhance engine durability and efficiency under extreme thermal conditions.
2. **Optimization of Cavity Geometries**: Further exploration into optimizing cavity designs holds the promise of improved fuel-air mixing and combustion efficiency. Investigating various geometries could lead to tailored configurations that maximize performance across different Mach numbers.
3. **Integration of Advanced Turbulence Models**: Exploring advanced turbulence models like Large Eddy Simulation (LES) offers the potential for accurately predicting turbulent flow behaviors within SCRAMJET combustors. This could provide deeper insights into combustion dynamics and support enhanced design strategies.
4. **The development of 3-dimensional models** for a more detailed study of geometry can be taken into consideration..

Références :

[1] E. Engman, «Numerical Simulation of Scramjet Combustion,» *Master thesis,* vol. 1, n° %1https://www.diva-portal.org/smash/get/diva2:1021892/FULLTEXT01.pdf, p. 78, 2008.

[2] R. Lorin, «https://fr.wikipedia.org/wiki/René_Lorin,» paris.

[3] H. v. Ohain, «https://en.wikipedia.org/wiki/Hans_von_Ohain,» german.

[4] Lorin, «https://migflug.com/jetflights/the-v1-flying-bomb/,» germany.

[5] T. BOMARC, «https://www.airplanesandrockets.com/rockets/bomarc-american-modeler-august-1958.htm,» USA.

[6] S.-4. Ganef, «https://armyrecognition.com/military-products/army/air-defense-systems/air-defense-vehicles/sa-4-ganef-2k11-krug-air-defense-missile-system-technical-data-sheet-13012155,» russia.

[7] R. T. Voland, «X-43A Hypersonic vehicle technology development,» *Acta Astronautica,* vol. 59, n° %1https://doi.org/10.1016/j.actaastro.2006.02.021, pp. 181-191, 2009.

[8] X-43, «https://www.nasa.gov/reference/x-43a/,» NASA.

[9] E. T. Curran, «Scramjet Engines: The First Forty Years,» *jourrnal of propulsion and power,* vol. 17, n° %1https://doi.org/10.2514/2.5875, 2001.

[10] J. Hank, «The X-51A Scramjet Engine Flight Demonstration Program,» *HYTASP-8: Program Overview I,* vol. 15, n° %1https://doi.org/10.2514/6.2008-2540, p. 198, 2008.

[11] J. J. Wang, «Scramjet operability range studies of an integrated hydrogen and hydrocarbon fuels,» *Virginia Polytechnic Institute and State University, Blacksburg,* vol. 13, n° %1VA, USA, Dissertation thesis, p. 200, 2008.

[12] Z. Peng, «Effect of Tube Size on Flame and Pressure Wave Propagation in a Tube Closed at One End: A Numerical Study,» *Combustion Science and Technology,* vol. 192, n° %1https://doi.org/10.1080/00102202.2019.1622534, p. 1713, 2019.

[13] Z. Peng., «Flame Propagation and Reflections of Pressure Waves through Fixed Beds of RTO Devices: A CFD Study,» *Industrial & Engineering Chemistry Research,,* vol. 58, n° %151, p. https://doi.org/10.1021/acs.iecr.9b04812, 2019.

[14] Z. Peng, «CFD investigation of flame and pressure wave propagation through variable concentration methane-air mixtures in a tube closed at one end,,» *Combustion Science and Technology,,* vol. 193, n° %17, p. https://doi.org/10.1080/00102202.2019.1685987, 2021.

[15] N. Bordoloi, «Numerical Investigation on the Effect of Inflow Mach Numbers on the Combustion Characteristics of a Typical Cavity-Based Supersonic Combustor,» *Research Article | Open Access,* vol. 2021, n° %114, p. https://doi.org/10.1155/2021/3526454, 2021.

[16] J. Tu, «A Practical Approach: Computational Fluid Dynamics,» *Elsevier, Amsterdam, Netherlands,,* vol. 4, 2023.

[17] C. Lia, «Numerical investigation on the performance of scramjet combustor with a novel strut configuration,» *Applied Thermal Engineering,* vol. 159, n° %1https://doi.org/10.1016/j.applthermaleng.2019.113894, p. 12, 2019.

[18] R. Masumoto, «Experimental Study on Combustion Modes in a Supersonic Combustor,» *Journal of propulsion and power,* vol. 27, n° %1https://doi.org/10.2514/1.B34020, p. 2, 2011.

[19] M. Oevermann, «Numerical investigation of turbulent hydrogen combustion in a SCRAMJET using flamelet modeling,,» *Aerosp. Sci. Technol.,* vol. 4, n° %1https://doi.org/10.1016/S1270-9638(00)01070-1., pp. 463–480,, 2000.

[20] M. T. GAUTAM CHOUBEY, «SCRAMJET COMBUSTION, Fundamentals and Advances,» *Butterworth-Heinemann ,* vol. Luleå University of Technology, n° %116, p. 198, 2022.

[21] T. L. D-21, «https://www.nationalmuseum.af.mil/Visit/Museum-Exhibits/Fact-Sheets/Display/Article/195778/lockheed-d-21b/,» usa.

[22] DARPA, «https://www.darpa.mil/about-us/timeline/falcon-htv-2,» usa.

[23] X.-5. Waverider, «https://www.researchgate.net/figure/Boeing-X-51A-WaveRider-scramjet-demonstrator-31_fig3_332867884,» air force.

[24] «Vajram-And-Ravi,» Ramjet vs Scramjet, 2023. [En ligne]. Available: https://vajiramandravi.com/quest-upsc-notes/ramjet-vs-scramjet/.

[25] «Ansys product page,» Ansys Fluent Fluid Simulation Software, [En ligne]. Available: https://www.ansys.com/products/fluids/ansys-fluent.

[26] J. Urzay, «Supersonic Combustion in Air-Breathing Propulsion Systems for Hypersonic Flight,» *Annual Review of Fluid Mechanics,* Vols. %1 sur %2https://doi.org/10.1146/annurev-fluid-122316-045217, n° %150, p. 593–627, 2018.

[27] Y. Y, «Numerical and experimental study on flame structure characteristics in a supersonic combustor with dual-cavity,» *Acta Astronautica,* vol. 117, n° %1https://doi.org/10.1016/j.actaastro.2015.09.005, pp. 376-389, 2015.